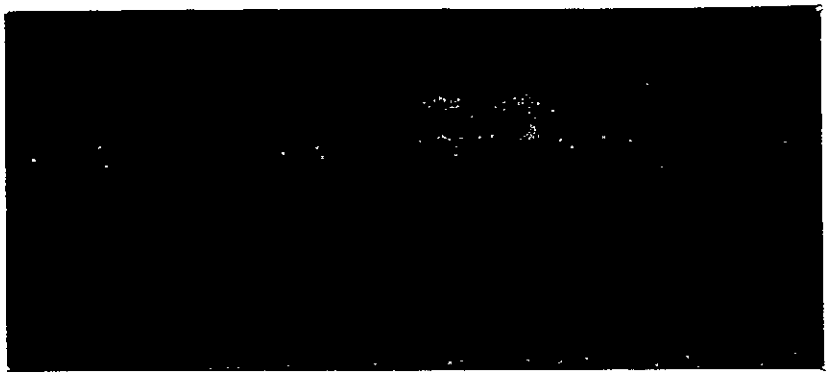

PLANETARY SCIENCE INSTITUTE

(NASA-CR-154512) PLANETARY ASTRONOMY PROGRAM Final Report (Planetary Science Inst., Tucson, Ariz.) 177 p HC A09/MF A01 CSCL 03A

N78-11955

Unclas
G3/89 15089

PLANETARY ASTRONOMY PROGRAM

Final Report
15 October 1977

NASW-2983

Submitted by:

Planetary Science Institute
2030 East Speedway, Suite 201
Tucson, Arizona 85719

CONTENTS

TASK 1: ASTEROID SPECTROPHOTOMETRY

(Principal Investigator: Clark R. Chapman)

During the 1976/1977 contract period, major advances were made in spectrophotometric observations of asteroids and in their interpretation. Major progress was achieved in data reduction. The purpose of this final report is to summarize briefly the accomplishments of the first three quarters, for which more details are available in our first three Quarterly Reports, and to provide greater details concerning the work accomplished during the Final Quarter. Appendices A and B contain manuscripts prepared in major part with Planetary Astronomy Program funding: "The Evolution of Asteroids and Meteorite Parent-bodies" (an invited review paper presented by Dr. Chapman to the annual Meteoritical Society meeting) and "The Asteroids" (a major review article to appear in the 1978 volume of Annual Review of Astronomy and Astrophysics, co-authored by Drs. Chapman and Hartmann at PSI and Dr. Williams of JPL).

SUMMARY OF WORK DURING FIRST THREE QUARTERS

The foundation of our program of asteroid spectrophotometry is acquisition of new data, although reduction and interpretation of that data are essential elements of the program as well. Data were obtained during the contract period during four observing runs at the Kitt Peak National Observatory: 3 runs on the 1.3-m telescope (Sept. 15-19, 1976; Nov. 14-17, 1976; and June 6-16, 1977) and 1 run on the 2.1-m telescope (Sept. 25-27, 1976). A total of 83 asteroids were observed, although a few included within that total represent the same object observed during different runs. All of the asteroids were measured in the spectral range 0.33 - 0.9 μm and a large minority were measured, in addition, between 0.9 - 1.07 μm.

This year has proven to be one of the most productive years for obtaining asteroid spectrophotometric data. Included among the asteroids measured are the exceptional asteroids 1620 Geographos and 944 Hidalgo. The great quantity of data has caused some pile-up in the data reduction programs, but preliminary results are expected to be available for some asteroids for presentation at the October 1977 DPS meeting in Boston.

During this year, our data reduction program was upgraded for inclusion as an interactive code for running on our HP-9825 computer. Improvements in standard star calibrations have been incorporated in the program and most raw data obtained during the past two years have been written onto HP-readable magnetic tape cartridges. Final reduction of all data is proceeding.

An observing trip was also made to Mexico during October 1976 to attempt measurement of the diameter of Pallas during a stellar occultation. Unfortunately, the occultation path passed south of us, so we could only report a negative observation.

Interpretive work has also progressed. Chapman has been working with Bowell, Gradie, Morrison, and Zellner in writing a paper on asteroid taxonomy, based on a classification program that utilizes the TRIAD data file (see Fourth Quarter Report, below).

Papers written and presentations delivered during the contract year include the following: (1) A final manuscript was prepared in February 1977, based on Chapman's invited review at IAU Colloquium 39 during the summer of 1976. This manuscript, entitled "The Evolution of Asteroids as Meteorite Parent-bodies", will appear in the Colloquium Proceedings (The Interrelated Origin of Comets, Asteroids, and Meteorites, A. H. Delsemme, Editor, Univ. of Toledo Publications, in press) and was included as Appendix A to our Second Quarterly Report. (2) Dr. Chapman presented an invited review paper to the Cambridge, England, meeting of the Meteoritical Society in July 1977. His extended abstract, "The Evolution of Asteroids and Meteorite Parent-bodies", attached as Appendix A, will appear in Meteoritics. (3) Drs. Chapman and Hartmann (in conjunction with Dr. Williams of JPL) have prepared an invited review paper on "The Asteroids" for the Annual Review of Astronomy and Astrophysics. It is attached as Appendix B.

FOURTH QUARTERLY REPORT

Plans have been finalized during the fourth quarter to obtain the extremely important observations of the nucleus of dying comet P/Arend-Rigaux during early November 1977. This observing run was originally planned for Kitt Peak Observatory, but for inexplicable reasons, time was not granted at that Observatory. Subsequently, last minute plans were made to obtain the data using the 88-inch telescope at Mauna Kea Observatory, using the spectrophotometer of T. McCord. Other faint asteroids will be observed as secondary objectives of the program. A proposal has been written to Kitt Peak requesting time for asteroid observations during spring 1978.

Further work has been accomplished in asteroid data-reduction. There is hope that some preliminary data may be in a form to be presented at the DPS meeting in Boston in October 1977.

Two manuscripts have been completed during the Fourth Quarter. They have been referred to above and are included as Appendices A and B.

A major interpretive effort has been carried out during the fourth quarter. Dr. Chapman hosted a meeting at PSI at which Dr. Bowell, Mr. Gradie, Dr. Morrison, and Dr. Zellner met to work on a manuscript in preparation concerning asteroid taxonomy. New data were entered into the TRIAD data file and a classification program generated classifications for over 560 different asteroids, according to the C-S-M-etc. taxonomy originally developed by Chapman, Morrison, and Zellner (Icarus 25, 104). Dr. Chapman worked on comparing the C-S-M taxonomy with earlier schemes developed by himself and with more recent schemes advanced by Gaffey and McCord. There is a reasonable degree of concordance among the various schemes (see Table I). The text of the article in preparation discusses the detailed relationships between the taxonomies, the advantages and disadvantages of each, and the relationships between observationally-based groupings and mineralogical types of asteroids.

Table I. Asteroid taxonomies and mineralogical classifications

	Taxonomic Class[a]	Mineralogical Class, Meteorite Analog, or Descriptor[b]	Type Asteroids[c]	Typical B-V[d]	Typical Albedo[d]
flat spectra	mostly C	C*, carbonaceous chondrite? (F + TB)	213, 2, 10, 88, 511, 1	0.63 - 0.74	0.04 - 0.07
		C2 or CM, carbonaceous chondrite (TA + TC)	324, 51	0.72 - 0.80	0.03 - 0.04
transitional spectra	M	metal or enstatite chondrite (RR)	16, 21, 22	0.70 - 0.72	0.09 - 0.11
	E	enstatite achondrite	44	0.72	0.35
	(U)	intermediate (various T)	166, 48	0.77	0.03
	(U)	basaltic achondrite	4, 69 (?)	0.77	0.23
	(U)	Trojan	624	0.77	0.04
reddish spectra	mostly S	metal-rich (plus silicate?) (RF)	9, 12	0.87 - 0.88	0.13 - 0.14
		metal plus olivine (RA-1)	7, 39	0.82 - 0.92	0.14 - 0.16
		metal plus pyroxene (plus minor olivine?) (RA-2 + TE)	29, 3, 6, 230, 25	0.87 - 0.91	0.10 - 0.17
		pyroxene-rich plus metal (RA-3)	89, 5, 63, 446	0.83 - 0.91	0.13 - 0.14
		metal-poor, opaque-poor, pyroxene-rich	8	0.88	0.14
high-contrast spectra	(U)	L ordinary chondrite?	1685	0.88	0.12
	R	LL ordinary chondrite or olivine achondrite?	349	0.96	0.26
	?	? (steep red spectrum)	170	?	?
	(U)	(carbonaceous?) chondrite type 3 (TD)	80	0.89	0.14

[a]Bowell et al (1978).

[b]Descriptor slightly modified from Chapman (1976). Letters in parentheses are corresponding compositional groups of Gaffey and McCord (1977a, b).

[c]Asteroids typifying the 34 spectral groups found by McCord and Chapman (1975a, b), augmented by the 44 Nysa group (Zellner et al 1977d).

[d]Typical colors and albedos are only indicative.

TASK 2: NATURE OF THE TROJAN ASTEROIDS

(Principal Investigator: William K. Hartmann)

Dr. Hartmann joined Dr. Dale P. Cruikshank for a highly successful observing run devoted to studying the peculiar Trojan asteroid 624 Hektor in February, 1977. Photometric observations were obtained both in the visual and at 20μ in the infrared. The observations revealed that we were observing Hektor as close to pole-on as it has even been seen. This was interesting in tying down the pole orientation, but disappointing from the point of view that the magnitude variation was only about 0.06 mag (clearly detected in the visual), making it difficult to detect the change in 20μ radiation with period, as shown in Figure 1, which shows the observations for 14 February. We are continuing a further analysis of the records, including data obtained on 13 February, so that it may ultimately be possible to determine the phase relations of the 20μ period. Our original intent was to discriminate a shape variation from an albedo variation by seeing whether the visual and 20μ peaks were correlated or anti-correlated, respectively. An irregular shape of Hektor is favored as an explanation of the light variations.

Our observations have allowed an improved measurement of the albedo and dimensions. Our results indicate Hektor is very dark, with visual albedo p_V 0.025 $\pm$ 0.005. The dimensions would be calculated as 128 km wide and 275 km long for the Dunlap-Gehrels cigar-shaped model.

Our work has led to consideration of the origin of such an unusual shaped object. It is the largest Trojan, making its origin as a fragment of a larger body seem less likely than if it were one of the smaller Trojans. We have made preliminary calculations of the possibility that 624 Hektor arose not as a fragment, but as a coalescence of two sub-spheroidal asteroids originally independent in the Trojan cloud. Collision velocities in the Trojan cloud could be lower than the typical collision velocity for belt asteroids. A low-velocity collision could result in a dumbbell-like configuration of two partially fractured bodies not completely broken apart on impact. Figure 2 shows some marginal evidence in favor of this interpretation. If Hektor were two ball-like objects in contact, each with different spectrophotometric properties, then the two end-on views should give different spectrophotometric signatures. Figure 2 shows that this is so, and that in fact, the end-on view in Minimum I (Dunlap-

Gehrels nomenclature) is markedly distinct from the other views, by more than the error-bar dimension.

Publication of the observations and interpretation is expected in 1978.

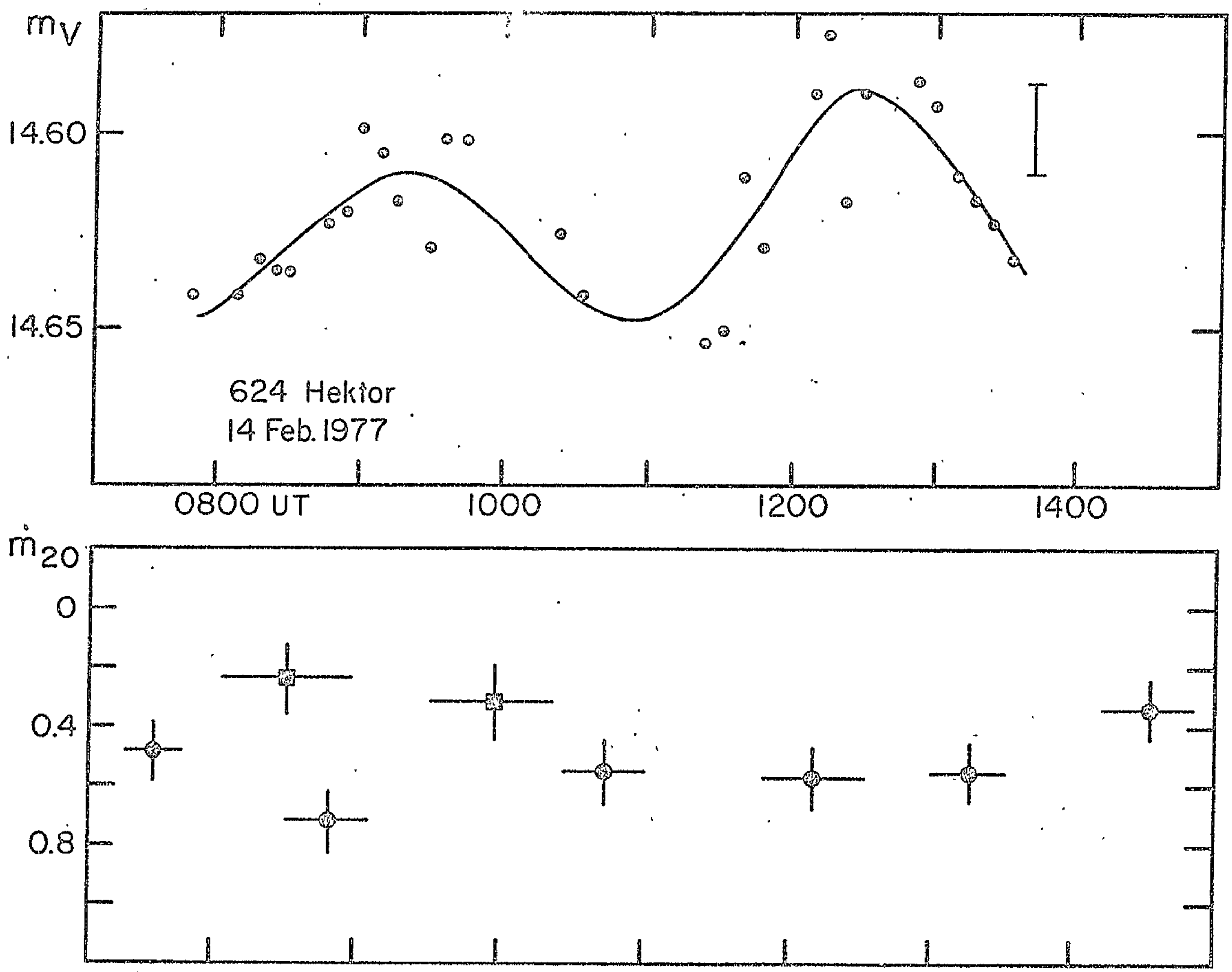

igure 1: Visual and 20μ infrared photometry of asteroid 624 Hektor on 14 Feb. 1977. The asteroid was seen nearly pole-on, minimizing light amplitude. A clear periodicity with 0.06 mag variation was found in the visual. At 20μ, where error bars are greater, the periodicity is not evident.

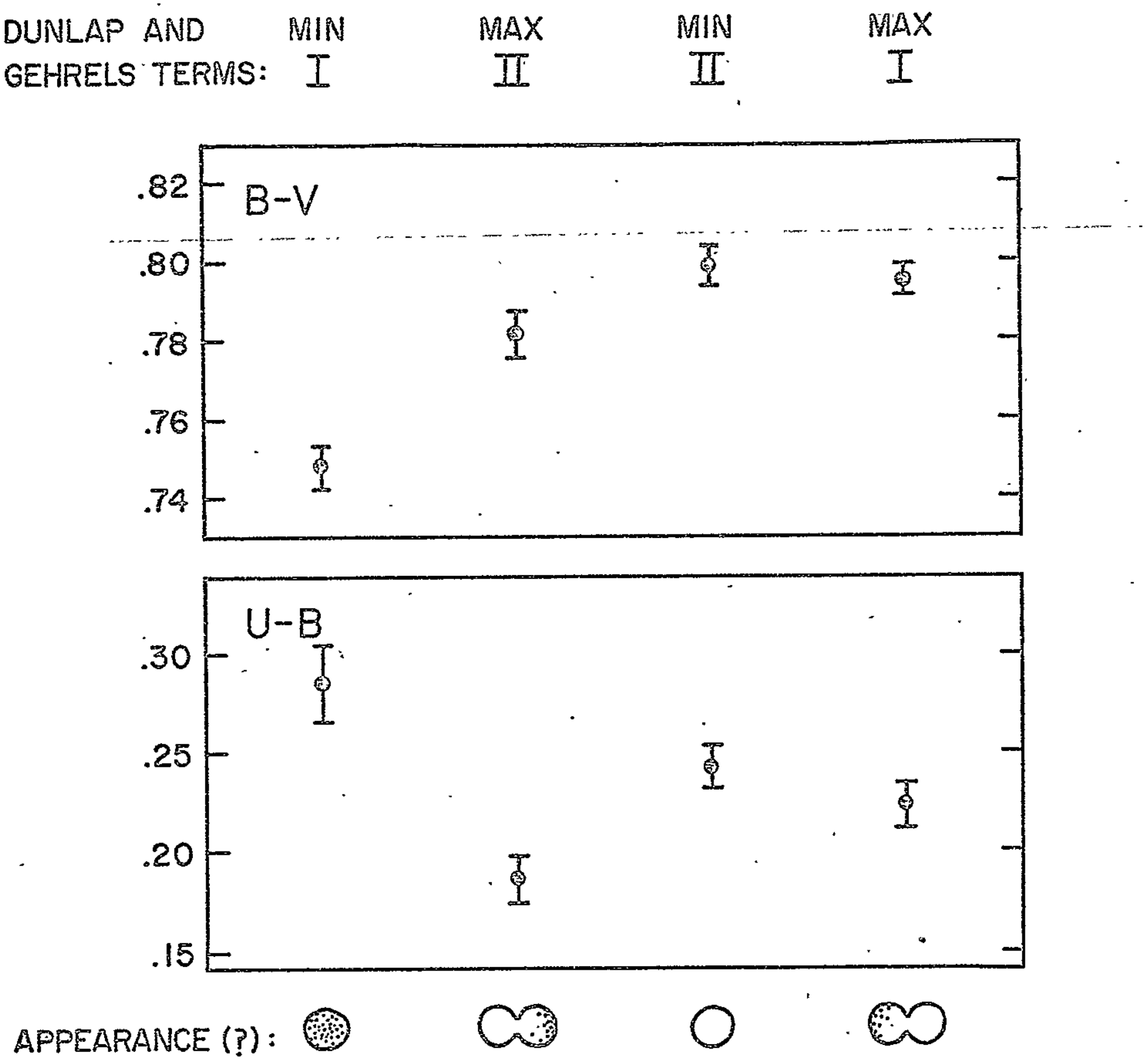

Figure 2: A hypothetical interpretation of Hektor is seen in the sketches at the bottom, where the asteroid is pictured as the result of a collision between two spheroidal bodies with different spectrophotometric properties. In this case, the two end-on views would differ, as is actually seen in the spectrophotometry.

TASK 3: INVESTIGATION OF THE DETERMINATION OF ASTEROID MASSES

(Principal Investigator: Donald R. Davis)

The main objective of this task was to search for close encounters between one of the ten largest asteroids and another of the numbered asteroids that would produce observable perturbations in the smaller asteroid's orbit. Analysis of observation would determine whether or not it would be feasible to measure the mass of the perturbing asteroid. Observations of perturbations in asteroid orbits has led to mass estimates for three asteroids, namely Ceres, Pallas and Vesta (Hertz, H.G., 1968, Science 160, 299; Schubart, J., 1975, Astron. & Astrophys. 39, 147), which are the only ones for which mass determinations are available. However, many other asteroids are now known to be much larger and presumably much more massive than previously believed, and consequently the orbital perturbation technique due to close encounters might be applicable to these objects.

Table II lists the largest asteroids which were the target bodies for close encounters. A search was made for other numbered asteroids which came within 0.1 AU of the target asteroid between 1970 and 1990. This search was performed using a program originally designed for multi-asteroid flyby mission opportunities. The target asteroid was substituted for the spacecraft in our study. Many close encounters were found during the course of the search, for example, 11 encounters involving 31 Euphrosyne and other asteroids were found. However, a close approach alone is not sufficient to produce an observable deflection; the relative velocity must also be sufficiently slow. At the 5 km/sec mean encounter speed of mainbelt asteroids, an extremely close encounter would be required to produce any observable deflection, hence most of the encounters occurred at too high speed to generate any significant orbital perturbation. The deflection angle, Θ, was adopted as a measure of the perturbation, where

$$\Theta = \pi - 2 \tan^{-1} (1 + rv^2/\mu),$$

with r = encounter distance, v = relative speed of encounter and μ = gravitational parameter of target asteroid.

μ was calculated assuming a density of 3 gm/cm^3. Θ is essentially the angle through which the asymptote of the hyperbolic approach trajectory is rotated. Table III summarizes the encounters that result in the largest deflections of the encountering asteroid orbit. The question remains, however, as to the feasibility of mass determination based on these encounters. However, before addressing that question, a discussion of the computations leading to Table III is required. The search program uses the orbits listed in the Minor Planet Ephemeris for

TABLE II - LARGEST ASTEROIDS (1976)

Asteroid	Diameter (km)
1 Ceres	1003
2 Pallas	608
4 Vesta	538
10 Hygiea	450
704 Interamnia	350
31 Euphrosyne	334
511 Davida	323
65 Cybele	309
52 Europa	289
451 Patientia	275
15 Eunomia	272

TABLE III

ENCOUNTERS FROM 1970-1990 RESULTING IN LARGEST DEFLECTIONS OF THE ENCOUNTERING BODY

Target Asteroid	Encountering Asteroid	Date	Closest Approach (AU)	Relative Speed km/s	Re-encounter Period (Years)
1 Ceres	534 Nassovia	12/24/75	.023	2.8	76
1 Ceres	1801 1963UR=52SP	11/19/84	.034	1.0	38
4 Vesta	197 Arete	1/26/76	.035	2.1	18
4 Vesta	126 Velleda	7/10/82	.012	3.8	78
4 Vesta	1044 Teutonia	1/25/79	.052	2.0	30
4 Vesta	1601 Patry	4/15/88	.048	1.2	42
10 Hygiea	64 Angelina	1/21/90	.061	2.0	21
10 Hygiea	1363 Herberta	6/25/82	.10	1.6	43
15 Eunomia	1313 Berna	3/24/69	.06	1.0	550
52 Europa	76 Freia	12/12/82	.01	2.6	44
65 Cybele	609 Fulvia	3/8/70	.09	0.8	37
511 Davida	348 May	10/3/80	.01	2.8	51

1977, augmented for a few asteroids by improved reference orbits from the Minor Planet Center, Cincinnati Observatory. The search program uses these two-body orbits to predict future encounters. This technique neglects orbital perturbation due primarily to Jupiter; the magnitude of the resulting error increases with the interval between the encounter date and the epoch dates of the orbits. To estimate the effect of this resulting error, several orbits were integrated from their epoch date to the encounter date; Table IV compares the fully integrated runs with the conic search results. Clearly planetary perturbations must be included in the final predictions. A project is currently underway at JPL under the direction of Dr. D. Bender to produce integrated asteroid orbits with epochs spaced every few years. When these results are available, refined predictions of encounter opportunities will be found. It is unlikely that many good encounters were missed during the conic search as the encounter distance criteria of 0.1 AU is quite large.

The feasibility of mass determination from the above-discussed encounters was addressed by modeling the orbit determination process using simulated observations. To do this, it is necessary to find the "observable", i.e. what are the perturbations in right ascension and declinations resulting from an encounter? The Vesta-Arete encounter was selected for detailed analysis for this pair is known to produce measurable perturbations; however, it is not an enormously large perturbation.

The encounter perturbations were calculated by numerical integrations in which Vesta was introduced as a perturbing body in addition to the planets Mercury to Neptune. The orbit of Arete was integrated twice; once with zero mass for Vesta and once using a Vesta mass of 1.2×10^{-10} solar masses. Figure 3 shows the resulting perturbation in right ascension, which is the principal observable perturbation for the mass determination process. This figure shows that an observable perturbation does result from this single encounter, but that high quality observations are required to obtain a good mass estimate.

An observation schedule was constructed based on Figure 3 and was the input to a Kalman filter orbit determination program which was modified to solve for the mass of a perturbing body on a known orbit. The Kalman filter technique produces an optimal estimate of the quantities to be determined that is equivalent to a least squares solution when the input measurement errors are uncorrelated and Gaussian distributed. This method has the advantage of considering measurements sequentially, rather than having to repeat the entire solution to ascertain the result of additional measurements. Table V lists the observations used in the mass determination process. Various combinations of bias and noise were added to the measurements along with different values of "a priori" estimates as to what the measurement errors really were. Table VI summarizes results

TABLE IV

EFFECT OF PLANETARY PERTURBATIONS ON CLOSE ENCOUNTERS. FOR EACH ENCOUNTERING PAIR THE UPPER ENTRY IS BASED ON THE CONIC REFERENCE ORBIT WHILE THE LOWER ENTRY INCLUDES PLANETARY PERTURBATIONS ON THE ORBITS.

Encountering Asteroids	Orbit Epoch	Encounter Date	Minimum Separation (AU)	Deflection Angle (")
4 Vesta	12/2/62	11/30/75	.081	0.13
197 Arete	11/23/56	1/26/76	.035	0.28
1 Ceres	12/2/62	12/28/75	.020	1.92
534 Nassovia	12/2/62	12/24/75	.023	1.67
*4 Vesta	12/2/62	5/23/72	.062	.15
1603 Neva	5/5/35	6/16/72	.086	.13
*4 Vesta	12/2/62	1/25/79	.052	.21
1044 Teutonia	12/20/51	2/21/79	.107	.09

*Vesta integration to 8/6/75

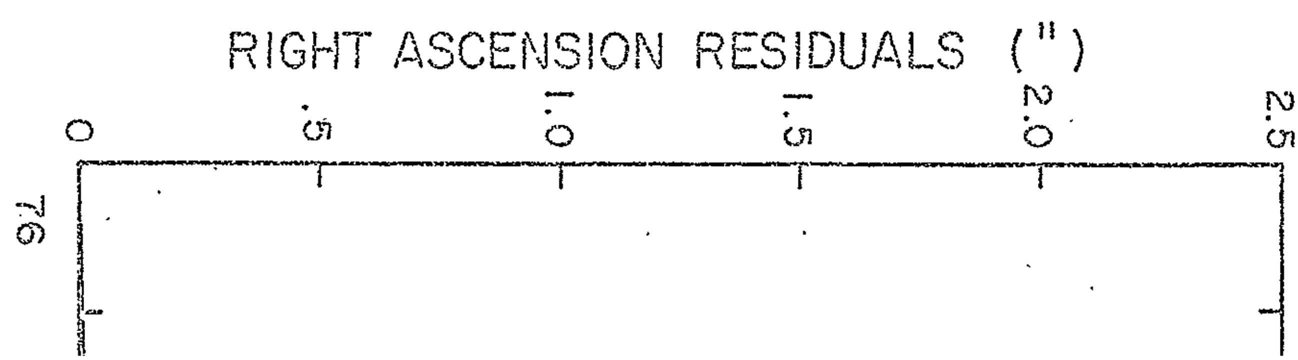

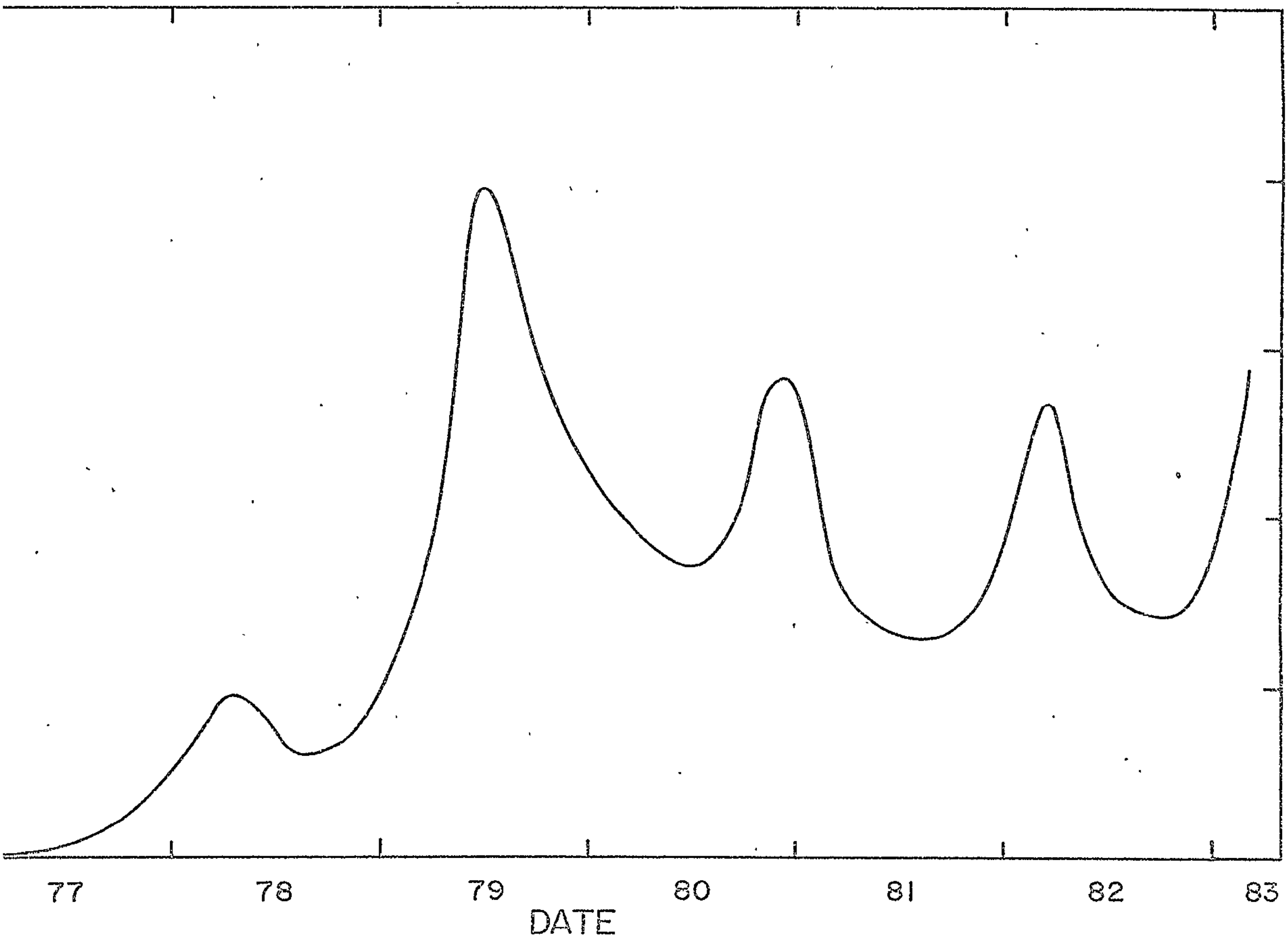
77
78
79
80
81
82
83
DATE

TABLE V

ARETE OBSERVATIONS FOR VESTA MASS DETERMINATION

Date	Julian Day	Right Ascension	Declination
2/26/79	2443930.5	259.51554	-19.627217
4/7/79	2443970.5	269.73373	-20.80407
5/17/79	2444010.5	271.38189	-22.40096
6/16/79	2444040.5	265.76601	-24.23964
7/16/79	2444070.5	259.22205	-25.82428
4/6/83	2445430.5	211.61586	- 0.86297
4/20/84	2445810.5	321.72147	-19.78834
6/19/84	2445870.5	340.66124	-17.90568
8/8/84	2445920.5	342.10084	-22.51729
8/7/84	2445980.5	332.89165	-25.35414

TABLE VI

MASS ESTIMATION OF 4 VESTA FROM ORBITAL PERTURBATION
OF 197 ARETE DURING 1976 ENCOUNTER

Number of Observations	Observation Noise/ Orbit Quality	A priori mass	A priori Standard Deviation	Mass Estimate	Standard Deviation
5	Precise Orbit 1" Bias 1.5" Noise	2^{-10}	2^{-10}	1.6^{-10}	3.5^{-11}
10	Fair Orbit 1" Bias 1.5" Noise	1^{-20}	2^{-10}	-6.7^{-11}	1.8^{-10}
10	Good Orbit 1" Noise	1^{-20}	2^{-10}	8.3^{-11}	1.1^{-10}
10	Precise Orbit 1" Noise	1^{-20}	2^{-10}	1.0^{-10}	4.2^{-11}

from the mass determination program for the Vesta-Arete encounter of 1976. This table shows that mass information can be recovered from a relatively small number of observations even in the absence of any a priori knowledge of the asteroid's mass. However, recovery of this information is dependent upon having a very accurate orbit of the perturbed body prior to the encounter and also upon obtaining high quality observations after the encounter.

A favorable encounter involving 1 Ceres and 534 Nassovia occurred in December 1975. Subsequent perturbations in the orbit of 534 Nassovia are shown in Figure 4 and are considerably larger than those resulting from the Vesta-Arete encounters. Simulated observations of 534 Nassovia were used to estimate the mass of Ceres, the results of which are shown in Table VII. A Ceres mass of 5.9×10^{-10} solar masses was used to generate the observation and the estimated value after 10 observations is 5.2×10^{-10} with a standard deviation of 2.1×10^{-10}. The estimated value differs from the true value by 12%, which is quite consistent with the conservative standard deviation. This case assumed no a priori knowledge of Ceres mass (0.0) and a large uncertainty in the initial estimate (6.0×10^{-10}) while the observation noise was 1". Additional observations would further improve the above estimates particularly in reducing the standard deviation of our estimate.

Several useful results were identified in this phase of the asteroid mass determination project. First, was the prediction of encounters potentially suitable for mass estimation. The Ceres-Nassovia encounter should produce observable perturbations in Nassovia's orbit over the next few years. High quality observations should readily provide an independent determination of Ceres' mass. Second, the "short arc" technique used here, i.e. observations before and after the encounter but over a limited time, can be used to estimate masses and should complement the "long arc" approach previously employed to determine masses. Third, although there probably will be other suitable encounters identified among those listed in Table III, there are not good encounters involving all asteroids, hence this method does not appear to be a general technique that could be applied to systematically explore asteroid masses. Rather it is applicable to specific cases and should provide independent estimates to those previously obtained or mass determinations being made at JPL based on Viking orbiter perturbations.

Additional sources of asteroid orbits were briefly considered, primarily the Palomar-Leiden Survey list of Class I orbits. However, even though the orbits are probably sufficiently good to recover the asteroid, they are generally not precise enough to permit reliable encounter predictions to be made.

FOLDOUT FRAME 1

FOLDOUT FRAME 2

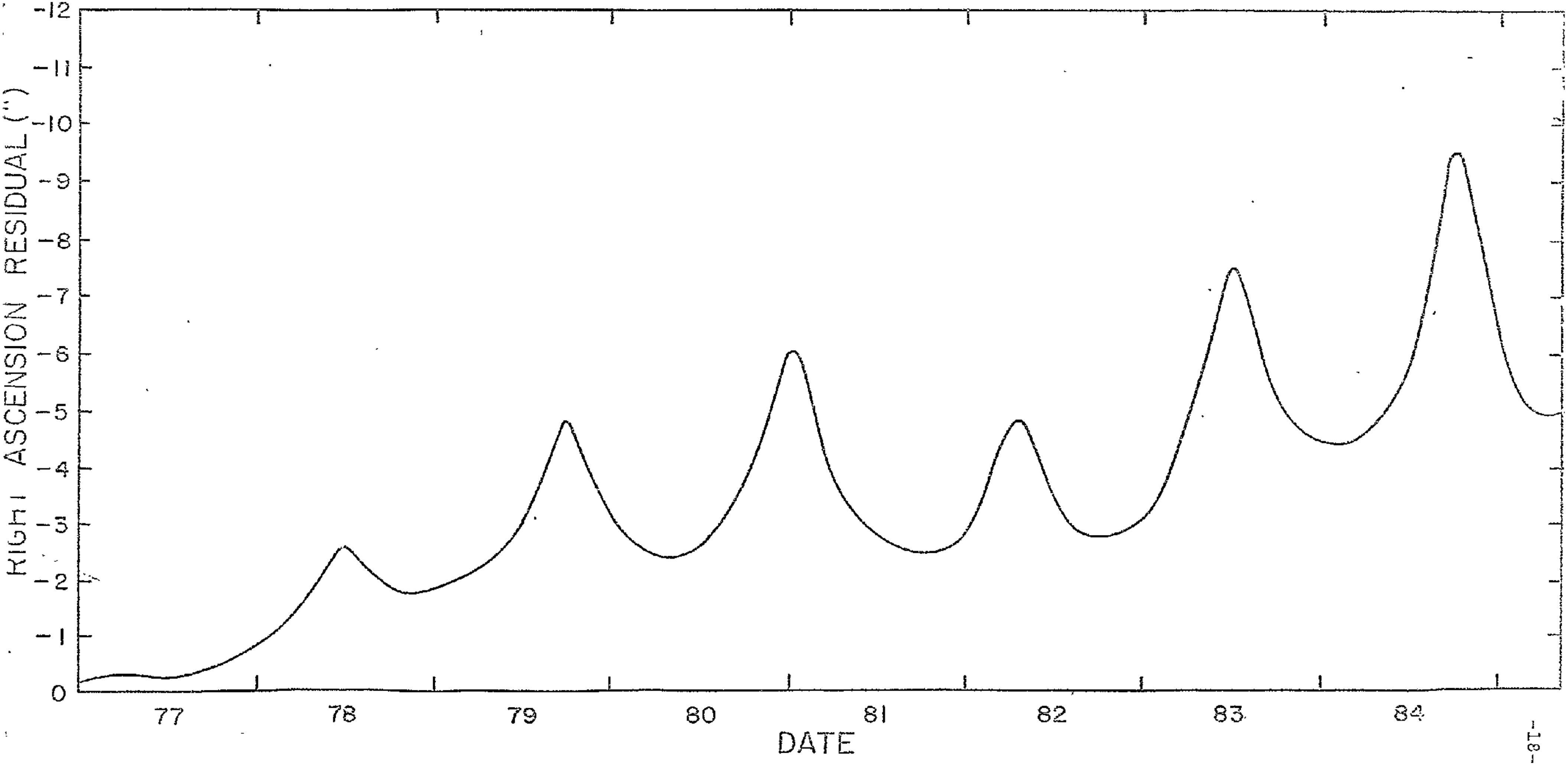

Figure 4

TABLE VII

MASS ESTIMATION OF 1 CERES FROM
ORBITAL PERTURBATIONS OF 534 NASSOVIA

Observation Number	Date	Residuals R.A. (")	Residuals DEC (")	Ceres Mass Estimate (Solar Mass Units)	Standard Deviation
1	5/28/78	2.5	0.4	1.7^{-10}	5.0^{-10}
2	6/17/78	1.8	0.2	1.8^{-10}	5.0^{-10}
3	7/7/78	1.6	0.0	1.8^{-10}	5.0^{-10}
4	9/20/79	7.6	2.2	2.4^{-10}	4.6^{-10}
5	10/10/79	0.1	0.0	2.4^{-10}	4.6^{-10}
6	10/30/79	0.0	0.0	2.4^{-10}	4.6^{-10}
7	12/3/80	2.3	0.2	5.0^{-10}	2.4^{-10}
8	12/23/80	0.2	0.0	5.1^{-10}	2.2^{-10}
9	1/12/81	0.1	0.0	5.1^{-10}	2.2^{-10}
10	2/2/81	0.1	0.0	5.2^{-10}	2.1^{-10}

The attached Exhibit A is the abstract submitted to the Boston meeting of the Division for Planetary Sciences of the American Astronomical Society to be held October 26-30, 1977. This meeting will provide an opportunity to alert observers to the necessity of obtaining observations of 534 Nassovia over the next few years.

Asteroid Mass Determinations: A Search for Further Encounter Opportunities. D. R. DAVIS, Planetary Science Inst., and D. F. BENDER, JPL - Asteroid mass measurements, which are currently available only for Ceres, Pallas and Vesta, have been based on observations of orbit perturbations arising from periodic close encounters between two asteroids (J. Schubart, 1974 Astron. Astrophys. 30, 289; H. G. Hertz, 1968 Science 160, 299). As many asteroids are substantially larger and hence more massive than previously believed, a search was undertaken to determine if there exist additional encounters involving one of the ten largest asteroids and another numbered asteroid. The search covered the interval from 1970 to 1990. The table below summarizes the best encounters found so far for producing observable changes. The magnitude of the perturbations resulting from the encounter was estimated based on an assumed asteroid mass. In order to ascertain observational requirements, a simulated observation schedule was constructed and a differential correction model was used to estimate the asteroid mass for various positional accuracies of the observations.

Asteroid	Encountering Asteroid	Date	Closest Approach (AU)	Re-Encounter Period (years)
1 Ceres	534 Nassovia	9/75	.02	76
1 Ceres	1801 1952 SP	11/84	.03	38
4 Vesta	197 Arete	1/76	.04	18
4 Vesta	686 Gersuind	1/73	.01	28
4 Vesta	1044 Teutonia	1/79	.05	30
4 Vesta	1603 Neva	5/72	.06	18
10 Hygiea	1363 Herberta	6/82	.10	43
65 Cybele	609 Fulvia	3/70	.10	37
52 Europa	76 Freia	12/82	.01	43
511 Davida	348 May	10/80	.01	51
704 Interamnia	993 Moultona	11/73	.01	51

KEY WORDS: (list up to ten)
ASTEROIDS, MASS, ORBIT IMPROVEMENT, PERTURBATIONS

Type of paper (check one)

1) oral presentation [X] 5 min.
[ ] 10 min.

2) read by title only [ ]

3) invited lecture [ ]

4) percent published elsewhere 0

Billing information:
We agree to pay $20 in partial support of the publication of the abstract in the B.A.A.S.

Date: 8/29/77

Planetary Science Institute
Institution to be billed

2030 East Speedway, Suite 201

Tucson, Arizona 85719

Joanne Metcalfe
Signature of Authorized Agent

TASK 4: SATURN'S RINGS: PHOTOMETRY, STRUCTURE, AND DYNAMICS

(Principal Investigator: Michael J. Price)

A. PHOTOMETRY

1. Azimuthal Clumping and Quadrant Asymmetry

Investigations of longitudinal clumping of particles within the ring system were made during the current Planetary Astronomy contract. Observations were hampered by poor observing conditions. Even so, UBV pinhole scans of Saturn's rings, perpendicular to the major axis across the west ansa were obtained on 1977 March 7 and April 7 using the Franz area-scanner mounted on the 72 inch aperture Perkins reflector at Lowell Observatory. Seeing conditions on March 7 were average-to-poor; on April 7, they were quite variable. Each night the rings were monitored continuously for $\sim$2 hours at a fixed position relative to the center of the system.

On March 7, real fluctuations ($\pm$ 3½ percent) in surface brightness of the rings were found on a time scale $\sim$5-10 minutes. Fluctuations were correlated in both B and V colors indicating their reality. On April 7, the photometry was not adequate to determine if brightness fluctuations were present. More observations will be made at the next Saturn apparition during the 1977/8 winter.

Insufficient observing time together with inadequate weather conditions prevented further study of the quadrant asymmetry until the next Saturn apparition during the 1977/8 winter.

2. Phase Effect

Observations to study differences in the phase effects of rings A and B were obtained on five nights during the 1976/7 Saturn observing season. The phase curve was adequately sampled. Scans were made in the three standard UBV colors using the Franz area scanner with a 100μ circular aperture. Data were taken with the 42 inch aperture reflector at Lowell Observatory. To expedite the analysis, information on the point spread function was also obtained using slit-scanning of selected comparison stars. Observing dates, and the corresponding phase angles, are listed in Table VIII.

Analysis of the photometric data to determine the absolute and relative surface brightnesses of rings A and B has not yet been completed at Lowell Observatory. Theoretical interpretation of the anticipated results has been completed at PSI.

TABLE VIII

SATURN'S RINGS: PHASE EFFECT

Date	Phase Angle (Degrees)
1977 February 3	0.2
1977 February 4	0.3
1977 February 13	1.2
1977 February 14	1.4
1977 May 4	6.3

Provided that the phase effect ratio between rings A and B does not vary by more than ∿15 percent, the concept of mutual shadowing within the ring system can safely be abandoned. Results on the study will be published in a paper entitled "On the Phase Effect in Saturn's Rings" which is currently in preparation.

3. Saturn Disk

UBV pinhole scans of the Saturn disk were made using the Franz area-scanner mounted on the 42 inch reflector at Lowell Observatory. Chord scanning of Saturn's disk over a wide range of latitudes was carried out on 1977 April 6 and May 9. Data for April 6 are illustrated in the accompanying Fig. 5. Limb-profiles, spaced parallel to the equator, were obtained over the entire southern hemisphere of the planet. Saturn was found to exhibit strong limb-brightening in the ultra-violet, moderate limb-brightening at the blue wavelengths, and strong limb-brightening in the visual region of the spectrum. Latitudinal variations in the disk profiles were found. In general, the degree of limb-brightening decreases towards the polar region. Pronounced asymmetry is apparent in the disk profiles in each color. The sunward limb is significantly brighter than the opposite limb. This asymmetry depends on phase angle; approaching zero at opposition, it reaches a maximum near quadrature.

The observations have been interpreted using an elementary radiative transfer model. The Saturn atmosphere was approximated by a finite homogeneous layer of isotropically scattering particles overlying a Lambert scattering cloud layer. The reflectivity of the clouds is a strongly dependent function of wavelength. The best-fitting model consists of a clear H_2 layer of column density ∿31 km·amagat above the clouds; the maximum permitted H_2 column density was ∿46 km·amagat. The phase-dependent asymmetry in the disk profiles is a natural consequence of the scattering geometry. The results are consistent with current knowledge of the Saturn atmosphere. The observations, and their analysis, will be published in a paper entitled "Saturn: UBV Photoelectric Pinhole Scans of the Disk" which is currently in preparation. The abstract of a paper to be presented at the Ninth AAS/DPS Meeting in Boston is contained in Appendix C.

PINHOLE SCANS OF SATURN DISK
SOUTHERN HEMISPHERE
1977, APRIL 6 - 4^h10^m to 4^h50^m U.T.

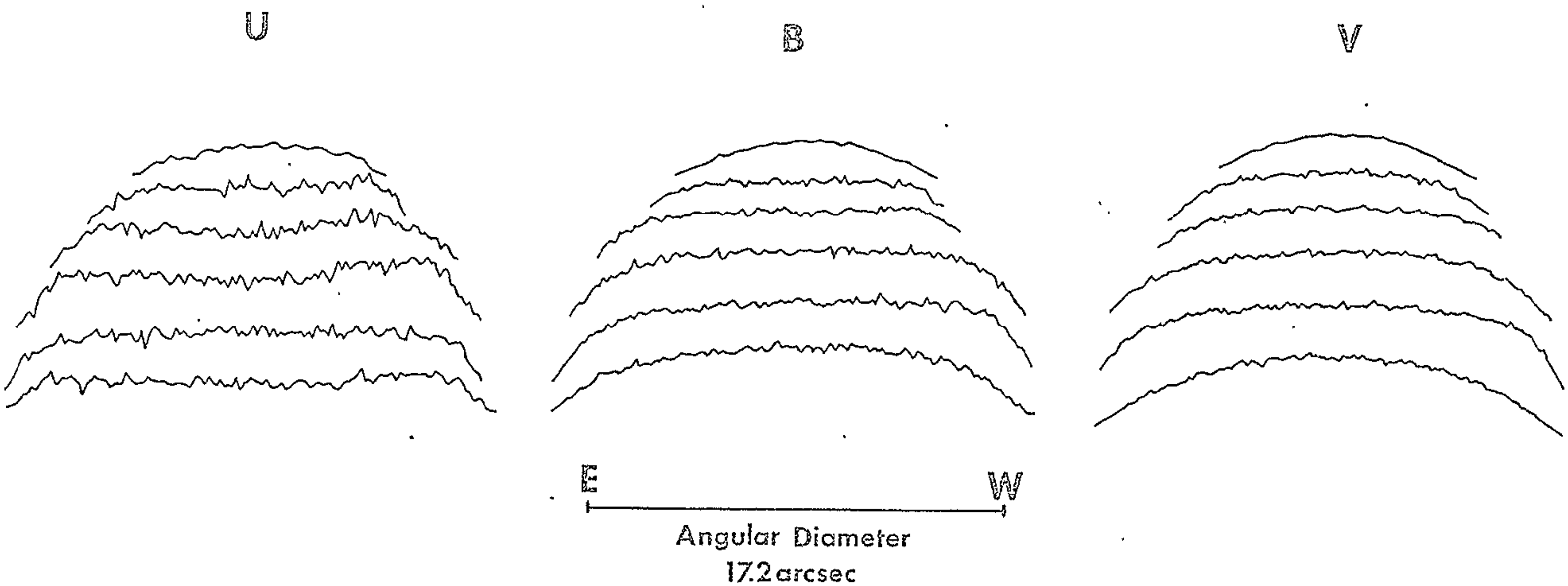

Figure 5

B. DYNAMICS

The longitudinal brightness variations observed in Saturn's ring (Franz and Price, unpublished observations) may result from a size distribution among the ring particles or it may arise from a physical clustering of ring particles. If this phenomena does reflect the real particle distribution in longitude, then what causes this azimuthal variation? To address this problem, a model was developed to examine the effect of longitude dependent harmonics in Saturn's gravity field on ring particles. The effects of such terms has been widely studied for Earth-orbiting satellites (Blitzer, L., 1966, JGR 71, 3557; Blitzer, L., Davis, D. and DeSulima, T., 1968, AIAA 6, 1199) and these results may be applied to Saturn.

The lowest order longitude dependent (tesseral) harmonic is the one arising from an equatorial ellipticity, the J_{22} term. The effect of this term on synchronous orbits of small eccentricity and inclination is to produce four equilibrium positions separated 90° in longitude. Two points are stable, namely those along extensions of the minor axis of the elliptical-shaped equator, while the other two are unstable. An orbit in the vicinity of a stable point exhibits large amplitude, long period oscillations about the stable point when viewed in a coordinate system rotating with the planet. The amplitude and period of the libration, which is predominately in longitude, is determined by the initial conditions and can be as large as 90°. However, if the initial location is too far from the stable points, the particle circulates rather than librates. The libration zone is quite narrow in the radial direction with the maximum width of the zone varying with J_{22}.

To ascertain the importance of these gravitational harmonic resonances, the location of resonances relative to the ring system must be known. Table IX gives the location of synchronous orbits about Saturn, which is the region where J_{22} resonance effects would be important together with pertinent ring parameters. Figure 5 shows the resonance location on a brightness profile of Saturn's ring system with the indicated resonance zone width determined by the difference between the equatorial and temperate rotation periods. If the actual rotation period for the mass distribution producing the J_{22} harmonic was known, then the actual synchronous orbit distance could be determined. It is interesting to note that the synchronous orbit distance is quite close to the region of peak brightness of the ring system.

Because the lowest order resonance, the J_{22} resonance, may be relevant to the structure of the ring system, a simple

TABLE IX

SYNCHRONOUS ORBIT DISTANCES FROM SATURN

Orbital Period	Distance from Saturn Using Keplerian Orbits (10^5 km)	Distance from Saturn including J_2 and J_4 correction (10^5 km)
10^h14^m = Equatorial Period	1.092	1.095
10^h38^m = Temperate Zone Period	1.121	1.124
Inner Edge of A Ring	∿1.20	---
Outer Edge of B Ring	∿1.16	---

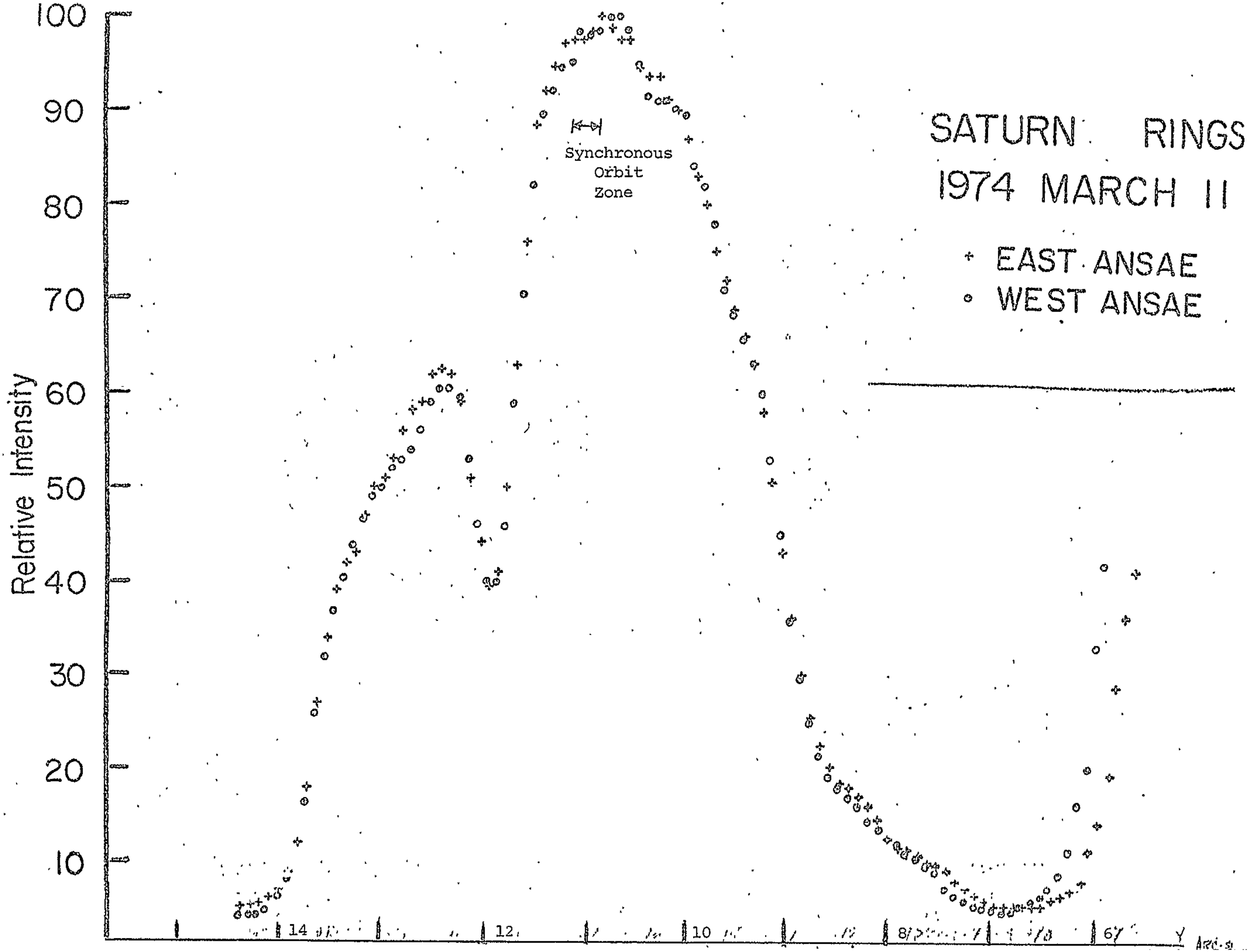
SATURN RINGS
1974 MARCH 11
+ EAST ANSAE
o WEST ANSAE
Synchronous
Orbit
Zone
Relative Intensity
100
90
80
70
60
50
40
30
20
10
14
12
10
8
6

model was constructed to see if resonance trapping of ring particles would produce a variation in the spatial density and if so , what would be the characteristics of the variation. The system of particles was taken to be moving initially in circular Keplerian orbits with a constant area density of uniform particles. The J_{22} perturbation was introduced and the size of the libration regions found. The initial conditions determine whether particles at particular locations within the ring librate or circulate. Within the libration zone the distribution of particles in longitude was found by first calculating the period and maximum amplitude of the libration orbit based on the initial conditions. The libration zone was divided into longitude increments $\Delta\lambda$, and the fraction of the period that particles spend in each zone $\Delta\lambda$ was found from the libration orbit. By summing over all libration orbits and weighting each orbit by the number of particles moving on it, a longitude distribution of particles in the libration zone was constructed.

In order to estimate the brightness variation in the ring it was assumed that outside the libration zone the distribution was uniform. Insofar as only the J_{22} perturbation is treated, this approximation is valid far away from the resonance; however, it does neglect the transition region where particles are circulating but might have a nonuniform spatial distribution. This effect should be incorporated if more sophisticated models are ever required.

The longitude brightness variation was then found by assuming that brightness is proportional to the particle density. The magnitude of the effect is proportional to the radial extent of the libration zone which is determined by the J_{22} coefficient and is given as

$$\Delta_{max} = 4 \sqrt{J_{22}}\ R_e ,$$

where Δ_{max} is the maximum radial deviation from the exact synchronous orbit distance, and R_e is the planet's equatorial radius.

Table X gives the maximum zone size for three levels of J_{22}. Table XI gives the particle density in the libration zone relative to the initial uniform distribution, where each longitude zone contains the area weighted average of librating and circulating particles. Finally, Table XII gives the longitude brightness variation in ring B for the two levels of J_{22}. In terms of the model developed here, J_{22} would have to be greater than $\sim 2 \times 10^{-5}$ for the effect to be observable, with a 2% brightness variation.

TABLE X

SIZE OF LIBRATION ZONES

J_{22}	Δ_{max} (km)	Ratio of Δ_{max} to B ring width
10^{-6}	240	.01
10^{-5}	760	.03
10^{-4}	2400	.10

TABLE XI

RELATIVE PARTICLE DENSITIES

INSIDE LIBRATION ZONES

Longitude Interval From Stable Longitude	Relative Density
0-10	1.41
10-20	1.38
20-30	1.32
30-40	1.17
40-50	1.17
50-60	1.02
60-70	.91
70-80	.91
80-90	1.0

TABLE XII

LONGITUDE BRIGHTNESS VARIATION OF RING B

Longitude Interval From Stable Longitude	Relative Brightness J_{22} 10^{-4}	10^{-5}
0-10	1.04	1.013
10-20	1.04	1.012
20-30	1.03	1.010
30-40	1.02	1.005
40-50	1.02	1.005
50-60	1.002	1.001
60-70	.99	.997
70-80	.99	.997
80-90	1.0	1.0

Although quantitative predictions cannot be made as J_{22} for Saturn is unknown, this model does lead to features that could be investigated observationally. First, the longitude variations should occur only in the outer part of ring B. In particular, the A ring would not be expected to show the longitude variation. Second, the time required to go from maximum to minimum brightness should be approximately one quarter of the rotational period of Saturn or about 2.5 hours. However, given the nature of the calculated profiles most of the brightness change occurs over a small longitude region from 15° - 55° and should occur on a time-scale of the order of an hour.

This model may be only part of the answer as to the nature of the longitude brightness variation in Saturn, but if any of the predicted characteristics could be observed, this technique provides a method for determining the gravitational coefficient J_{22} for Saturn which would have possible interesting implications for the interior structure of Saturn and perhaps other giant planets.

C. STRUCTURE

A portion of our study of ring systems was to gather observational data on the probable shapes of particles in ring systems governed by collisions. Our earlier study (Greenberg, Davis, Hartmann and Chapman, 1977, Icarus 30, 769) showed that collisions at low speeds are possible in the Saturn rings, and that fragmentation may have governed the evolution of the ring particles. Our initial hypothesis was that aligned particles of non-spherical shape might play a role in explaining the observed brightness asymmetries in Saturn's rings. Therefore, Dr. Hartmann has made a series of shape measurements of all particles generated in his experiments at Ames Research Center on fragmentation of basalt spheres and irregular igneous rocks. These bodies were fragmented at velocities of 26.0 to 50.4 m/sec.

If particles were aligned, the extreme light variations that would be observed would depend on the ratio of minimum to maximum cross section, or BC/AC, where A, B, and C are principal diameters. This reduces to an extreme light variation of B/A. Measurements of 46 particles showed a median ratio of 0.69 and a similar mean of 0.71, illustrated in Figure 6 . An interesting trend is shown in Figure 7 , which indicates that the largest fragments (defined as maximizing mass of fragment/mass of initial body) tended to be more spherical than the smallest fragments. Extreme light ratios of less than 0.4 were found among the smallest fragments, but no large fragments had extreme light ratios less than about

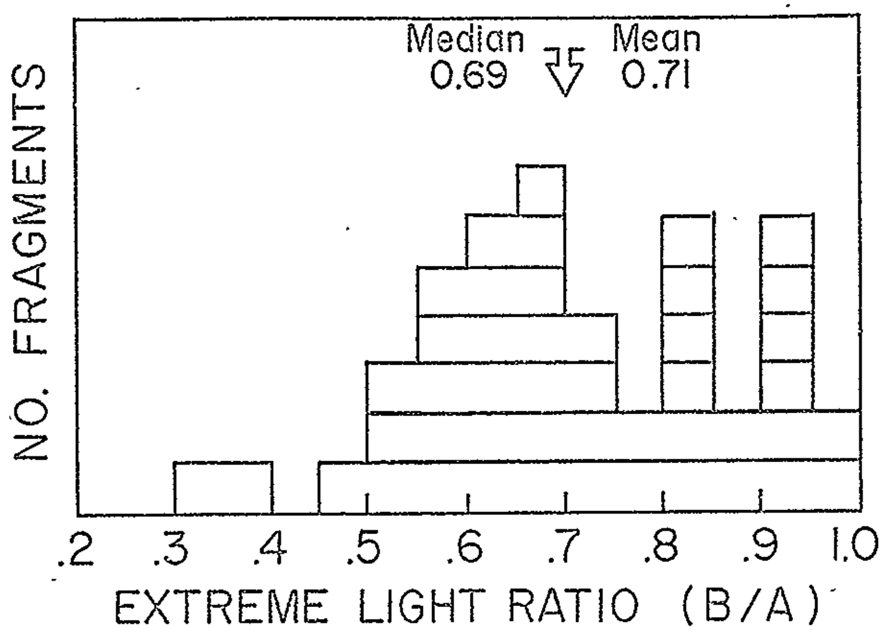

Figure 6: Histogram of frequencies of fragments of different shapes. Abscissa shows maximum light ratio that could be observed if particle were rotating around its principle axis. Alignment of particles by tidal or other forces could affect photometry of ring system.

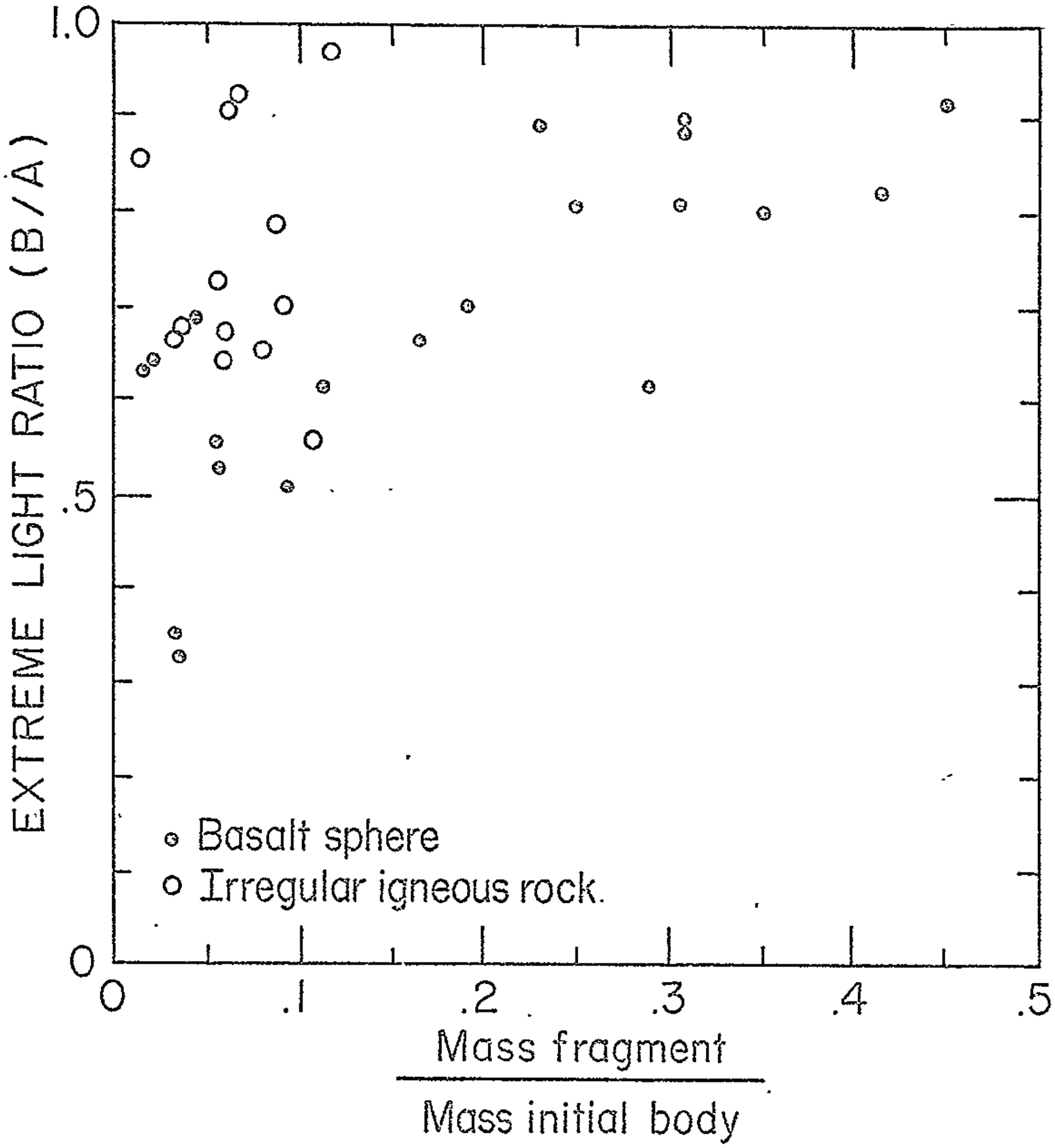

Figure 7: Relation of shape (light ratio) and fragment size (scaled to size of parent object). Data suggest that the smallest fragments have the greatest range of shapes and the largest fragments are the most nearly spherical.

0.8. We have not carried out further application of these data to models of photometric variations or asymmetries in Saturn's rings, partly because other models, such as density wave theories, have been proposed to explain the quadrant asymmetries, and partly because of the more fruitful theoretical investigation of effects to explain the light variations observed by Drs. Price and Franz.

We have also noted that scattering theories of radiation transfer in the rings have tended to assume spherical particles, and that elongated particles, particularly in the presence of any mechanisn of preferential alignment, could modify the scattering theory as well as the more straightforward models of direct reflection. However, our data on shapes of macroscopic (mm-cm dimension) fragments do not establish shapes of wavelength-scale scatterers. Further investigation of this problem might be useful.

TASK 5: URANUS: AEROSOL DISTRIBUTION IN THE ATMOSPHERE

(Principal Investigator: Michael J. Price)

Studies of the phenomenon of limb-brightening on Uranus resulted in the production of several related papers during the course of the current Planetary Astronomy contract. In a Letter, Franz and Price (1977, Astrophys. J. 214, L145) reported pinhole photoelectric area-scanning photometry of the Uranus disk which demonstrated directly the existence of both limb and polar brightening in the 7300Å CH_4 band. Polar brightening, which appeared to be present also at continuum wavelengths, was interpreted as being caused by scattering in a thin aerosol haze located over the polar regions. A reprint is contained in Appendix D.

Full details of the 1976/7 observational program are reported in a paper entitled "Limb-Brightening on Uranus: The Visible Spectrum. II", recently submitted for publication in Icarus. A preprint is contained in Appendix E. New narrow-band (100Å) photoelectric area-scanning photometry of the Uranus disk is reported. Observations were concentrated on the two strong CH_4 bands at 6190Å and at λ7300Å. Adjacent continuum regions at λ6400Å and at λ7500Å were also measured for comparison. Both slit and pinhole scans were made in orthogonal directions. Disk structure in each waveband is apparent through lack of circular symmetry in the intensity distribution over the Uranus image. Polar brightening is especially prominent in the λ7500Å waveband.

Coarse quantitative determinations of the true intensity distribution over the Uranus disk were made. For the λ6190Å CH_4 band, Uranus exhibits a disk of essentially uniform intensity except for a hint of polar brightening. For the λ7300Å CH_4 band, moderate limb-brightening is apparent. Specifically, the true intensities at the center and limb of the planetary disk are approximately in the proportion 1:2. Extreme limb-brightening, with a corresponding intensity ratio greater than 1:4, is not permitted by the observational data.

Theoretical analysis of the limb profile of Uranus in the λ7300Å CH_4 band has been completed. The results are contained in a paper, currently in preparation, entitled "Limb-Brightening on Uranus: An Interpretation of the λ7300Å Methane Band." Our earlier observational results have been interpreted on the basis of a simple radiative transfer model containing an elementary vertical inhomogeneity. The Uranus atmosphere is approximated by a finite upper layer of conservatively scattering particles below which lies a semi-infinite honogeneous H_2-CH_4 gas. Isotropic scattering is assumed. The measured degree of limb-brightening is consistent with an upper layer of optical thickness ~ 0.1 together with a CH_4/H_2 mixing ratio $\sim 2 \times 10^{-3}$ in the lower atmosphere. CH_4 appears to be overabundant by a factor ~ 3 compared with the solar value. Our conclusions are discussed in the context of recent models of the Uranus atmosphere by Danielson (1977, Icarus 30, 462) and by Trafton (1976, Astrophys. J. 207, 1007). The abstract of a paper to be presented at the Ninth AAS/DPS Meeting in Boston is contained in Appendix F.

APPENDIX A

THE EVOLUTION OF ASTEROIDS AND METEORITE PARENT-BODIES (Invited Review)

Clark R. Chapman, Planetary Science Institute,
2030 E. Speedway, Suite 201, Tucson, AZ 85719

As distinct from other planetary scientists, meteoriticists are studying planets unknown. Rocks fall from the sky, they are measured, and inferences are made concerning conditions on other planets -- but <u>what</u> planets? Evidently they are asteroids or comets, for if rocks don't reach Earth from the moon, they certainly don't come from much more distant and much larger planets. And all other bodies are defined to be asteroids and comets. If dead, devolatilized comets are also called "asteroids", then virtually all meteorites come from asteroids.

There are other ways of learning about asteroids than by drawing inferences from stones that fall from the skies. They are the techniques of astronomy. While these techniques are often more limited than meteoritical techniques, they provide kinds of information about asteroids that are impossible to infer from meteorites (e.g. orbital characteristics and physical shapes) or can be inferred from meteorites only through elaborate models (e.g. parent-body sizes). All meteoritical and astronomical data would be much more useful, of course, if we could identify individual asteroids (or at least groups of asteroids) as the parents of individual meteorites (or at least classes of meteorites). Here again, the astronomical techniques --

despite their limitations -- hold promise of providing the required links.

Much astronomical data has been gathered about asteroids during the past decade. We know the colors, albedos, diameters, shapes, spin periods, and orbital family relationships for hundreds of bodies. Progress has been made in understanding the orbital dynamical evolution of asteroids and their collisional interactions. Models for the evolution of meteorite parent-bodies may now be compared with expectations, for instance, of asteroid collision rates based on our knowledge of the frequency of asteroids of different compositional classes and of their collisional cross-sections.

Results of these observational and theoretical programs provide a general picture of consistency: substantial parent-bodies for most meteorite types appear to exist in the main asteroid belt or among the Apollo and Amor asteroids, to the degree we can confidently interpret asteroid spectra in terms of major mineralogies and ascribe such assemblages to different meteorite types. Collisional and dynamical evolution of the asteroids can indeed yield the observed numbers of meteorites on Earth. Inferences about the early accretion and subsequent collisional evolution of asteroids that are consistent with the physical and orbital properties of present-day asteroids are also consistent with many of the inferences that have been based on meteoritical and cosmochemical research; for instance, regolith environments have existed in the past, and may still exist on some asteroids, to provide for the creation of brecciated and gas-rich meteorites.

But there are also certain important inconsistencies emerging from the synthesis of astronomical and meteoritical data, and fascinating new questions emerge. For example, while we can readily identify the Earth-approaching asteroids as the parent-bodies for many ordinary chondritic meteorites, it is increasingly unlikely that sizable parent-bodies for either these short-lived asteroids or chondritic meteorites will be found in the main asteroid belt. What are the cosmochemical implications if we must identify the ordinary chondritic parent-bodies as cometary cores? Alternatively, it may be necessary to identify the so-called S-type main-belt asteroids as ordinary chondrites, but that would require that an as-yet-not-understood process is modifying the infrared spectra of those asteroids.

Other interesting problems concern Vesta: It seems to be the only large candidate parent-body for the eucrites, howardites, and diogenites. Yet as Wetherill has said, it is hard to understand how eucritic basaltic surface flows, formed near the beginning of solar system history, can have been preserved on Vesta for all this time, given the very high collision rates to which all asteroids have been subjected over the intervening duration. And we still do not understand how to deliver fragments of Vesta to the Earth in sufficient quantities to account for the observed numbers of basaltic achondrites.

Still other questions concern such diverse bodies as Ceres and the Martian satellite Phobos. Both bodies are inferred to be of carbonaceous chondritic composition, on the basis of their albedos, spectra, and bulk densities. How can such a large body as Ceres have failed to melt if a neighboring, smaller body like Vesta did melt? How can a carbonaceous body be in Martian orbit, well inside the zone where carbonaceous material is believed to have accreted (the outer part of the asteroid belt and beyond)? Personally, I believe that it is not yet proven that Ceres and Phobos are carbonaceous.

The major result of asteroid research of the 1970's, I believe, is the recognition that asteroid collisions have probably been much more frequent than was believed; this recognition has emerged from observational studies of asteroid albedos and sizes combined with improved collisional modelling. Collisions, both erosive and catastrophically destructive, have been very important through the last 4 aeons, quite apart from the possibly even higher collision frequencies in still earlier times. Most asteroids, even quite large ones, must be regarded as fragments. Original surface layers of asteroids must have been destroyed to depths of many tens of kilometers. There are many implications for meteoritics, including questions of accessibility of phases formed deep in differentiated parent-bodies, modification of chronological systematics, and the extent of regolith environments in parent-bodies.

APPENDIX B

THE ASTEROIDS

Clark R. Chapman

Planetary Science Institute
Tucson, Arizona 85719

James G. Williams

Jet Propulsion Laboratory
Pasadena, California 91103

and

William K. Hartmann

Planetary Science Institute
Tucson, Arizona 85719

Running Head: Same as above

Address and telephone number of author
to whom proofs are to be sent:

Dr. Clark R. Chapman
Planetary Science Institute
2030 East Speedway, Suite 201
Tucson, Arizona 85719

(602) 881-0332

Submitted to: Annual Review of Astronomy and Astrophysics

Slightly Revised: October 20, 1977

CONTENTS

I. INTRODUCTION

The asteroids are small rocky bodies that orbit in modestly eccentric and inclined orbits, mainly between the orbits of Mars and Jupiter. With the comets, they are the only known population of residual planetesimals from the earliest epochs of solar system history. Despite their collisional evolution, their thermal and geological evolution apparently has been modest compared with that for main planets and their orbital evolution has been modest compared with that of comets. Thus they, along with their fragments among the meteorites, hold special clues for us about the early development of the solar system. Their dynamical and collisional evolution continues to contribute to the major geological events (impact cratering) on the less geologically active planets, such as the moon and Mercury.

The modern era of asteroid studies commenced with the 12th IAU Colloquium, held in Tucson, Arizona, in 1971 ("Physical Studies of Minor Planets"; cf the proceedings, edited by Gehrels 1971). Since then, progress in understanding asteroids has been exceedingly rapid, spurred especially by several astronomical observing programs that started about 1970. Especially noteworthy are the determinations of asteroid sizes and mineralogical compositions and theoretical understanding of asteroid dynamical and collisional evolution. These have begun to yield a fruitful synthesis with studies of meteorites, classes of which are now thought to derive from asteroids.

We regret that space limitations prohibit us from referencing most of the cogent literature of the past decade; we are restricted to especially significant or recent papers and those that review subfields of asteroid science. Further, we regret that we cannot tabulate recent physical and orbital data for more than a handful of bodies. Reference is made to the computerized TRIAD file of asteroid data (Bender et al 1978) and recent published compilations by contributors to that file.

II. OBSERVATIONAL CHARACTERISTICS

A. Photometry

Photometry is the only technique pertinent to physical properties of asteroids (chiefly size and albedo) that was regularly applied until the last few years. Detailed photometric programs yield lightcurves (Sect. II B) and phase angle variations (see review by Gehrels 1970). The B magnitude of an asteroid, on the standard UBV system, varies (1) inversely as the square of the (known) distances from both Sun and Earth; (2) directly with the geometric albedo and with the reflecting cross-section (neither of which is known independent of the other and both of which vary with spin and with viewing aspect); and (3) in an unknown manner with respect to scattering geometry (the unknown dependences with incidence and reflection angles for each surface element are integrated into an effective phase relation for the whole face of the object).

The adopted fundamental brightness parameter for asteroids is the <u>absolute magnitude</u> B(1,0): the B magnitude "at 0° phase angle" reduced to 1 AU distances from Earth and Sun. The latest tabulation, based on photoelectric data supplemented by photographic photometry, is by Gehrels & Gehrels (1977) and is included in TRIAD. Phase variations have been measured for few asteroids, so tabulated magnitudes are extrapolated from observed phases to 0° phase by a single relationship for all asteroids that artificially excludes the opposition effect (brightness surge at $\sim 7^{\circ}$ phase); beyond 10°, the adopted correction is 0.023 mag /deg (see Gehrels & Gehrels 1977 for details). Although the adopted correction for opposition effect is based on data for the anomalous asteroid 20 Massalia, the effect is probably due to surface texture and is similar for all measured asteroids (Gehrels & Taylor 1977). But phase corrections vary among asteroids and probably depend on both regolith texture and surface composition, which may depend on asteroid size. Since Gehrels' correction is based on diverse photographic magnitudes for a modest non-bias-corrected sample of asteroids, it may not be representative and could even lead to systematic diameter-dependent errors. Indeed faint Palomar-Leiden Survey asteroids (van Houten et al 1970) vary with 0.039 mag/deg and Bowell (1977) reports different phase variations for C and S asteroids (composition types, Sect. II E). To avoid confusion, Gehrels' corrections have been adopted for cautious use until more phase dependences are studied. In the meantime, one may expect large errors in some tabulated magnitudes such as the case of Ceres (Taylor et al 1976), for which a change of 0.3 mag was found due to an anomalous phase factor.

B. Rotations

Asteroid magnitudes vary periodically as they spin, mostly due to changes in cross-section for nonspherical bodies but partly due to albedo variations and scattering anomalies. Amplitudes are typically 0.1 to 0.3 mag but can exceed 1 mag. Early unreliable photographic photometry was replaced in the 1950's and 60's by photoelectric photometry (the methodology is described and results summarized by Taylor 1971). In the 1970's useful results are being achieved not only by photoelectric photometry but also by photographic and even visual photometry (results for 1975 and 1976 are referenced by Schober 1977). Lagerkvisk (1975) and Degewij & Gehrels (1976) have attempted photographic photometry of faint, small asteroids; the latter is a statistical analysis of very faint uncataloged objects. E. Tedesco is maintaining the TRIAD file on lightcurves.

Lightcurves dominated by shape exhibit two maxima and two minima per period for obvious geometrical reasons. Variability due solely to albedo features can yield any number of maxima per period, but most commonly one. Ambiguity concerning period is uncommon, but Vesta is now believed to rotate in $10^{h}.68$ rather than the earlier value of $5^{h}.34$. A few asteroid lightcurve amplitudes are too small to reveal rotation periods and a few others spin too slowly to be conveniently measured (the longest reported period so far is $\sim 32^{h}$ for 654 Zelinda).

Odd-order terms in the Fourier analysis of a lightcurve tend to imply "spottedness" due to albedo or scattering effects and even-order terms imply nonspherical shape (cf Lacis & Fix 1971). The effect of odd-order terms on the amplitude is typically 0.04 mag or less, suggesting a high degree of compositional uniformity on measured asteroids (found also by constancy with spin of color and of polarimetric properties).

Lightcurves provide data on asteroid shapes and spin-vectors. Maximum amplitudes are observed when the rotation axis is perpendicular to the line of sight, assuming an asteroid has had time to dissipate energy and spin about its dynamically stable minimum axis, as seems generally likely (McAdoo & Burns 1974). Over the course of several months or years, an asteroid may be measured from several aspect angles with respect to its spin axis (which may be assumed not precessing, except for especially small objects that may have suffered a recent collision). Such data provide information on ecliptic latitude and longitude of the spin axis (a recent example is given by Sather 1976), but Dunlap (1971) has shown that the technique requires pre-knowledge of the asteroid shape. The technique of "photometric astrometry" (cf Taylor 1971) depends on light-curve timings at different epochs and in principle yields the spin vector, including the sense of direction. (Thermal radiometry is also sensitive to prograde vs retrograde rotation: Morrison 1977.) In general the quantity of photometric data available on individual asteroids has been sufficient to determine only weakly (at best) the numerous unknowns: shape, spottedness, and spin vector. Earlier conclusions that asteroid spin axes have large tilts must be reevaluated, although the large Trojan, 624 Hektor, does have a rotation pole near the ecliptic. The only secure parameter measured from light-curves for a significant sample of asteroids is rotation period (tabulated for about 160 objects), and even that may be subject to occasional misinterpretation.

C. Diameters and Albedos

Because asteroids are small and far away, their diameters once were obtained from absolute magnitudes (Sect. II A) by <u>assuming</u> a geometric albedo (typically 0.1 to 0.2). Such diameters (e.g. as tabulated by Pilcher & Meeus 1973) are systematically too small and have relative errors exceeding a factor of 3, since asteroid albedos are now known to range from ∿0.025 to ∿0.35.

DIRECT MEASUREMENTS Direct measurements of the diameters of the first four asteroids were attempted using filar and double-image micrometers and interferometers (reviewed by Dollfus 1971). Little confidence can be placed in these results since (a) asteroid sizes are comparable to diffraction disks, (b) systematic errors are not easily evaluated, (c) results were inconsistent (especially for Pallas), and (d) similar direct measurements of larger objects, such as Neptune and the Galilean satellites, were moderately erroneous. Recently, the new technique of speckle interferometry has been applied to Vesta (Worden et al 1977), yielding a diameter within 5% of values determined by radiometry and polarimetry (see below).

OCCULTATIONS Precise diameters and shapes for asteroids may be obtained from photometry of occultations of stars by asteroids. These events are common (several occur per night somewhere on Earth involving asteroids brighter than 12.5 mag and stars $\lesssim$2 mag fainter). But predictions cannot normally be made for the usually faint, uncataloged stars. 'Predictable' events occur about once a year, but are difficult to observe since the paths are narrow (the diameter of the asteroid) and uncertainties in asteroid and star positions result in errors in the location of the path approaching 1000 km. Despite several coordinated attempts during the past decade, photoelectric observations have never been obtained for more than a single chord of an asteroid, which provides only a lower limit on diameter. Visual timings of events lasting a few seconds have yielded diameters for 6 Hebe (Taylor & Dunham 1977) and 433 Eros (O'Leary et al 1976) that agree with results from radiometry and polarimetry, but are too imprecise to calibrate those less direct techniques.

Occultations of asteroids by the dark limb of the moon are easily predictable and observable from wide areas on Earth but, due to rapid lunar motion, photometry with timing resolution better than 0.01 sec is required. Uncertainties in asteroid shape, limb-darkening, and albedo features, combined with rough topography on the lunar horizon, complicate interpretation of photometric traces. The technique has yet to be successfully applied to an asteroid.

RADIOMETRIC METHOD Current knowledge of asteroid diameters comes from two indirect methods. The first is based on a comparison of visible and mid-IR magnitudes (Allen 1970). For asteroids of the same size at the same distance, one of a lower albedo will be fainter in the visible but, at the same time, hotter and hence will radiate more at 10 or 20 μm. Quantitative application of the technique requires knowledge of the emissivity and thermal inertia of the surface, the rotation period, and the angular dependence of the reflected and radiated radiation. Radiometry over a range of Sun-asteroid-Earth geometries can help specify some parameters. Thermal modelling assumptions are discussed most recently by Morrison (1977) and Hansen (1977). Derived diameters are insensitive to modelling assumptions for very dark objects of rock-like composition with low thermal inertias. Present models may introduce systematic errors up to 20% in inferred albedos; especially uncertain are the relatively high albedo objects of potentially metallic composition (S and M classes, Sect. II E).

POLARIMETRIC METHOD There is an empirical relationship between geometric albedos of powdered materials (crushed rocks, meteorites, and lunar soils) and the slope of the polarization-vs-phase curve (Widorn 1967, KenKnight et al 1967). As recently calibrated in the laboratory by Zellner et al (1977a, 1977b), the relationship is insensitive for albedos $\lesssim 0.05$. The technique has the potential for inherent systematic errors approaching those of the radiometric technique and there is significant scatter of the laboratory data about the nominal calibration curve. Asteroid albedos determined from polarimetry agree with those determined by radiometry (for albedos >0.05) to within a couple of percent.

BEST-KNOWN DIAMETERS Over 160 asteroids have been measured radiometrically (summarized by Morrison 1977) and about a third that number polarimetrically (Zellner & Gradie 1976). The radiometric technique is based on sound physical principles but is subject to modelling uncertainties while the polarimetric technique is based on an empirical relationship for which there is only an incomplete physical understanding. Various observational uncertainties in both visible and IR photometry introduce appreciable scatter in radiometric diameters (e.g. most published radiometry is based on comparisons of radiometry with tabulated values of B(1,0) without regard for individual variations in visible or IR phase coefficients or lightcurve phase). Morrison (1977) has tabulated best-known diameters and albedos for 187 asteroids, including all objects >250 km diameter, by applying roughly equal weighting to radiometric and polarimetric results. D. Morrison and B. Zellner, respectively, are responsible for the TRIAD data files on radiometry and polarimetry.

It is possible to estimate diameters of unmeasured asteroids from other photometric properties (color index, visible phase coefficients, minimum polarization) known to correlate roughly with albedo. Such estimates may be very misleading in individual cases. For instance, the very-high-albedo E-type asteroids have UBV colors very similar to those of the much more common very-low-albedo C-type asteroids. Asteroids having physical or orbital parameters indicating probable C-type may have albedos

$\sim$0.04, while probable S-types may be $\sim$0.15. Because C-types are predominant in the belt, a geometric albedo $\sim$0.06 is applicable to a statistical ensemble of bodies about which nothing is known. The proportion of S to C bodies is reasonably invariant with size for diameters >50 km, but may change at smaller diameters. (S- and C-types are defined in Sect. II E.)

D. Masses and Densities

Estimates have been made of the masses of Ceres, Pallas, and Vesta from the accumulated perturbational changes in orbital longitudes of other asteroids in nearly commensurate orbits. From the motion of 197 Arete, Hertz (1968) derived a mass for Vesta of 2.4 x 10^{23} gm with a probably underestimated formal error of $\pm$10%. From mutual perturbations of Ceres, Vesta, and Pallas, Schubart (1974, 1975) has obtained 1.17 x 10^{24} gm for Ceres and 2.26 x 10^{23} gm for Pallas; Schubart's estimated percentage errors are 4 times worse for Pallas than for Ceres.

It may be possible to improve on these mass determinations slightly and possibly extend the technique to one or two additional asteroids. It may also be possible to determine masses for a few large asteroids from their perturbations on Mars' orbit by analyzing accurate ranges to spacecraft orbiting or landed on Mars. But definitive measurements of asteroid masses await close approaches by spacecraft.

An important constraint on the internal constitution of asteroids is density. Combined with the best-known diameters, the above masses yield 2.2, 1.9, and 2.9 gm cm^{-3} for Ceres, Pallas, and Vesta, respectively. Likely errors exceed 1/2 gm cm^{-3} for Ceres and Vesta and 1 gm cm^{-3} for Pallas. Morrison (1976) has determined the relative diameters of Vesta and Ceres to higher precision, which yields an apparently significant density ratio between the two of 1.33 ± 0.17, dominated by the difficult-to-estimate uncertainties in mass. Thus Ceres and Vesta are apparently of different bulk composition. If one can trust the derived densities, Ceres and Pallas have bulk densities similar to the most primitive carbonaceous chondrites and Vesta is more similar to terrestrial and ordinary chondritic rocks. Such compositions are consistent with geochemical inferences based on surface mineralogy (Sect. II E).

Estimates of the mass of the entire asteroid belt may be made assuming asteroid interiors are composed of compositions inferred for surface mineralogical assemblages (Sect. II E) and applying bias-corrected statistics for the proportions of different compositional types to measured brightness-frequency distributions (Sect. II E & G). Asteroids >100 km diameter total about 3.0×10^{24} gm and the total for the entire belt does not greatly exceed three times the mass of Ceres alone; this estimate is consistent with that of Kresák (1977).

E. Spectrophotometry and Surface Compositions

ASTRONOMICAL OBSERVATIONS Rocks and minerals differ in their wavelength-dependent reflectance of visible and near-IR sunlight. Early programs of asteroid colorimetry (reviewed by Chapman et al 1971), interpreted in terms of colors of meteorites, were not definitive. More recent extensive programs of UBV photometry (Zellner et al 1975, Zellner et al 1977c, Degewij et al 1978), maintained in the TRIAD files by E. Bowell, have yielded reliable colors for hundreds of asteroids. While this is an efficient reconnaissance technique that distinguishes several broad types, the blue portion of the spectrum is not highly diagnostic of mineralogy.

Spectrophotometry in ~24 filters has been published for ~100 asteroids by Chapman, McCord, and coworkers (most presented by Chapman et al 1973a, McCord & Chapman 1975a, b) and is being reduced for 150 others (maintained in TRIAD by M. Gaffey and C. Chapman). These spectra reveal absorption features near 1 μm in spectra for many asteroids.

Spectral windows beyond 1 μm contain important electronic and molecular absorption features, but faint objects cannot be measured because of the lesser brightness of the sun and detector insensitivity. Broadband measurements at J, H, and K wavelengths, combined with visible photometry, provide data unsuited to defining absorption features but appear to be sensitive to metallic iron (Veeder et al 1977; for other data cf Chapman & Morrison 1976 and Gradie et al 1977). Measurements beyond 3 μm, accomplished so far only for Ceres (Lebofsky 1977), are sensitive to water of hydration. Interferometric spectra to 2.5 μm (with resolution of $\sim 35\ cm^{-1}$) have been published for Vesta and 433 Eros by Larson & Fink (1975) and Larson et al (1976). Both spectra reveal the 2 μm pyroxene band. The technique can be extended toward 4 μm but only for bright asteroids. Far-ultraviolet reflectance data have been obtained for a few asteroids from above the Earth's atmosphere (Caldwell 1975), but are not highly diagnostic of composition.

Spectral observations of emitted thermal radiation beyond 5 μm could provide useful compositional information, but little has been learned from differences in 10 μm and 20 μm radiometry and occasional measurements at longer wavelengths.

COMPOSITIONAL INTERPRETATION It is less easy to interpret reflection spectra of solid surfaces than gaseous spectra. Absorption bands are broad and few in number, and physical factors unrelated to composition (e.g. particle size) influence spectra. Nevertheless such spectra are highly diagnostic for many common minerals (cf Adams 1975). The clearest inferences are possible for spectra dominated by the signature of a single mineral that has diagnostic features. Pyroxenes dominate reflection spectra of many rocks because of their intermediate opacity (transparent minerals reflect light chiefly from surface facets despite long pathlengths traversed in the material, while high-opacity substances hardly transmit light at all and so also exhibit primary surface reflections). Pyroxenes have strong IR absorptions involving the Fe^{2+} ion within the crystal lattice; bandcenters vary predictably depending on proportions of calcium, iron, and magnesium in the crystal, yielding a precise tool for determining pyroxene composition. Other minerals (e.g. olivine and plagioclase) have important IR bands. Transparent minerals with featureless spectra may constitute a significant portion of a mineral assemblage and remain undetectable whereas opaque minerals manifest themselves by reducing or blocking the spectral features of pyroxenes or similar minerals. The soundness of such approaches to interpreting asteroid spectra was proven when the prediction of a 2 μm pigeonite band on Vesta, based on the observed 0.9 μm band (McCord et al 1970), was confirmed by Larson & Fink (1975).

These approaches to interpreting asteroid spectra are somewhat complicated by the fact that the silicate absorption features are subdued on many asteroids and absent on others. Interpretations for asteroids lacking deep bands variously invoke the absence of strong-featured minerals, blocking by an opaque phase, and apparent presence of the spectral signature (not involving distinct absorption bands) of nickel-iron alloy. These potentially challengeable interpretations are strengthened by a combination of (1) matching spectral traits against a library of lab spectra of various meteorites and other rocks, (2) attempts to model spectra of simple artificial multi-component mineral assemblages, and (3) geochemical considerations of cosmically abundant elements and plausible mineral assemblages. Early work on interpreting asteroid spectra is referenced and briefly summarized by Chapman (1976). Inclusion of albedo data with spectral data in mineralogical interpretation was done by Chapman et al (1975). The most recent and definitive interpretation, with discussion of meteoritical analogs, is that of Gaffey & McCord (1977a).

COMPOSITIONAL TYPES Thirty-five recognizably different visible and near-IR spectral types are grouped in Table 1 into 16 groups of significantly different inferred mineralogical assemblages. Most asteroids fall into two broad types: the C-type (inferred to be akin to carbonaceous chondrites) and the S-type (various silicate-metal mixtures, perhaps akin to stony-iron meteorites). The inference that the very dark C-types are carbonaceous has been strengthened by Lebofsky's (1977) discovery of a water of hydration band on the C*-type asteroid Ceres. The silicate absorption features are obvious in most spectra of S-types, but the inference that there is also a metal phase (nickel-iron alloy) present has been more controversial. The IR measurements of Veeder et al (1977), combined with the analysis of soil maturation effects by Matson et al (1977), argue against the chief alternative to the nickel-iron interpretation. Soon radar-backscatter measurements of large S- and M-type asteroids should prove or disprove the inferred large abundance of metal on these asteroid surfaces.

The C and S types are recognized by bimodalities in several observational parameters, including depth of the negative branch of polarization-vs-phase curves (an opacity-related parameter that separates the groups most clearly), albedo, and color index. Particular ranges in five parameters were used by Chapman et al (1975) to define these types. The definitions have been slightly modified by Bowell et al (1978), who have classified ∿560 asteroids. They added a few new types, including M-type (a mnemonic for "metal", which is apparently the spectrally important phase present, although possibly mixed with featureless silicates as in enstatite chondrites) and E-type (a mnemonic for the possible interpretation as "enstatite achondrite"; cf Zellner et al 1977d). Anomalous asteroids, such as Vesta, are considered "unclassified" (U-type).

An attribute of the C-S-M-etc. taxonomy of Bowell et al (1978) is that it permits numerous asteroids observed by one of the reconnaissance techniques (e.g. UBV photometry) to be given probable classifications and calls attention to anomalous objects. Furthermore, such an albedo-sensitive taxonomy is useful for studying the statistical and distributional properties of asteroids. Correction for observational selection biases against low-albedo and more distant asteroids were first applied to a sample of ∿100 asteroids by Chapman et al (1975) and more recently to a sample three times larger by Zellner & Bowell (1977). Sampling bias is dominated by apparent brightness, so corrections are performed by weighting each observed asteroid of mean opposition magnitude B(a,0) by the ratio of total asteroids of that apparent magnitude to the number in the sample. Apparently there are ∿560 mainbelt asteroids $\gtrsim$50 km diameter, of which 76% are C, 16% S, 5% M, and 3% other. S-types constitute 2/3rds of asteroids at the inner edge of the mainbelt, but only 15% in the middle of the belt decreasing to 6% at the 2:1 resonance. Zellner and Bowell find that large asteroids avoid Kirkwood gaps more completely than small ones, but contrary to earlier suggestions they see no evidence for a compositional correlation with proximity to gaps.

F. Surface Textures and Regoliths

The physical state of an asteroid surface affects the manner in which cratering impacts redistribute or eject material. In early epochs, when collisional velocities were lower, the development of particulate surface layers (regolith) probably assisted accretion (Hartmann 1978). Asteroidal regoliths, both ancient ones and those evolving today, are hypothesized as environments for the creation of many types of gas-rich, brecciated meteorites (cf Pellas 1972, Rajan 1974).

Few observations conclusively reveal the surface structure of asteroids. Polarization data are interpreted as indicating <u>dusty</u> surfaces; a dusting is the easiest way to produce the intricate surface structure required. Radar penetrates to greater depths, but it is unclear whether the extreme roughness found for Eros at scales $\gtrsim 4$ cm radar wavelengths (Jurgens & Goldstein 1976) necessarily rules out a deep regolith. Microwave measurements of Ceres and Vesta have been interpreted (Conklin et al 1977) in terms of regoliths -- a dusty surface for Ceres, more compacted for Vesta.

Qualitative theoretical considerations have led to hypotheses that most asteroid regoliths are very thin (Chapman 1976) or many kilometers deep (Anders 1975). A quantitative model by Housen et al (1977) predicts deep regoliths on the largest asteroids, but negligible regoliths on rocky bodies $\lesssim 10$ km diameter or on relatively unconsolidated bodies $\lesssim 1$ km diameter. Early in an asteroid's life, the surface level of a typical region actually rises, due to blanketing from large anomalous cratering events elsewhere on the body; later, rapid net erosion may occur on typical regions prior to catastrophic fragmentation of the whole body. Repetitive gardening of the surface by small impacts is inefficient in competition with erosion and blanketing, so asteroid regoliths should have a coarse texture. The model suggests that most small- to moderate-sized asteroids should be surrounded by the ejecta from the last major cratering event, probably masking any local compositional variations; this is consistent with the apparent polarimetric and colorimetric uniformity nearly all asteroids display as they rotate.

Asteroid surfaces may superficially resemble Phobos, as photographed by Viking. Yet ejecta from Phobos cannot immediately escape Mars' gravitational potential well and may reaccumulate on Phobos, yielding an anomalously thick regolith (Soter 1971), a situation that does not apply to asteroids.

G. Size Distribution

Relative to the few big asteroids, smaller ones are increasingly abundant. The size distribution has been derived from the bias-corrected statistics of Zellner & Bowell (1977) for diameters $\gtrsim$50 km and may be supplemented at smaller diameters by photographic magnitude surveys. The first survey was the McDonald Survey or MDS (Kuiper et al 1958), which is nearly complete to apparent photographic magnitude 15 or 16. Corrections were made for minor incompletenesses in coverage as well as the plate-measurers' completeness factors near the limiting magnitude of the plates. Frequency relations of B(1,0) were obtained for each of three concentric zones in the belt; an error in tabulated completeness factors for the outer zone was corrected by van Houten (1971). The Palomar-Leiden Survey or PLS (van Houten et al 1970) sampled asteroids down to mag 20 in a

$12^{\circ} \times 18^{\circ}$ part of the ecliptic during two successive months. The factor of $\sim$50 extrapolation from this small region to the whole belt involves assumptions which have been questioned (cf Kresák 1971; Kiang 1971; Dohnanyi 1971, and discussions of same by van Houten; also see Sect. IV H).

Comparisons of the revised MDS and PLS reveal a discrepancy of a factor of two in the region of overlap between $11 < B(1,0) < 13$. One reason may be the small PLS sample in this range (Van Houten [1971] says it is 12). Second, the "revised" MDS values for objects fainter than $B(1,0) = 10.0$ are based on extrapolations of an average of one linear fit and one curving fit to the MDS plot of log number vs magnitude. But a linear extrapolation (MDS eq. 7) is without justification, especially now that PLS data and direct diameter measurements confirm the curving relation given by MDS eq. 6.

Fig. 1 shows the bias-corrected size-frequency data of Zellner and Bowell. The differences between the shapes of the smooth curves drawn through the C data and through the S+M data are not significant. The dashed extrapolations are hypothetical, but they must satisfy the PLS data, which constrain at least one curve to bend upwards at small diameters.

III. ASTEROID COLLISIONS

A. Erosion and Fragmentation

Although an individual asteroid is small compared with the volume of the belt, its geometric cross-section sweeps out a huge volume over 10^9 years. Thus interasteroidal collisions, at velocities of $\sim$5 km sec^{-1}, are common and the resulting erosion and fragmentation determines the asteroid size distribution, probably forms Hirayama families, and liberates some of the meteorites and cratering projectiles that strike the Earth and other terrestrial planets.

Most calculations of asteroid collisional evolution are based on a particle-in-a-box approach, with the box taken to be the effective volume of the asteroid belt (8.5×10^{25} km^3, according to Dohnanyi [1969]). Wetherill (1967) found that the particle-in-a-box approach underestimates collision timescales by factors of 1.5 to 2. Two parts of a continuum of asteroid collisions may be distinguished by the ratio of diameters of the larger and smaller colliding bodies (D/D_s). If D/D_s > some parameter γ, the smaller body craters the larger one. Such erosive collisions gradually reduce the size of the larger body, provided the ejecta that escape exceed the mass of the projectile, which is true for even the largest asteroid in the present 5 km sec^{-1} velocity regime. For colliding bodies more nearly equal in size ($D/D_s < \gamma$), catastrophic collision occurs and the larger object fragments into a distribution of smaller pieces.

The size ratio γ depends on velocity and the physical traits of the bodies involved -- their material strength, density, and gravitational field. The kinetic energy of the projectile is partitioned into fracturing and comminution of both bodies, heat, and the kinetic energy of the ejecta. The partitioning has been examined in detail for cratering on semi-infinite surfaces (O'Keefe & Ahrens 1976), but may be roughly applied to asteroid collisions. Some laboratory measurements have been made of such parameters as the energy per unit volume necessary to rupture an object (for basalt, $\sim 3 \times 10^7$ ergs cm^{-3}; Greenberg et al 1977, Hartmann 1978), the size of the largest fragment for excessive energy densities, and the size and velocity distributions of the smaller fragments.

Material properties help establish γ. An impact of given energy makes a much larger crater, or disrupts a much larger body, in weak material than in strong material; the resulting ejecta velocities are concomitantly much reduced for weak material. For 5 km sec^{-1} collision velocities in the belt, $\gamma = 18$ may be appropriate for hard, rocky bodies sufficiently small that the gravitational binding strength is << the material strength. $\gamma \gtrsim 7$ for iron. Presumably $\gamma >> 18$ for gravitationless carbonaceous bodies; but for a weak body of moderate size or larger, energy sufficient to fracture the body is often insufficient to disperse the fragments. In that case γ is determined by the gravitational, rather than material, strength of the target body.

The size distribution of a fragmental event may be roughly log-normal, but it is commonly represented by a truncated incremental power-law frequency distribution of the form $dN/dD = a\ D^{-b}$, for diameter D bigger than some lower limit determined by mass conservation. For size ratios near γ, a barely sufficient energy is delivered to the target to rupture it and the fragmental distribution is found to have $b \approx 3$. For cratering events and destructive collisions involving excessive energy densities ($D/D_s << \gamma$), there is more comminution and $b \gtrsim 4$ (Hartmann 1969, Greenberg et al 1978). A weakness in Dohnanyi's (1969) analytical treatment is that he adopted $b = 3.4$ for all cases, cratering <u>and</u> catastrophic fragmentation.

Full consideration of relevant physical processes and experimental data may reveal weaknesses in earlier considerations of asteroid collisional evolution (e.g. Wetherill 1967, Dohnanyi 1969, Napier & Dodd 1974). The characteristic lifetime against catastrophic destruction varies roughly as $\sqrt{D}$ in these theories and the asteroids evolve to a size distribution that varies within narrow limits about b = 3.5 (earlier theories gave b = 3.0). Chapman et al (1977) have modelled most of the physical processes discussed above, including the mutual interaction of populations of bodies of different strengths (to simulate C and S types); they find collisionally evolved size distributions for C and S types qualitatively resembling the observed curving distributions (Fig. 1), which cannot be characterized by a single value of b.

The nonlinear shape of the size-distributions, first noted by Kuiper et al (1958), was interpreted by Anders (1965) and Hartmann & Hartmann (1968) as indicating a remnant accretionary population of asteroids with a "tail" of smaller collisional fragments from several of the original bodies. The shape of the power-law-like size distribution for smaller asteroids did appear consistent with the size distributions observed in nature and in the laboratory for fragmented rocks (Hartmann 1969). The major downward revision of asteroid albedos in the 1970's caused an upward revision in collisional cross-sections, hence decrease in lifetimes against destruction by catastrophic collision. Virtually all rocky asteroids must now be thought of as fragments. Chapman (1974), noting evidence (now obsolete) that the nonlinearity might be confined to the S-types, suggested they could be bodies preserved from early epochs despite the much greater collision rates if they were very strong, such as metallic cores of geochemically differentiated bodies. More recent observations (Fig. 1) show that the C-type bodies also fail to exhibit a simple linear fragmental distribution. Chapman et al (1977) suggest this may result from variable strength of inherently weak C objects dominated by gravitational strength at larger sizes, combined with their collisional interaction with S bodies. However, a definitive explanation of the observed size distribition awaits further research. A major conclusion that has emerged during the 1970's is that, unless asteroids are much stronger than we believe, nearly all of them (including all but the largest ones) must be fragments of precursor bodies.

Chapman & Davis (1975) suggested the asteroids might be a collisional remnant from a much vaster population of bodies in early epochs. The lifetimes of the largest asteroids against catastrophic fragmentation are probably a few x 10^9 yr, which is consistent with collisional depletions ranging from only a factor of 2 up to a huge factor. Chapman & Davis offered a highly model-dependent estimate of an early population $\sim$300 times that present today.

At the opposite extreme, Alfvén & Arrhenius (1970a, b) believe that accretion of asteroids competes effectively with fragmentation. This requires that asteroids have organized motions that result in collision velocities << 5 km sec^{-1}. Napier & Dodd (1974) argue that formation of such jet streams requires volume densities vastly greater than exist in the asteroid zone. The observational evidence for jet streams (Arnold 1969) is of questionable statistical significance. Moreover the preferred orientation of the node and perihelion, which distinguishes a jet stream from a Hirayama family (Section IV I), has been demonstrated to be due to observational selection in at least one case (Kresák 1971).

B. Asteroid Rotations

Alfvén & Arrhenius (1970a) suggest that the typical rotation periods of asteroids (8 to 9 hr) are too long to explain by rotational instability, that any modification of "original" periods by collisions should result in shorter periods for smaller fragments (not clearly observed), and therefore that the observed rotations are primordial.

Although asteroid rotation periods (cf Burns 1975) are independent of size down to a few km diameter, there is a suggestion of excess angular momenta for a few numbered objects less than 3 km diameter and from statistical analysis of lightcurves of very faint asteroids by Degewij & Gehrels (1976). Proper interpretation of these data require the understanding that unless an asteroid is very small or strong, it will be catastrophically fragmented by any collision sufficient to markedly change its spin. Harris (1977) has shown that most asteroids are rotating at an appropriate equilibrium rate for a collisionally interacting population. The more rapid rotation of small asteroids suggests they have at least moderate strengths; if the $\sim$100 km diameter S- or M-type asteroids are indeed strong metallic cores, they might show a detectably greater dispersion about the 8 to 9 hr mean period. Asteroid precession, if observed, would also yield information on collision frequencies and material strengths; but few asteroids have been observed well enough to determine whether or not they are rotating about their body axes.

Asteroid lightcurve maximum amplitudes have been taken by Anders (1965) and others as a measure of whether or not an asteroid is a fragment (large amplitude) or original accretion (small amplitude). Apart from the lack of compelling reasons for assuming original accretions to be spherical, other effects apparently control asteroid shape. The smallest asteroids, which certainly are recent fragments, have smaller amplitudes than moderate-sized bodies (Bowell 1977). As for the larger asteroids, gravitational compression would constrain those made of very weak materials to roughly spherical shapes, even if they were fragmental (Johnson & McGetchin 1973); this effect is apparent for C-type objects > 100 km diameter (Chapman 1976).

IV. DYNAMICS AND ORBITAL EVOLUTION

A. Introduction

We have just considered how asteroid collisions produce fragments, large and small. Perturbative forces of planets redistribute them, sometimes onto orbits that cross those of the terrestrial planets, resulting in impact or further orbital evolution. The asteroids are depleted and gaps are created in the distribution of orbits. Thus dynamical evolution may link the asteroid belt and the meteorites that strike Earth. This section leads to consideration of meteorite origin, geochemical evolution of parent bodies, and cratering. Furthermore, we discuss clues in the present orbital distributions about early epochs in the origin of the asteroids and the planetesimal swarms from which planets accreted.

Two types of orbital resonances are known to be important for asteroids. First, commensurabilities in periods of an asteroid and planet (usually Jupiter) cause variations with typical periods of centuries. Second, when the rate of the longitude of node or perihelion of an asteroid matches a frequency of one of the fundamental, long-period oscillations of the planetary system, an asteroid is in a secular resonance; such secular perturbations have timescales of a few million years. A third type of behavior, libration of the argument of perihelion, is not usually classed as a resonance.

B. Commensurabilities and Kirkwood Gaps

If an asteroid and planet nearly repeat their relative positions after an integral number of revolutions of both bodies, then perturbing forces systematically repeat. For such a resonance, a phase angle is defined of the form $\sigma = Q\lambda - P\lambda_j + (P - Q)\,\tilde{\omega}$, where Q and P are integers, λ and λ_j are the mean longitudes of the asteroid and the j^{th} planet, and $\tilde{\omega}$ is the longitude of perihelion of the asteroid. P:Q is the ratio of periods of planet and asteroid. The most common ($P \neq Q$) commensurabilities depend on asteroid orbital eccentricity, but inclination-dependent resonances are possible for which $\tilde{\omega}$ must be replaced by the node Ω. Also possible are resonances controlled by the eccentricity (e) or inclination (i) of the planet, in which case $\tilde{\omega}_j$ or Ω_j replaces $\tilde{\omega}$. Most commensurabilities are eccentricity-controlled since terms occur in the expansion of the perturbing potential at one lower power of the eccentricity than of the inclination; this power is the difference $|P-Q|$, called the degree. Resonances may be shallow, for which σ circulates slowly and large amplitude oscillations in the orbit have the period of that circulation, or deep, for which σ cannot take on all values but librates about some value (usually near 0° or 180°) and large orbital oscillations have the period of this libration.

Librations frequently act to prevent close approaches between an asteroid and planet. Librating asteroids are preserved for P:Q = 4:3 (279 Thule), 3:2 (Hilda type), and 2:1 (Hecuba type, i.e., 1362 Griqua, 1921 Pala, and 1922 Zulu), with Jupiter the perturbing planet. For each case, σ librates about a value near 0°. When the asteroid and Jupiter are passing the same longitude so that $\lambda = \lambda_J$ (which together with $\sigma \approx 0$ means that the mean anomaly $\lambda - \tilde{\omega} \approx 0$), the asteroid is always near perihelion; when the asteroid is near aphelion, Jupiter's longitude cannot be similar. This results in striking stabilization. Some Hilda-type asteroids have aphelia nearly reaching Jupiter's orbit, but they are safe from Jupiter encounters closer than 1 AU.

Objects for which σ oscillates most are least stable. Commensurabilities at 1:1 (Trojans) and 3:1 (887 Alinda and 1915 Quetzalcoatl) also contain librators. Both of the latter are Mars-crossers and could have been placed in librating orbits during a close encounter with Mars.

The best examples of libration due to commensurability are the Trojan asteroids of Jupiter (Table 2) at the 1:1 commensurability, librating about $\sigma = \pm 60^{\circ}$. Everhart (1973) started 221 hypothetical objects in low inclination, circular orbits between 4.68 and 10.4 AU and calculated their orbital evolution under the influence of Jupiter and Saturn. Twenty-five of them librated about the Jupiter Trojan points for >1000 yr, of which 10 lasted the length of the integration, $\sim$30,000 yr. All seven Saturn Trojans were stable for similar durations. The real Jupiter Trojan 1173 Anchises and 6629P-L were found to be stable for $\sim$160,000 yr integrations. No Saturn Trojans have yet been discovered, although the limited searches to date do not rule out their existence.

Everhart also studied a type of 1:1 libration called horseshoes which, in a coordinate system rotating with the orbital rate of the planet, are large C-shaped loops enclosing both Trojan points and the third Lagrangian point, which lies on the side of the sun opposite the planet. Jupiter horseshoes were not very stable, consistent with the fact that none have been discovered, but several Saturn horseshoes seemed moderately stable. Weissman & Wetherill (1974) have studied Trojan and horseshoe orbits associated with Earth, yielding stability for as long as 10,000 yr on Trojan-type orbits. They argue that modest eccentricities and inclinations for the planets and librators will not disrupt stability, which is supported by the existence of Jupiter Trojans with _e_ up to 0.15 and _i_ up to 34°.

Horedt (1974) examined whether, if Jupiter lost mass, outer satellites might escape and become Trojans. Evidently such satellites would avoid the Trojan points, escaping always from the sunward side of Jupiter, in accord with Hill's zero-velocity surfaces in the restricted three-body problem. The minimum in the potential energy barrier over which the satellite has to escape occurs at the sunward Lagrangian point while, contrary to popular misconception, the Trojan points represent local potential energy maxima in the rotating coordinate system (potential energy is taken to be negative for gravitational interactions).

It seems paradoxical that asteroid groupings appear at the 1:1 and 3:2 commensurabilities, while those at 2:1, 3:1, 5:2 and 7:3 appear as Kirkwood gaps. For _a_ > 3.95 AU, all reliably observed minor planets are commensurate, with the possible exception of 944 Hidalgo which, in any case, may be an extinct comet (cf Marsden 1972). As discussed above, any noncommensurate asteroids would long since have been eliminated by close Jupiter encounters, but at smaller semimajor axes _a_, noncommensurate objects become stable and we see Kirkwood gaps partly by contrast. The origin of these gaps, apparently due to a combination of dynamical and collisional processes, has been much studied.

Both Hilda (3:2) and 2:1 type asteroids have first-order commensurabilities with P-Q = 1, but there are 24 numbered asteroids of the former type (see Table 3) and only 3 of the latter, despite observational biases favoring the latter. The brightest 3:2 librator has B(1,0) $\sim$ 3 mag brighter than the brightest 2:1 librator. Giffen (1973) studied the averaged planar elliptic restricted three-body problem for the two commensurabilities and found that intriguing changes result from a finite value for the eccentricity of Jupiter's orbit. Periodic solutions were found for both commensurabilities when an integral number of libration periods equalled the period of the longitude of perihelion. For the nonperiodic cases, Giffen plotted $\underline{a}$ vs $\underline{e}$ and σ vs $\underline{e}$ at systematic times, such as each maximum of $\underline{a}$. If the points lie on smooth so-called invariant curves, an integral of the motion exists and the orbit is stable. For the 3:2 case, initial $\underline{e}$ from 0.1 to 0.3 and initial $\underline{a}$ of 3.920 - 4.015 AU gave invariant curves. For the 2:1 case, initial $\underline{e}$'s from 0.1 to 0.34 were checked and only those >0.30 gave invariant curves. Giffen hypothesizes that cases without invariant curves might rule out the existence of such asteroids, but he suggests no mechanism for their elimination and concludes that their possible existence is not yet disproven.

The existence of the invariant curves demonstrates stability against the close approaches to Jupiter which radically change orbits and remove real objects by collision or gravitational ejection from the solar system. But nonexistence of invariant curves does not demonstrate limited lifetimes for low-eccentricity cases unless such orbits can be shown to evolve to higher eccentricities so that close Jupiter approaches occur. Alternatively a librating object might simply move out of the Kirkwood gap. One of Giffen's cases which was increasing in $\underline{e}$ and *a* was further followed by Scholl & Giffen (1974) and Froeschlé & Scholl (1976); its variation of *a* and *e* is bounded and of moderate amplitude, so the apparently least stable of Giffen's orbits lacking invariant curves is stable. A dynamical means for emptying the 2:1 gap thus remains unknown.

Giffen's suggested nonexistence of 2:1 librators with $e \leq 0.3$ may be checked observationally. Franklin et al (1975) note that the three numbered librators (1362, 1921 and 1922) now have *e* between 0.34 and 0.47, supporting Giffen's suggestion, but that *i*'s of 19° - 36° are far from Giffen's 0° case. Thirty-three unnumbered objects, with orbit qualities ranging from hopeless to very good, lead to libration when integrated. The best one is 1928UF=1928WC= the original 1125 China, which was measured on eight nights over a 1½ month span. Its *e* of 0.22 and low *i* seems to violate Giffen's hypothesis, but the object has not been recovered.

The Kirkwood gaps at 2:1, 3:1, 5:2 and 7:3 have been studied by Scholl & Froeschlé (1974, 1975) and Froeschlé & Scholl (1976) using the planar elliptic case. With 10^4 and 10^5 yr integrations, they show that commensurabilities, except for the 7:3, include some orbits with *e* oscillating between modest values and values >0.3. Since only a fraction of orbits in gaps show large changes in *e*, it is unclear how the gaps are depopulated. Scholl & Froeschlé adopt Jefferys' (1967) suggestion that increased collision probabilities of periodically eccentric bodies with other asteroids may deplete the gaps. But even if the present asteroid population is a decayed remnant of a larger population (Chapman & Davis 1975), *e*'s would have to greatly exceed 0.3 to deplete even part of the gaps, since high *e*'s exist elsewhere in the belt where population densities are much higher in the gaps. For the 3:1 case there is an alternative to collisions for part of the gap, since objects with $e > 0.27$ can be eliminated by close Mars encounters.

Of course, the dynamical models so far applied to the problem of Kirkwood gaps are simpler than reality. Enhanced eccentricities appear to result from the complex intermingling of a commensurability and the longer period secular perturbations due to perihelion rotation. The calculation of perturbations due to Jupiter's precessing, variable e orbit provides several additional frequencies to mix with commensurabilities beyond the one zero frequency present in the fixed ellipse case. These may affect a larger fraction of gap orbits. Future studies should also investigate inclined asteroid orbits.

Franklin et al (1975) exemplified a new kind of 2:1 librator, called apparent apocentric librators, for which σ librates about 180° rather than 0°. When σ librates, $\tilde{\omega}$ circulates and vice versa. Greenberg & Franklin (1975) have explained the behavior of $\tilde{\omega}$ and e when the forced oscillations in e due to the nearby 2:1 commensurability exceed e itself, appropriately averaged over an oscillation. The temporarily small values of e occur for asteroids with proper $e \sim 0.04$, about the same size as forced oscillations in e due to long-period secular perturbations. Greenberg & Franklin explained the behavior of σ as well: when forced oscillation in e due to the 2:1 commensurability dominate the motion of $\tilde{\omega}$, driving it into rapid circulation, the circulation frequency is exactly that needed to cause libration of σ with a 180° phase. Such temporary apocentric librators occur at a slightly beyond the main librating region. Analogous temporary <u>pericentric</u> librators occur just inward from the main librating region. Temporary librators are not deep enough into resonances to be as strongly modified as ordinary librators; the secular perturbations are strong enough to push them into and out of the narrow region of e at the edges of the resonance where libration occurs. (These phenomena have yet to be generalized to other commensurabilities.)

Wiesel (1974a, b) developed a theory of phase mixing of an initial asteroid distribution and applied it to the 2:1, 3:1, and 5:2 Kirkwood gaps. He developed the two integrals of the resonant motion to first order in e for the planar case with a circular Jupiter orbit. The distribution is calculated after the phases of resonant terms for different objects have become randomly distributed. For smooth initial a-e distributions, the largest depletion is about 50%, with a corresponding augmentation on the inward side of the resonance. The effect is much smaller for initial distributions mimicking the belt adjacent to the 2:1 gap. Wiesel points out that a mechanism that relies solely on the dynamical redistribution of librators to depopulate the gaps is doomed since so few objects near gaps are librators. Since gaps are wider than libration regions, a mechanism is needed that selectively removes librators and adjacent circulators. The missing mechanism may be collisions, but Wiesel points out that for reasonable initial distributions near the 3:1 and 5:2 gaps, the increase in average e, hence collision rate, due to the librations is quite modest.

Zimmerman & Wetherill (1973) showed that asteroids adjacent to the 2:1 gap collide and inject fragments into the libration region. Libration periodically augments small initial e's to as much as 0.3 to 0.4, but prevents close approaches to Jupiter. If librating fragments suffer further high-velocity collisions while e's are large, some resulting fragments will be put in nonlibrating orbits that can approach Jupiter. On a timescale of $\sim 10^5$ yr, such approaches random-walk the orbits into different paths (important implications for deriving meteorites are discussed in Sect. IV E). Thereby we may collisionally populate and depopulate the Kirkwood gaps, but destructive collisions seem to be required. Lesser collisions cannot modify the orbit sufficiently and the probability of a destructive collision approaches unity before the effects of lesser collisions could accumulate. This problem requires further work.

There is yet another possibility: Jupiter's $\underline{e}$ causes extra periodicities in $\underline{e}$ for a librating object so that the range of $\underline{e}$ and σ variation is increased. To be stable against close Jupiter encounters, orbits must be stable for the full range of variation of Jupiter's $\underline{e}$ (0.027 to 0.062). Orbits which librate only part of the time would be eliminated by close Jupiter encounters if they can leave libration with $\underline{e} \gtrsim 0.3$.

We have used the word "stability" to describe orbits that can exist for the age of the solar system. Empirical evidence suggests that a minimum approach distance to Jupiter (the major dynamical destabilizer in the outer asteroid belt) of $\sim$1 AU is the limit for such stability, but the limit has yet to be theoretically computed. We have seen that some commensurabilities can increase stability, by increasing minimum approach distances. But other librating orbits are unstable, as exemplified by comets which exhibit temporary librations of a few cycles and are suddenly terminated by a close approach to Jupiter (Marsden 1970, Franklin et al 1975), which results in eventual ejection from the solar system or collision with a planet.

Heppenheimer (1975) studied the effect of a changing Jupiter/Sun mass ratio (e.g. in early solar system history) on evolution of degree one commensurabilities, especially that at 2:1. He identified two adiabatic invariants for 0° $\underline{i}$ orbits and a circular Jupiter orbit. For slowly increasing mass ratio, circulating orbits adjacent to the libration region become librating orbits. Transition from circulation to libration is reasonable since the width of the libration region scales as the square root of the mass ratio; an example is transition from low *e* circulation to a higher *e* libration. If transitions could occur between high *e* circulators and libration, then a decreasing mass ratio might transfer librators into circulators which pass close to Jupiter and would be terminated. While slow mass change of Sun or Jupiter could change the number of librators, it would not provide an obvious way to empty the Kirkwood gaps. (A brief way to calculate the width of the 2:1 resonant region was given by Walsh & Zimmerman, 1971.)

Because the strength of a commensurability involves $e^{|P-Q|}$ or $\sin i^{|P-Q|}$, low-degree commensurabilities have wider resonance regions, hence are more probable, than high-degree ones. For asteroids of modest *e* or *i*, resonances involving *i* can occur only for even values of $|P-Q| \geq 2$ while *e*-controlled commensurabilities occur for any value of $|P-Q| \geq 1$; hence, we know of many *e*-controlled librators but no *i*-controlled librators.

1685 Toro crosses the orbits of Earth and Mars and approaches Venus' orbit; the above generalities do not apply to such orbits that approach planets closely; high-degree resonances then become possible. Toro's complex behavior -- near commensurabilities with both Earth (5:8) and Venus (5:13) -- has led a succession of authors (most recently Williams & Wetherill, 1973) to run numerical integrations for up to 5000 yr. Since Earth and Venus have a near-commensurability of 13:8, Toro's two commensurabilities can be simultaneously important and both are capable of temporary librations. But Toro's librations with respect to at least one commensurability must be temporary, since Venus and Earth are only roughly commensurate. The 5:8 librations with Earth last for at least 3400 yr while the 5:13 librations with Venus last for a nonoverlapping time span of at least 1000 yr. A transition occurs as perihelion precession increases the closest approach distance of Toro from Earth and decreases the Venus closest-approach distance; the planet with strongest peak forces (nearly impulsive) controls the librations. The librations tend to prevent the closest encounters, although it is uncertain how efficiently. If collisions can be avoided by such librations, the mean lifetimes of planet-crossing asteroids might be increased. Mars perturbations set an upper limit of ∼3 m.y. for the Toro librations, which is an order of magnitude smaller than typical lifetimes of such objects against planetary impact or ejection. It is not certain how much such resonances can lengthen the lifetimes of typical planet-crossers; we require more statistics. Several other Earth-approaching objects have been studied; one has been known to librate (887 Alinda), 1627 Ivar may have an 11:28 librating commensurability with Earth, and 1221 Amor apparently does not librate (Janiczek et al 1972). Ip & Mehra (1973) have called some objects "librators" because of periodic oscillations of elements (always expected near a commensurability), although they failed to establish that σ oscillates between fixed limits in many cases.

Knowledge about commensurabilities remains incomplete. Most theoretical work involves necessarily restrictive assumptions about a very complex problem. Numerical integrations can model the complexities; for investigations of real asteroids, timescales of both ∼1 libration period (a few hundred yr) and ∼1 perihelion or nodal precession period (several x 10^3 yr) are important. Such long integrations are expensive but they have revealed the surprising temporary apocentric librators and the switch of libration mode for Toro. Finally, continued discoveries of librators contribute to understanding commensurabilities; two of the three known 2:1 librators and one of the two 3:1 librators were recovered in the past few years.

C. Secular Resonances

Secular resonances have been less intensively studied than commensurabilities, but are clearly important for the morphology of the asteroid belt. They arise if the rate of the node or perihelion of an asteroid matches one of the discrete frequencies in the trigonometric series that describes planetary inclinations and nodes or eccentricities and longitudes of perihelion. If planetary nodes and perihelia precessed at constant rates, then the resonant values for an asteroid would correspond to these rates. The actual description of planetary precessions corresponds to an eigenvector-eigenvalue problem. Perturbations with periods depending on precession periods are (misleadingly) called secular perturbations. They yield periodicities in the e's and i's and periodic and linear changes in the nodes and longitudes of perihelion.

There are three dominant resonant frequencies for the asteroid belt. An asteroid with an average (more exactly a proper) nodal rate of $-25''.7$/yr, or one with a proper longitude of perihelion rate of $27''.8$/yr or $4''.3$/yr, is resonant and can oscillate substantially in i or e with timescales of $\sim 10^6$ yr. The strong effects of such a resonance are exemplified (for the Lost City meteorite) by Lowrey (1971) and Williams (1975a). The asteroids are strongly depleted (like the Kirkwood gaps) at these three resonant frequencies. The recognition of gaps around secular resonances is recent since digital computers are required for practical calculation of the resonance locations in a-e-i space.

The depopulation of the secular resonance gaps is more easily understood than for the Kirkwood gaps. For the 27"8/yr resonance, Williams (1973b) showed that a resonant inner-belt asteroid could easily attain sufficiently large e oscillations to become Mars-crossing. Mars probably clears the 4"3/yr resonance also, but the -25"7/yr nodal resonance requires a separate study. None of the non-planet-crossing main-belt asteroids with accurate orbits and $a < 2.5$ AU are seen in the three strongest secular resonances. There appear to be some resonant planet-crossers and there may be resonant main-belt objects with larger a, although calculations of the latter are sensitive to error. It is actually surprising that no resonant inner-belt objects are known for it seems it should be possible for low e secular librators to exist without becoming Mars-crossers.

D. Argument of Perihelion: Libration

The argument of perihelion ω of an asteroid librates about 90° or 270° when a combination of e and i exceeds a critical value. 1373 Cincinnati is the only numbered asteroid known to show ω libration (cf description by Marsden 1970). Although its aphelion reaches 5.2 AU, the libration about 90° prevents close approaches to Jupiter. In fact all asteroids with large e or i have minimum perihelion distance and maximum aphelion distance when ω passes through 90° or 270° and the perihelion and aphelion points are farthest from the plane of the planets. This additional effect of secular perturbations helps stabilize such orbits against close planetary encounters. The recently discovered Mars-crosser 1974 UB also shows ω libration about 90°.

E. Material Transport from the Asteroid Belt

Problems of extracting meteoritic material from the asteroid belt have been reviewed by Wetherill (1974) and Wetherill & Williams (1977). Wetherill (1976) finds that the Apollo objects can be the primary source bodies for a large fraction of the meteorites. But the lifetimes of Apollos are too short for any significant number to have remained in such orbits since the origin of the solar system. Thus a source is required for both meteorites and Apollos; one possible source is the main asteroid belt.

One transport mechanism (Zimmerman & Wetherill 1973) was partly outlined in Sect. IV B. Fragmental debris knocked into the 2:1 resonance region develops high e and secondary collisions decouple some material from libration. The debris with greater e approaches Jupiter, which results in some material being random-walked into Earth-crossing orbits. Some debris goes Earth-crossing within 10^4 yr of the second collision and much of the rest within 10^5 yr. A second mechanism (Williams 1973a, b) uses secular resonances to transport collision debris to Earth. Debris injected into secular resonance gaps in the inner belt is augmented in e until it becomes Earth-crossing on a timescale of $\sim 10^6$ yr. Encounters with Earth decouple the debris from the resonance. Initial Earth-crossing orbits are distinct for the two mechanisms (orbits with aphelia near Jupiter and resonant orbits, respectively) but Earth perturbations rapidly smear out the distinctions so there are not yet observational tests of the relative importance of the mechanisms (only three meteorite orbits are known). These resonant mechanisms select debris from objects near the 2:1 Kirkwood gap (and possibly others) and from near the secular resonance gaps, leaving most asteroids unsampled.

A significant meteorite source mechanism must match observed timescales and mass fluxes on Earth. Both mechanisms are rapid enough to be compatible with typical 10^7 yr cosmic-ray exposure ages for stony meteorites. Also both mechanisms may yield $\sim 10^{8\pm1}$ gm/yr impacting Earth, which is about a factor of 10 lower than observed. While these mechanisms likely contribute <u>some</u> meteorites and could plausibly supply a substantial fraction of them, the production rates fail by at least two orders of magnitude to supply the observed number of Apollo objects (Wetherill 1976). A recent evaluation of the combined effects of secular, Mars, and Earth perturbations on fragments derived from some large, low <u>i</u> asteroids in the inner belt demonstrates that such bodies are an entirely adequate source for the stony and metallic differentiated meteorites (Wetherill & Williams 1977), consistent with some inferred mineralogies for those asteroids.

Peterson (1976) has proposed transport using the Yarkovsky effect. The effect on the yield and lifetimes of the stability of the spin state remains to be evaluated.

Much work remains to be done. For example, secular resonances in the outer belt might transport debris into Jupiter-crossing orbits more readily than into Earth-crossing orbits, with subsequent evolution resembling the end of the 2:1 gap process. One hopes to restrict the dynamically possible processes so as to identify particular asteroids with particular meteorite classes.

We have discussed resonance transportation only for the present solar system. When the planets were forming, resonances would have shifted position, modifying planetesimal orbits in the asteroid belt and elsewhere.

F. Poisson's Theorem

The most misunderstood result on orbital stability in the solar system may be Poisson's theorem on the invariability of semimajor axes. Consider gravitational interactions between noncommensurate, mutually noncrossing point masses. It is often stated that there are no secular terms in a of second order in planetary masses, but there are secular terms of third order containing the factor m^3t. What is frequently missed is that this result is demonstrated only for timescales $\ll 10^4$ yr, limited by the timescale of node and perihelion precession periods. The existence proof for these terms involves trigonometric expansion of the potential energy of interaction, where the arguments of cosines involve a linear combination of the mean longitudes, nodes, and longitudes of perihelion. The proof involves expanding the truly secular terms in Ω and $\tilde{\omega}$ out of the arguments so that a linear term in time is introduced into the coefficients. The same approximation introduces linear terms in time into the e's and i's which, in fact, can be demonstrated to be long-periodic at that order. The third-order secular term in the semimajor axes is really periodic of very long period and the linear term in time results from expanding part of the trigonometric term in a power series in time. This restriction in the development was pointed out by Eginitis (1889) but has been little noted since. For timescales comparable to the age of the solar system, there has been no analytic demonstration of the existence of terms in either a, e, or i of planets and asteroids with coefficients which are truly linear in time, though such terms may exist.

It should be possible to calculate the largest pure and mixed secular terms in a, e, and i while retaining all of the secular changes inside the trigonometric arguments. Such a project is natural for one of the computer codes which manipulate series; it would contribute to our knowledge of the true dynamical stability of the solar system.

Ovenden (1972, 1973) formulated what he calls the principle of "least interaction action," suggesting it is responsible for the arrangement of semimajor axes of planets and satellites. He states that calculation of the present configuration of planets is improved if a body of 90 Earth masses had been in the asteroid belt until 1.6×10^7 yr ago; then the present configuration is a stage in evolution toward a new minimum of "interaction action."

One objection to Ovenden's dynamical procedure concerns timescale. His calculation of the evolutionary rates of planetary $\underline{a}$'s uses the aforementioned third-order secular term in $\underline{a}$. But this term is periodic, not linear, in time for $\gtrsim 10^4$ yr, so the calculation of a $\sim 10^7$ yr event is unjustified. Another objection concerns the meaning of least interaction action and the assumed evolution toward it. Experience with numerical integrations of several bodies does not indicate that a system of strongly interacting orbits evolves smoothly into a system of weakly interacting orbits; rather some objects are ejected from the system in unbound orbits until the remaining system stabilizes. It is very different for a system to stabilize by eliminating its least stable members than by evolution of all objects toward stability. Once stable, there is no reason to expect the system to evolve further toward minimum interaction action. If Ovenden's principle has any validity in predicting configurations, it is probably not because the configurations change until they reach a minimum, but because the minimum configuration is the most difficult from which to remove members.

Lunar and meteoritical chronologies provide further fundamental inconsistencies to Ovenden's hypothesis for the creation of the asteroids $\sim 10^7$ yr ago by destruction of a huge planet. A recent observation by

Van Flandern (1975) on the regularity of orbits of comets with $\sim 10^7$ yr periods has been linked to Ovenden's hypothesis, but far less exotic explanations exist than an exploded planet (e.g. collision between a large comet and an asteroid or observational biases in the data).

G. Planetary Masses

Minor planets provide a useful tool for measuring masses of some planets. Duncombe et al (1973) and Greenberg (1976) have summarized the use of commensurable asteroids to measure Jupiter. The mass of Saturn has been determined from three Trojans (Scholl, 1973).

H. Catalogs and Selection Effects

The permanently numbered asteroids are cataloged each year in the Ephemerides of Minor Planets. Orbits therein result primarily from photographic programs plus some visual programs. New discoveries result from astrometric programs and supernova and asteroid search programs. Most asteroids are discovered near opposition. Photography is often concentrated near the ecliptic and is not uniform in time (e.g. because of moonlight). At least three observations over a duration of a month or more are required to permit identification with observations made in earlier years which were too few in number, or covered too short a span, to give an accurate orbit. This is the most common way new asteroids are cataloged. For instance, 1940 Whipple got its first accurate orbit from a 45-day arc in 1975 which led to identification of 6 previous observations at 5 oppositions back to 1932. Sometimes lower-accuracy orbits are linked by recognizing their similarily. Short-arc orbits or unlinked data are common for asteroids near the plate limit. (Each year several hundred objects are seen while only several dozen are cataloged.) Finally, an accurate orbit at one opposition may be used to generate predictions which lead to subsequent recovery. This third procedure for cataloging objects is used for unusual objects, such as Apollos. To guard against misidentifications most asteroids are cataloged only if seen at three or more oppositions (very rarely two). Care was not always taken in the past, partly for lack of computers; there are about 30 minor planets with catalog numbers less than 1565 that are presently lost. There are always several dozen multiple opposition objects with good orbits awaiting observation at one more opposition prior to cataloging. Over a thousand single-opposition orbits await linkage with another opposition.

The annual Ephemerides of Minor Planets, published by the Institute of Theoretical Astronomy at Leningrad, lists all cataloged asteroids, giving orbital elements and predicted positions near opposition. The Minor Planet Circulars, compiled by the Cincinnati Observatory, list observations, newly numbered orbits, preliminary orbits, and new ephemerides. Finally, the IAU Circulars give observations, orbits, and ephemerides for priority objects (e.g. Earth-approachers).

Selection effects in the numbered asteroids are discussed by Kiang (1966) and Kresák (1967). Slightly less than half are brighter than mean opposition magnitude B(a,0)=15.0, the limit of bias-free completeness. Newly cataloged asteroids tend to range from 15.5 to 17.5. The sample of all 2042 numbered asteroids is biased against high inclinations and in other ways. Participating observatories are few, so that climate and observatory latitude favor discoveries of asteroids coming to favorable opposition at certain times of the year in certain parts of the sky. A strong effect is discovery of asteroids near perihelion, when they are brightest. The peaking of the number of known perihelia near 0°, $\sim$3 times that at 180°, is partly a selection effect but partly due to long-period perturbations that cause asteroids with perihelia approximately aligned with Jupiter's to have smaller perihelion distances than those oriented around 180°. Because of the power-law size distribution of asteroids, the closer perihelia in one part of the sky favor discovery of smaller objects. Such selection effects are enhanced by the fact that most asteroids are independently observed at several oppositions before the observations are linked.

The Palomar-Leiden Survey (PLS, see Sect. II G) sampled fainter minor planets. Plates were timed and positioned so that most objects could be followed between two months. Of the $\sim$1800 discovered objects with acceptable orbital elements, $\sim$1100 were seen in both months and are of high accuracy; the remainder have an order-of-magnitude worse accuracy. The selection effects for this survey of 2% of the total number of asteroids within the Palomar Schmidt's grasp are easier to assess than for numbered asteroids since the procedures were uniform and specified. The restriction to a 12% strip about the ecliptic strongly selects against high i objects; those with i > a few degrees were missed unless their nodes were in the photographed area. The faintest surveyed objects exhibit a bias for perihelia near the survey area.

The faintest cataloged objects are a biased sample and the brightest PLS objects are a sample of small numbers. The discovery of new asteroids will push the completeness limit to fainter objects. This will further clarify the distortions in the vicinity of the juncture of the two data sets (Sect. II G).

I. Families

The orbital elements of main-belt asteroids show clusters called families. They are probably debris resulting from catastrophic collisions. From the orbital properties of families and physical studies of their members, we may learn about the collisional and dynamical evolution of asteroids and about the interior properties of precursor bodies. There have been few papers on families since the classical papers by Hirayama (1928), Brouwer (1951), and Arnold (1969). We discuss here the technique of family identification and some partial results of a study in progress.

Asteroid orbits are affected by planetary perturbations, especially Jupiter's. For most asteroids, the long-period (secular) perturbations are largest. When these periodic perturbations are removed from the present elements, one obtains proper elements which may be thought of as mean elements. The proper elements, *a*, *e*, and *i* show the distinctive family clusterings. The long-recognized families Eos (Fig. 2), Themis, and Koronis are heavily populated and well defined, but families with as few as four members are recognizable. Using the numbered asteroids and high-quality PLS orbits, Williams (1975b) searched for clusters among ∿2800 objects. 104 families, containing 44% of the asteroids in the sample, were found which appeared to be statistically significant. The size of the families in proper *a-e-i* space suggests a typical rms speed of 270 m sec^{-1} from the center of mass. The violence of family-producing events ranges from cases where a large body still exists and the family members are ejecta from a gigantic cratering event to cases where the parent body was thoroughly broken up. Families were not examined for clusterings of proper longitude of node and perihelion since "jet streams" can be the spurious result of observational selection (most family members are fainter than the completeness limit; see Sect. IV H). The discovery of new asteroids will help to fill out many small families and will place major portions of some families above the bias-free completeness limit.

Comparisons of the physical properties of family members permits us to look inside a former asteroid. Spectrophotometric sampling of the brightest members of several families (McCord & Chapman 1975b) reveals heterogeneity of compositional types in many cases. UBV studies of the Eos and Koronis families suggest compositional similarity of members, but the Nysa family may be more complex (Gradie & Zellner 1977). Attempts to interpret the association of the Nysa family with a compositionally distinct companion family (Zellner et al 1977d) and the disparate members of the Eunomia family (Chapman 1976) in terms of geochemically plausible precursor bodies have proven to be difficult.

J. Apollo, Amor, and Mars-Crossing Asteroids

Earth-approaching asteroids are particularly fascinating. First, they are links between many meteorites that fall to Earth and their distant parent bodies. Second, some of them are possible candidates for mining endeavors in space (Gaffey & McCord 1977c). Third, the Earth is an active participant in a cosmic target-shoot with these objects.

Apollo asteroids have perihelion distances $q < 1.0$ AU while Amors have perihelia somewhat larger than 1 AU, although different authors define different upper limits such as 1.15, 1.30, or 1.38 AU. There is little significance to the Apollo/Amor boundary for we know that two Amors (1915 Quetzalcoatl and 1580 Betulia) have perihelia that evolve back and forth across 1.0 AU. Also, one must calculate orbital evolution in order to determine if an object with $q < 1.0$ AU can intersect the Earth's orbit.

Table 4 lists asteroids with $q < 1.5$ AU in order of perihelion distance. Note that the range of inclinations, up to 68°, is nearly twice that for main-belt asteroids and that there is a great variety of <u>e</u>'s and <u>a</u>'s. The large range of absolute magnitudes is expected for a sample of close-approaching objects; though the brightest Amor objects are 433 Eros and 1036 Ganymed, it is unlikely that the brightest Apollo has been found yet. The table shows that perihelia tend to avoid the mean distances of Venus and Earth; perhaps objects with such perihelia would have more frequent close planetary encounters, hence shorter lifetimes. The exception to this avoidance appears to be 1685 Toro, but it seems to avoid both Earth and Venus due to a resonant commensurability (Sect. IV B).

Table 4 illustrates a cutoff in aphelia near 4.2 AU which, without the certainty that evolutionary calculations would provide, suggests that we lack objects that approach Jupiter closer than ~ 1 AU, the same limit seen for main-belt objects. Apollo/Amor lifetimes are apparently controlled by the terrestrial planets and are typically a few x 10^7 yr rather than the $\sim 10^6$ yr expected for the Jupiter-approaching objects such as meteors and fireballs. Perhaps some Apollos and Amors were perturbed from short-lived orbits into longer-lived orbits by the terrestrial planets. Aphelia $\gtrsim 4.0$ AU might suggest bodies derived by the Kirkwood gap meteorite transport mechanism (Sect. IV E), but the largest value is for an orbit (for 6344P-L) of only modest accuracy. While no clear-cut examples exist, there are several cases of aphelia ~ 4 AU which might result if a higher-aphelion object were perturbed onto a longer-lived orbit by close encounters with terrestrial planets.

Many Apollos were discovered in the late 40's and early 50's, but only two were found in the 60's (both from the PLS). The 1970's have yielded numerous Apollos, partly due to the dedicated search for them by E. Shoemaker and E. Helin. Because of their large angular velocities at discovery, rapid follow-ups are necessary if the objects are not to be lost; occasionally objects disappear into the daylit sky within days. Unidentified objects trailing $\gtrsim 0\overset{\circ}{.}7$/day at opposition are mainly unusual objects such as Apollos, Amors, and Mars-crossers, while those trailing 0.5 - $0\overset{\circ}{.}7$/day tend to be high-$\underline{i}$ main belt objects, but may be more unusual. Also <u>any</u> object near opposition moving the wrong way (prograde) or nearly perpendicular to the ecliptic are strong suspects. Any such unusual objects should be reported by telegram to the Central Bureau for Astronomical Telegrams (cable: Satellites New York; postal address: 60 Garden St., Cambridge, Mass. 02138). The first rough positions should be followed by accurate ones and further positions should be sought on subsequent nights. All accurate asteroid positions should be sent to the Cincinnati Observatory. Much of the recent success in discovering unusual objects has been due to observers being alert to the possibility of discovery and responding rapidly when a suspect is found.

None of the known Apollos has been independently rediscovered at a different opposition. Several authors, most recently Wetherill (1976), have used this fact to try to place approximate limits on the number of Apollos with diameters $\geq$ 1 km. Constraining the upper limit by lunar and terrestrial crater counts, Wetherill estimates that there are ∿700 such Apollos. When he includes the search data of Shoemaker, Helin & Gillett (1977), Wetherill estimates ∿600 Apollos and a similar number of Amors. This last fact raises a serious problem concerning the origin of the Apollos:

7-0

since the dynamical lifetimes of Amors are at least 10 times those of Apollos, few Apollos can be derived by evolution through an Amor stage. Calculations of methods for supplying Apollos directly from the main belt also run into difficulties (Sect. IV E), leading Wetherill to conclude that most Apollos are extinct comet nuclei. This conclusion is bolstered by Sekanina's (1973) report that several small meteor streams seem to match orbits of several Apollos.

V. RAMIFICATIONS FOR PLANETARY EVOLUTION

A. Asteroids as Planetesimals

"Planetesimals" is a term referring to asteroid-sized bodies -- from objects hundreds of km across down to dust grains -- that were involved in forming and cratering planets. Remnants of these populations exist, or have existed, in orbits that protect bodies from collision or ejection. Known remnants include comets, main-belt asteroids, Apollos, and Trojans. Crater-forming projectiles and meteorites must be derived from one or more of the known populations, although a few could conceivably be derived from an as-yet-unknown population. Arguments have persisted over which bodies are the "parent bodies" for the meteorites, but the term is deceptively vague. Levin (1977) has emphasized the distinctions between initial parent bodies (presumably large bodies on which meteoritic rocks originally formed and were subsequently modified by metamorphic and other processes), intermediate parent bodies (on whose regolithy surface many gas-rich, brecciated, and xenolithic meteorites were formed), and last parent bodies (in which meteorites were shielded from cosmic rays prior to fragmentation and capture by the Earth). Whatever the relationship among the various types of parent bodies, they are all representatives of, or descendants of, the same grand family of planetesimals that initially populated the solar system. Differences among them involve such factors as initial solar distance (which determined the ice/silicate ratio) and distance from the gravitational effects of large outer planets, which determined the probability of accumulating into a planet, being left as a swarm in situ (asteroids), or ejection into the Oort cloud (comets). The clear separation of classes of planetesimals is blurred by recent work suggesting appreciable mixing of material between planetary zones (Hartmann 1976, Wetherill 1977).

The lunar cratering record (cf Hartmann 1972) exemplifies how the remnant planetesimal population has been decreasing with time as objects remaining in short-lived orbits are exhausted. The lunar cratering flux was high in early epochs, perhaps with some major spikes, but has tailed off since 4 b.y. ago. The lunar post-mare crater size distribution is similar to that expected from impact of an evolved fragmental population, but there is some evidence for anomalous population in the cratering record on Mercury and on some of the oldest lunar units (Strom & Whitaker 1976).

B. Early Orbital Evolution

Lecar & Franklin (1973) examined the evolution of several hundred hypothetical objects distributed in orbits interior to Jupiter. After only 2400 years most objects beyond 3.97 AU (3:2 commensurability) were removed by Jupiter perturbations, as were higher *e* objects just inside the commensurability. Many 3:2 and 4:3 librators remained there throughout the 2400-yr integration. Lecar and Franklin's final distribution for the outer belt resembles the true belt in that nonresonant belt objects exist only for *a* smaller than for the 3:2 commensurability, though the predominant outer boundary of the true belt appears trimmed by a further ¼ AU. Presumably this difference represents the additional depth from which Jupiter has been able to eject objects between 2400 yr and the age of the solar system.

Lecar and Franklin thought their discrepancy with the true belt was larger than it really is because they compared their results with the PLS rather than the cataloged asteroids. A rarely noted PLS result is that few objects were found between the 2:1 and 3:2 commensurabilities. While 47 of the first 1800 numbered asteroids exist in this interval, only four of ∿1100 PLS objects with accurate orbits were found, one of which was already numbered. The four (319, 6550P-L, 6030P-L, and 9594P-L) have B(a,0) of 16.1, 17.4, 18.5, and 19.6, a distribution very unlike the usual power-law (Sect. II G) for which each fainter magnitude interval contains about 2¼ times as many objects as the adjacent one. This puzzling lack of small noncommensurate objects beyond 3.3 AU may imply that very little collisional fragmentation has occurred, but it is not known why.

Lecar and Franklin also performed integrations over 6000 yr for hypothetical objects between Jupiter and Saturn. Most were ejected from the solar system, but bands remained at 6.8 and 7.5 AU. Everhart (1973) found some of these orbits stable for >50,000 yr. These zones are near the 2:3 and 4:7 commensurabilities with Jupiter and 5:3 and 10:7 with Saturn. It is not known whether these zones are stable for the age of the solar system, but no such objects have yet been discovered.

Birn (1973) integrated hypothetical, initially circular orbits interior to Jupiter and found that boundaries of stability between planets occur at first-order commensurabilities with the adjacent planet. To speed up his integrations, he increased the masses of the planets over present values, but that modifies the dynamics; perturbations on the position of an object scales with the mass to the power 1, ½, and 0 for short-period, commensurate, and "secular" terms so that the relative importance of different terms differs from reality. Alfvén et al (1974) explain the outer-belt boundary by a process other than pure gravitational dynamics. They calculate that it should occur at 3.47 AU (2/3 Jupiter's a) due to condensation of grains in a partially corotating plasma.

Weidenschilling (1975) has addressed the question of why an asteroid planet failed to grow. When a planet grows large enough, remaining planetesimals are random-walked into orbits of higher e and i. As Jupiter-crossing planetesimals increase in e, they should first cross the asteroid belt, then Mars, and then Earth at which time their ejection probability coincidentally becomes significant. He notes the inverse correlation of bombardment time with present planetary masses in these zones and suggests that this intense bombardment may have inhibited the growth of Mars and, especially, the asteroids. Similar disruption by high-velocity bodies with different origins has been suggested by Wetherill (1975). While such bombardment certainly could have depleted the asteroid population, the present size-distribution is controlled by the interasteroidal collisions at 5 km sec^{-1} due to moderate e's and i's. The origin of these velocities is not known, but probably cannot be explained by collisions since they tend to catastrophically fragment bodies rather than change orbits.

This raises yet another objection to the "exploded planet" theory for the origin of the belt (Sect. IV F). Such an explosion would produce orbits that cross at the distance of the explosion. But the separation of orbits in the belt exceeds the distance between the inner belt and Earth. Nearly circular orbits exist from the belt's innermost edge to its outermost edge, a range of 1.9 AU and, if the Trojans are included, this spread is 3.3 AU. Planetary perturbations cannot make crossing eccentric orbits into separated circular orbits. To accomplish this feat by collisions, without disrupting a body, would require $\gtrsim 10^3$ collisions just under the threshold for disruption. As improbable as such a scenario would be for a single body, it is absurd to rely on such a process for reordering orbits of multitudes of asteroids.

C. Geochemical Evolution of Asteroids

The recent deluge of data on the physical properties of asteroids permits us to begin to consider them as "planets" in their own right and to discuss how they evolved to their current form. To the extent that meteorites are, in fact, asteroid fragments, we can discuss the geochemical evolution of these bodies more knowledgeably than for any other planets besides the moon and Earth. Indeed the meteorites most indicative of geochemical and thermal evolution in large parent bodies -- the most differentiated meteorites -- are almost certainly derived from the asteroid belt. There is a concordance between spectral identification of surface mineralogies for inner-belt asteroids and dynamical probabilities of deriving meteorites from them (Wetherill & Williams 1977) as well as between the measured sizes of these bodies and dimensions inferred from cooling curves for many metallic meteorites. Furthermore, the large asteroid Vesta seems to be uniquely well suited as the parent body for basaltic achondrites (Consolmagno & Drake 1977) despite the lack of a clear transport mechanism from Vesta to Earth.

It is also plausible that many carbonaceous chondrites are derived from the asteroid belt, if for no other reason than that C-type asteroids predominate in the belt. But a real problem concerns the ordinary chondrites, the most common type of meteorite. No definitely confirmed asteroid analog for ordinary chondrites has been found in the main belt so far. It may be quantitatively possible to obtain sufficient yield from as-yet-unobserved asteroids, but it seems increasingly improbable. Moreover, the association of ordinary chondrites with Apollo asteroids (Chapman et al 1973b, Levin et al 1976) combined with the difficulties we have mentioned before in deriving most Apollos from the main belt lends credence to the idea that ordinary chondrites are of cometary origin. Although this idea does violence to many prejudices concerning the likely environments in comet cores, inferences from measured properties of chondrites, and models for the condensation of the solar nebula, it must be taken seriously. We must then examine possible ways of forming ordinary chondrites in the outer solar system or ways that major constituents of comet cores might have been derived from the inner solar system. The asteroid belt might yet be salvaged as a location for parent bodies of ordinary chondrites if (1) the common S-type asteroids are actually ordinary chondrites rather than the preferred stony-irons and if (2) further dynamical investigations uncover major additional transport mechanisms for both meteorites and Apollo asteroids.

A preliminary model for the geochemical evolution of asteroids has been descirbed and updated by Chapman (1976, 1977). These ideas are too new, and the data are increasing too rapidly to warrant summary here. We conclude our review with one of the most interesting questions: the nature of heating processes in the early solar system. Asteroids evidencing thermal evolution provide an extreme measure of the efficacy of heating processes since small objects cool so rapidly. The fact that the third largest asteroid appears to have been heated substantially while the largest retains a primitive composition illustrates the complexity of the problem (cf Matson et al 1976). Short-lived radionuclides such as Al-26 (Lee et al 1976) may have been injected into different asteroids in different amounts or at different times with respect to accretion. Another possible mechanism -- electrical induction by the solar wind during the presumed T Tauri phase of solar evolution -- may be most effective for moderately large (but not the largest) asteroids (Herbert & Sonett 1977). Collisions among asteroids, or between asteroids and high-velocity planetesimals, may have contributed to heat budgets, but it is likely that collisional melts, of which we may have a few meteoritic examples (nahklites; cf Bogard and Husain 1977), were locally restricted on parent bodies.

ACKNOWLEDGMENTS

This review was supported in part by the NASA Planetary Astronomy Program (NASA Contract NASW-2983). Another part of this work was one phase of research carried out at the Jet Propulsion Laboratory, California Institute of Technology, under NASA Contract NAS 7-100. We thank numerous colleagues (including B. Marsden, D. Morrison, and G. Wetherill) for critical reviews of earlier drafts of this manuscript. D. Davis and J. Metcalfe helped in the late phases of the project. This is PSI Contribution No. 55.

Literature Cited

Adams, J. B. 1975. In Infrared and Raman Spectroscopy of Lunar and Terrestrial Minerals, ed. C. Karr, Jr. pp 91-116. New York: Academic Press.

Alfvén, H., Arrhenius, G. 1970a. Astrophys. Space Sci. 8:338-421.

Alfvén, H., Arrhenius, G. 1970b. Astrophys. Space Sci. 9:3-33.

Alfvén, H., Ip, W.-H., Burkenroad, M. D. 1974. Nature 250:634-36.

Allen, D. A. 1970. Nature 227:158-59.

Anders, E. 1965. Icarus 4:399-408.

Anders, E. 1975. Icarus 24:363-71.

Arnold, J. R. 1969. Astron. J. 74:1235-42.

Bender, D., Bowell, E., Chapman, C., Gaffey, M., Gehrels, T., Zellner, B., Morrison, D., Tedesco, E. 1978. Icarus. In press.

Birn, J. 1973. Astron. Astrophys. 24:283-93.

Bogard, D. D., Husain, L. 1977. Geophys. Res. Lett. 4:69-71.

Bowell, E. 1977. Bull. Am. Astron. Soc. In press ; also in Relationships Between Comets, Minor Planets, and Meteorites, ed. A. H. Delsemme, Univ. of Toledo Publications. In press.

Bowell, E., Chapman, C. R., Gradie, J., Morrison, D., Zellner, B. 1978. Icarus. (submitted)

Brouwer, D. 1951. Astron. J. 56:9-32.

Burns, J. A. 1975. Icarus 25:545-54.

Caldwell, J. 1975. Icarus 25:384-96.

Chapman, C. R. 1974. Geophys. Res. Lett. 1:341-44.

Chapman, C. R. 1976. Geochim. Cosmochim. Acta 40:701-19.

Chapman, C. R. 1977. In Relationships Between Comets, Minor Planets, and Meteorites, ed. A.H. Delsemme, Univ. of Toledo Publications. In press.

Chapman, C. R., Davis, D. R. 1975. Science 190:553-56.

Chapman, C. R., Davis, D. R., Greenberg, R. 1977. NASA TM X-3511, 72-73.

Chapman, C. R., Johnson, T. V., McCord, T. B. 1971. See Gehrels 1971, pp 51-65.

Chapman, C. R., McCord, T. B., Johnson, T. V. 1973a. Astron. J. 78:126-40.

Chapman, C. R., McCord, T. B., Pieters, C. 1973b. Astron. J. 78:502-05.

Chapman, C. R., Morrison, D. 1976. Icarus 28:91-94.

Chapman, C. R., Morrison, D., Zellner, B. 1975. Icarus 25:104-30.

Conklin, E. K., Ulich, B. L., Dickel, J. R., Ther, D. 1977. See Chapman 1977.

Consolmagno, G. J., Drake, M. J. 1977. Geochim. Cosmochim. Acta 41:1271-82.

Degewij, J., Gehrels, T. 1976. Bull. Am. Astron. Soc. 8:459.

Degewij, J., Gradie, J., Zellner, B. 1978. Astron. J. (submitted)

Dohnanyi, J. S. 1969. J. Geophys. Res. 74:2531-54.

Dohnanyi, J. S. 1971. See Gehrels 1971, pp 263-95.

Dollfus, A. 1971. See Gehrels 1971, pp 25-31.

Duncombe, R. L., Klepczynski, W. K., Seidelmann, P. K. 1973. Fund. Cosmic Phys. 1:119-65.

Dunlap, J. L. 1971. See Gehrels 1971, pp 147-54.

Eginitis, D. 1889. Annales de L'Observatoire de Paris 19:H.1-H.16.

Everhart, E. 1973. Astron. J. 78:316-28.

Franklin, F. A., Marsden, B. G., Williams, J. G., Bardwell, C. M. 1975. Astron. J. 80:729-46.

Froeschlé, C., Scholl, H. 1976. Astron. Astrophys. 48:389-93.

Gaffey, M. J., McCord, T. B. 1977a. Space Sci. Rev. (submitted)

Gaffey, M. J., McCord, T. B. 1977b. Proc. Lunar Sci. Conf., 8th. In press.

Gaffey, M. J., McCord, T. B. 1977c. Tech. Rev. 79:50-59.

Gehrels, T. 1970. In Surfaces and Interiors of Planets and Satellites, ed. A. Dollfus, pp 371-75. New York: Academic Press.

Gehrels, T., ed. 1971. Physical Studies of Minor Planets, NASA SP-267. Washington: NASA. 687 pp.

Gehrels, T., Gehrels, N. 1977. See Chapman 1977.

Gehrels, T., Taylor, R. C. 1977. Astron. J. 82:229-37.

Giffen, R. 1973. Astron. Astrophys. 23:387-403.

Gradie, J., Leake, M., Morrison, D. 1977. Meteoritics. In press.

Gradie, J., Zellner, B. 1977. Science 197:254-55.

Greenberg, R. 1976. In Jupiter, ed. T. Gehrels, 122-132. Tucson: Univ. Ariz. Pres

Greenberg, R., Davis, D. R., Hartmann, W. K., Chapman, C. R. 1977. Icarus 30:769-79.

Greenberg, R., Franklin, F. 1975. MNRAS 173:1-8.

Greenberg, R., Wacker, J. F., Hartmann, W. K., Chapman, C. R., 1978. Icarus (submitted)

Hansen, O. L. 1977. Icarus 31:456-82.

Harris, A. W. 1977. Icarus (submitted)

Hartmann, W. K. 1969. Icarus 10:201-13.

Hartmann, W. K. 1972. Astrophys. Space Sci. 17:48-64.

Hartmann, W. K. 1976. Icarus 27:553-559.

Hartmann, W. K. 1978. Icarus 33. In press.

Hartmann, W. K., Hartmann, A. C. 1968. Icarus 8:361-81.

Heppenheimer, T. A. 1975. Astron. J. 80:465-72.

Herbert, F., Sonett, C. 1977. Astrophys. Space Sci. Submitted.

Hertz, H. G. 1968. Science 160:299-300.

Hirayama, K. 1928. Jap. J. Astron. Geophys. 5:137-62.

Horedt, Gp. 1974. Icarus 23:459-64.

Housen, K. R., Wilkening, L.L., Greenberg, R., Chapman, C.R. 1977. Bull. Am. Astron. Soc. In press.

Ip, W.-H., Mehra, R. 1973. Astron. J. 78:142-47.

Janiczek, P. M., Seidelmann, P. K., Duncombe, R. L. 1972. Astron. J. 77:764-73.

Jefferys, W. H. 1967. Astron. J. 72:872-75.

Johnson, T. V., McGetchin, T. R. 1973. Icarus 18:612-20.

Jurgens, R. F., Goldstein, R. M. 1976. Icarus 28:1-15.

KenKnight, C. E., Rosenberg, D. L., Wehner, G. K. 1967. J. Geophys. Res. 72:3105-29.

Kiang, T. 1966. Icarus 5:437-49.

Kiang, T. 1971. See Gehrels 1971, pp 187-95.

Kresák, L. 1967. Bull. Astron. Inst. Czech. 18:27-36.

Kresák, L. 1971. See Gehrels 1971, pp 197-210.

Kresák, L. 1977. Bull. Astron. Inst. Czech. 28:65-82.

Kuiper, G. P., Fujita, Y., Gehrels, T., Groeneveld, I., Kent, J., Van Biesbroeck, G., van Houten, C. J. 1958. Astrophys. J. Suppl. Ser. 3:289-334.

Lacis, A. A., Fix, J. D. 1971. See Gehrels 1971, pp 141-46.

Lagerkvist, C.-I. 1975. Astron. Astrophys. 45:439-40.

Larson, H. P., Fink, U. 1975. Icarus 26:420-27.

Larson, H. P., Fink, U., Treffers, R. R., Gautier, T. N. III. 1976. Icarus 28:95-103.

Lebofsky, L. A. 1977. MNRAS (submitted)

Lecar, M., Franklin, F.A. 1973. Icarus 20:422-36.

Lee, T., Papanastassiou, D. A., Wasserburg, G. J. 1976. Geophys. Res. Lett. 3:109-11

Levin, B. J. 1977. See Chapman 1977.

Levin, B. J., Simonenko, A. N., Anders, E. 1976. Icarus 28:307-24.

Lowrey, B. E. 1971. J. Geophys. Res. 76:4084-89.

Marsden, B. G. 1970. Astron. J. 75:206-17.

Marsden, B. G. 1972. Proc. IAU Colloq. 45, pp. 239-43.

Matson, D. L., Fanale, F. P., Johnson, T. V., Veeder, G. J. 1976. Proc. Lunar Sci. Conf., 7th, pp 3603-27.

Matson, D. L., Johnson, T. V., Veeder, G. J. 1977. Proc. Lunar Sci. Conf., 8th, In press.

McAdoo, D. C., Burns, J. A. 1974. Icarus 21:86-93.

McCord, T. B., Adams, J. B., Johnson, T. V. 1970. Science 168:1445-47.

McCord, T. B., Chapman, C. R. 1975a. Astrophys. J. 195:553-62.

McCord, T. B., Chapman, C. R. 1975b. Astrophys. J. 197:781-89.

Morrison, D. 1976. Geophys. Res. Lett. 3:701-04.

Morrison, D. 1977. Icarus 31:185-220.

Napier, W. McD., Dodd, R. J. 1974. MNRAS 166:469-89.

O'Keefe, J. D., Ahrens, T. J. 1976. Proc. Lunar Sci. Conf., 7th, pp 3007-25.

O'Leary, B., Marsden, B. G., Dragon, R., Hauser, E., McGrath, M., Backus, P., Robkoff, H. 1976. Icarus 28:133-46.

Ovenden, M. W. 1972. Nature 239:508-9.

Ovenden, M. W. 1973. In Recent Advances in Dynamical Astronomy, ed. B. D. Tapley and V. Szebehely, pp 319-32. Dordrecht :Reidel.

Pellas, P. 1972. In From Plasma to Planet, ed. A. Elvius, pp 65-92. New York: John Wiley.

Peterson, C. 1976. Icarus 29:91-111.

Pilcher, F., Meeus, J. 1973. Tables of Minor Planets. Privately published. (Library of Congress Catalog Card #73-80379). 104 pp.

Rajan, R. S. 1974. Geochim. Cosmochim. Acta 38:777-88.

Sather, R. E. 1976. Astron. J. 81:67-73.

Schober, H. J. 1977. Astron. Astrophys. In press.

Scholl, H. 1973. Astron. Astrophys. 25:203-9.

Scholl, H., Froeschlé, C. 1974. Astron. Astrophys. 33:455-58.

Scholl, H., Froeschlé, C. 1975. Astron. Astrophys. 42:457-63.

Scholl, H., Giffen, R. 1974. Proc. IAU Symp. No. 62, pp 77-80.

Schubart, J. 1974. Astron. Astrophys. 30:289-92.

Schubart, J. 1975. Astron. Astrophys. 39:147-48.

Sekanina, Z. 1973. Icarus 18:253-84.

Shoemaker, E. M., Helin, E. F., Gillett, S. L. 1977. Geologica Romana. In press.

Soter, S. 1971. CRSR 462 Cornell Univ., Ithaca, NY.

Strom, R. G., Whitaker, E. A. 1976. NASA Tech. Memo, X-3364, pp 194-96.

Taylor, G. E., Dunham, D. W. 1977. Icarus (submitted)

Taylor, R. C. 1971. See Gehrels 1971, pp 117-31.

Taylor, R. C., Gehrels, T., Capen, R. C. 1976. Astron. J. 81:778-86.

Van Flandern, T. 1975. Bull. Am. Astron. Soc. 7:467.

van Houten, C. J. 1971. See Gehrels 1971, pp 292-295.

van Houten, C. J., van Houten-Groeneveld, I., Herget, P., Gehrels, T. 1970. Astron. Astrophys. Suppl. 2:339-448.

Veeder, G. J., Matson, D. L., Smith, J. C. 1977. Astron. J. In press.

Walsh, T. F., Zimmerman, P. D. 1971. Nature 230:233-34.

Weidenschilling, S.J. 1975. Icarus 26:361-66.

Weissman, P. R., Wetherill, G. W. 1974. Astron. J. 79:404-12.

Wetherill, G. W. 1967. J. Geophys. Res. 72:2429-44.

Wetherill, G. W. 1974 Ann. Rev. Earth Planet. Sci. 2:303-31.

Wetherill, G. W. 1975. In Lunar Science VI, pp. 866-68 (Abstr.)

Wetherill, G. W. 1976. Geochim. Cosmochim. Acta 40:1249-1317.

Wetherill, G. W. 1977. Proc. Lunar Sci. Conf., 8th. In press.

Wetherill, G. W., Williams, J. G. 1977. Proc. 2nd Intl. Conf. Origin and Distribution of Elements (I.A.G.C.), In press.

Widorn, T. 1967. Ann. Univ. Sternw. Wien 27:112-19.

Wiesel, W. E. 1974a. Harvard CFA Preprint Series, No. 191.

Wiesel, W. E. 1974b. Harvard CFA Preprint Series, No. 204.

Williams, J. G. 1973a. Eos, Trans. Am. Geophys. Union 54:233.

Williams, J. G. 1973b. Bull. Am. Astron. Soc. 5:363.

Williams, J. G. 1975a. J. Geophys. Res. 80:2914-16.

Williams, J. G. 1975b. Bull. Am. Astron. Soc. 7:343.

Williams, J. G., Wetherill, G. W. 1973. Astron. J. 78:510-15.

Worden, S. P., Stein, M. K., Schmidt, G. D., Angel, J. R. P. 1977. Icarus In press.

Zellner, B., Andersson, L., Gradie, J. 1977c. Icarus 31:447-55.

Zellner, B., Bowell, E. 1977. See Chapman 1977.

Zellner, B., Gradie, J. 1976. Astron. J. 81:262-80.

Zellner, B., Leake, M., Lebertre, T., Duseaux, M., Dollfus, A. 1977a. Proc. Lunar Sci. Conf., 8th. In press.

Zellner, B., Leake, M., Morrison, D., Williams, J. G. 1977d. Geochim. Cosmochim. Acta In press.

Zellner, B., Lebertre, T., Day, K. 1977b. Proc. Lunar Sci. Conf, 8th. In press.

Zellner, B., Wisniewski, W. Z., Andersson, L., Bowell, E. 1975. Astron. J. 80:986-95.

Zimmerman, P. D., Wetherill, G. W. 1973. Science 182:51-53.

Table 1. Asteroid taxonomies and mineralogical classifications

	Taxonomic Class[a]	Mineralogical Class, Meteorite Analog, or Descriptor[b]	Type Asteroids[c]	Typical B-V[d]	Typical Albedo[d]
flat spectra	mostly C	C*, carbonaceous chondrite? (F + TB)	213, 2, 10, 88, 511, 1	0.63 - 0.74	0.04 - 0.07
		C2 or CM, carbonaceous chondrite (TA + TC)	324, 51	0.72 - 0.80	0.03 - 0.04
transitional spectra	M	metal or enstatite chondrite (RR)	16, 21, 22	0.70 - 0.72	0.09 - 0.11
	E	enstatite achondrite	44	0.72	0.35
	(U)	intermediate (various T)	166, 48	0.77	0.03
	(U)	basaltic achondrite	4, 69 (?)	0.77	0.23
	(U)	Trojan	624	0.77	0.04
reddish spectra	mostly S	metal-rich (plus silicate?) (RF)	9, 12	0.87 - 0.88	0.13 - 0.14
		metal plus olivine (RA-1)	7, 39	0.82 - 0.92	0.14 - 0.16
		metal plus pyroxene (plus minor olivine?) (RA-2 + TE)	29, 3, 6, 230, 25	0.87 - 0.91	0.10 - 0.17
		pyroxene-rich plus metal (RA-3)	89, 5, 63, 446	0.83 - 0.91	0.13 - 0.14
		metal-poor, opaque-poor, pyroxene-rich	8	0.88	0.14
high-contrast spectra	(U)	L ordinary chondrite?	385	0.88	0.12
	R	LL ordinary chondrite or olivine achondrite?	349	0.96	0.26
	?	? (steep red spectrum)	170	?	?
	(U)	(carbonaceous?) chondrite type 3 (TD)	80	0.89	0.14

[a] Bowell et al (1978).

[b] Descriptor slightly modified from Chapman (1976). Letters in parentheses are corresponding compositional groups of Gaffey and McCord (1977a, b).

[c] Asteroids typifying the 34 spectral groups found by McCord and Chapman (1975a, b), augmented by the 44 Nysa group (Zellner et al 1977d).

[d] Typical colors and albedos are only indicative.

Notes to Tables 2, 3, and 4

These tabulate Trojans, Hildas, and Earth-approaching ($q < 1.5$ AU) asteroids. Columns give catalog number, name, semi-major axis, eccentricity, inclination, perihelion and aphelion distances, and absolute and mean opposition B magnitudes. P and F indicate Trojan clouds preceding or following Jupiter in its orbit. The least secure Trojan orbits are for PLS objects 2706 and 9507. 334 Chicago and 1256 Normannia are excluded from the Hildas since they do not librate. The last column in the Earth-approachers table indicates observational status, hence orbital accuracy. Several magnitudes were provided by E. Roemer in advance of publication.

Table 2. Trojans

NUMBER	NAME	A	E	I	Q1	Q2	B(1,0)	B(A,0)	
588	ACHILLES	5.21	.148	10.3	4.44	5.98	9.44	16.15	P
617	PATROCLUS	5.21	.141	22.1	4.47	5.94	9.16	15.86	F
624	HEKTOR	5.12	.025	18.3	4.99	5.25	8.67	15.29	P
659	NESTOR	5.26	.110	4.5	4.68	5.84	9.69	16.44	P
884	PRIAMUS	5.19	.120	8.9	4.56	5.81	9.87	16.55	F
911	AGAMEMNON	5.15	.067	21.9	4.81	5.50	8.92	15.57	P
1143	ODYSSEUS	5.21	.093	3.1	4.73	5.70	9.44	16.15	P
1172	ANEAS	5.17	.102	16.7	4.64	5.69	9.42	16.08	F
1173	ANCHISES	5.17	.141	6.9	4.44	5.89	10.13	16.79	F
1208	TROILUS	5.17	.093	33.7	4.68	5.65	9.79	16.45	F
1404	AJAX	5.21	.113	18.1	4.62	5.80	10.27	16.97	P
1437	DIOMEDES	5.08	.046	20.6	4.85	5.32	9.23	15.82	P
1583	ANTILOCHUS	5.28	.054	28.3	4.99	5.56	9.81	16.58	P
1647	MENELAUS	5.22	.028	5.6	5.08	5.37	11.50	18.22	P
1749	TELAMON	5.27	.111	6.1	4.68	5.85	11.20	17.96	P
1867	DEIPHOBUS	5.20	.045	26.8	4.97	5.44	10.60	17.30	F
1868	THERSITES	5.18	.108	16.9	4.62	5.74	10.75	17.43	P
1869	PHILOCTETES	5.26	.061	4.0	4.94	5.58	12.32	19.07	P
1870	GLAUKOS	5.21	.031	6.6	5.05	5.37	11.90	18.61	F
1871	ASTYANAX	5.33	.034	8.6	5.15	5.51	12.30	19.12	F
1872	HELENOS	5.11	.043	14.8	4.89	5.32	11.50	18.11	F
1873	AGENOR	5.25	.091	21.9	4.77	5.73	11.70	18.44	F
	2706P-L	5.07	.119	1.2	4.47	5.68	14.14	20.72	P
	4139P-L	5.14	.003	17.6	5.13	5.16	12.44	19.08	P
	4523P-L	5.15	.049	.9	4.89	5.40	12.38	19.03	P
	4572P-L	5.17	.057	9.3	4.87	5.46	12.88	19.55	P
	4655P-L	5.25	.031	17.1	5.08	5.41	11.93	18.67	P
	6020P-L	5.24	.094	1.4	4.75	5.73	13.06	19.79	P

Table 2 (Cont.)

6540P-L	5.26	.059	9.1	4.95	5.57	12.79	19.54	P
6541P-L	5.25	.087	8.1	4.80	5.71	12.82	19.57	P
6581P-L	5.32	.030	4.9	5.16	5.48	12.10	18.91	P
6591P-L	5.31	.042	7.4	5.08	5.53	12.32	19.11	P
6629P-L	5.07	.007	4.2	5.03	5.10	12.30	18.95	P
6844P-L	5.21	.103	8.2	4.67	5.74	13.80	20.58	P
9507P-L	5.08	.114	5.0	4.50	5.66	11.96	18.54	P

ORIGINAL PAGE IS
OF POOR QUALITY

Table 3. Hildas

NUMBER	NAME	A	E	I	Q1	Q2	B(1,0)	B(A,0)
153	HILDA	3.98	.154	7.8	3.36	4.59	8.85	14.21
190	ISMENE	3.95	.170	6.2	3.28	4.62	8.58	13.92
361	BONONIA	3.93	.214	12.7	3.09	4.77	9.65	14.96
499	VENUSIA	3.96	.222	2.1	3.08	4.84	10.22	15.57
748	SIMEISA	3.95	.176	2.3	3.26	4.64	9.85	15.18
958	ASPLINDA	3.94	.191	5.7	3.19	4.70	11.13	16.45
1038	TUCKIA	3.93	.243	9.2	2.97	4.88	11.69	16.99
1162	LARISSA	3.94	.110	1.9	3.51	4.38	10.34	15.66
1180	RITA	3.98	.173	7.2	3.29	4.67	10.23	15.60
1202	MARINA	3.95	.197	3.4	3.17	4.73	11.41	16.74
1212	FRANCETTE	3.95	.184	7.6	3.23	4.68	10.90	16.24
1268	LIBYA	3.93	.106	4.4	3.51	4.35	9.99	15.30
1269	ROLLANDIA	3.94	.074	2.7	3.65	4.23	9.75	15.07
1345	POTOMAC	3.98	.179	11.4	3.27	4.70	10.81	16.18
1439	VOGTIA	3.98	.115	4.2	3.52	4.44	11.24	16.61
1512	OULU	3.93	.162	6.6	3.30	4.57	10.50	15.81
1529	OTERMA	4.00	.194	9.0	3.22	4.77	11.29	16.68
1578	KIRKWOOD	3.96	.223	.8	3.08	4.84	11.84	17.18
1746	BROUWER	3.97	.197	8.4	3.19	4.75	10.90	16.26
1748	MAUDERLI	3.92	.234	3.3	3.00	4.84	11.70	16.99
1754	CUNNINGHAM	3.99	.163	12.0	3.34	4.64	10.60	15.99
1877	MARSDEN	3.96	.213	17.5	3.11	4.80	12.40	17.74
1902	SHAPOSHNIKOV	3.97	.224	12.5	3.08	4.87	10.60	15.96
1911	SCHUBART	3.98	.162	1.7	3.33	4.62	11.30	16.67
1941	WILD	3.99	.278	3.9	2.88	5.10	12.50	17.89
	2033P-L	3.99	.168	3.5	3.33	4.66	13.66	19.05
	2159P-L	3.93	.165	5.6	3.28	4.57	11.68	16.98
	2554P-L	3.98	.238	3.5	3.03	4.92	13.94	19.30

2696P-L	3.93	.213	2.9	3.10	4.77	15.30	20.61
2709P-L	4.04	.272	3.3	2.94	5.13	15.83	21.27
4282P-L	3.96	.199	8.3	3.17	4.75	15.36	20.71
4652P-L	3.97	.120	6.7	3.49	4.44	13.44	18.79
4710P-L	4.03	.243	6.8	3.05	5.01	15.51	20.94
6847P-L	3.97	.300	8.8	2.78	5.16	16.19	21.55

	1972RB	2.17	.492	5.2	1.10	3.23	20.00	22.02	RECOVERABLE?
1580	BETULIA	2.20	.490	52.0	1.12	3.27	15.66	17.76	SECURE
1627	IVAR	1.86	.397	8.4	1.12	2.60	14.23	15.27	SECURE
	1972RA	2.36	.523	9.0	1.13	3.60	18.50	21.04	RECOVERABLE
433	EROS	1.46	.223	10.8	1.13	1.78	11.88	11.00	SECURE
887	ALINDA	2.52	.544	9.1	1.15	3.88	15.39	18.30	SECURE
	4788P-L	2.55	.545	10.8	1.16	3.93	17.89	20.87	LOST
719	ALBERT	2.58	.540	10.8	1.19	3.98	16.87	19.93	LOST
1036	GANYMED	2.66	.542	26.3	1.22	4.10	10.86	14.08	SECURE
	1963UA	2.65	.530	11.1	1.24	4.05	17.80	20.99	SECURE
1916	1953RA	2.27	.450	12.8	1.25	3.30	15.60	17.91	SECURE
1951	LICK	1.39	.062	39.1	1.30	1.48	15.80	14.47	SECURE
	1971SC	2.21	.390	12.0	1.34	3.07	16.50	18.62	LOST?
	1974UB	2.12	.359	36.3	1.36	2.89	14.00	15.89	SECURE
1474	BEIRA	2.73	.490	26.8	1.39	4.07	13.02	16.40	SECURE
	2108P-L	2.32	.385	2.6	1.43	3.21	19.60	22.03	LOST
1134	KEPLER	2.68	.467	15.0	1.43	3.93	15.39	18.66	SECURE
	4548P-L	2.17	.340	17.5	1.43	2.91	18.55	20.58	LOST
1009	SIRENE	2.63	.454	15.8	1.44	3.82	16.92	20.08	RECOVERABLE?
1139	ATAMI	1.95	.255	13.1	1.45	2.44	14.35	15.68	SECURE
	1963RH	2.38	.379	21.1	1.48	3.28	14.20	16.79	LOST
	1975AD	2.37	.375	20.1	1.48	3.26	14.00	16.55	SECURE
1198	ATLANTIS	2.25	.335	2.7	1.49	3.00	16.79	19.03	LOST

Table 4 (Cont.)

NUMBER	NAME	A	E	I	Q1	Q2	B(1,0)	B(A,0)	STATUS
1566	ICARUS	1.08	.827	23.0	.19	1.97	17.62	12.23	SECURE
	1974MA	1.76	.760	37.7	.42	3.09	15.00	15.62	LOST?
	1936CA ADONIS	1.87	.764	1.4	.44	3.30	18.60	19.66	SECURE
	1976UA	.84	.451	5.9	.46	1.22	21.50	17.10	RECOVERABLE
1864	DAEDALUS	1.46	.615	22.1	.56	2.36	16.34	15.48	SECURE
1865	CERBERUS	1.08	.467	16.1	.58	1.58	17.50	12.19	SECURE
	1937UB HERMES	1.64	.624	6.2	.62	2.66	18.10	18.20	LOST
1981	1973EA	1.78	.650	39.8	.62	2.93	16.40	17.10	SECURE
1862	APOLLO	1.47	.560	6.4	.65	2.29	17.00	16.20	SECURE
1685	TORO	1.37	.436	9.4	.77	1.96	14.90	13.41	SECURE
	1976AA	.97	.182	18.9	.79	1.14	18.36	10.91	SECURE
	6743P-L	1.62	.493	7.3	.82	2.42	18.41	18.42	LOST
1620	GEOGRAPHOS	1.24	.335	13.3	.83	1.66	16.67	14.08	SECURE
	1976WA	2.41	.656	24.3	.83	3.99	16.30	18.95	RECOVERABLE
	1947XC	2.25	.630	1.0	.83	3.67	16.00	18.25	LOST
	1959LM	1.34	.379	3.3	.83	1.85	14.00	12.32	LOST
	1950DA	1.68	.502	12.1	.84	2.53	16.90	17.20	LOST?
1866	SISYPHUS	1.89	.540	41.1	.87	2.92	13.70	14.84	SECURE
	1973NA	2.39	.633	67.9	.88	3.91	15.40	18.01	LOST?
1863	ANTINOUS	2.26	.606	18.4	.89	3.63	16.50	18.77	SECURE
	1975YA	1.29	.298	64.0	.91	1.67	17.50	15.37	RECOVERABLE
	6344P-L	2.58	.635	4.6	.94	4.21	23.02	26.06	LOST
	1960UA	2.26	.537	3.7	1.05	3.48	18.10	20.39	RECOVERABLE
1915	QUETZALCOATL	2.52	.583	20.5	1.05	3.99	19.30	22.22	SECURE
1917	CUYO	2.15	.505	24.0	1.06	3.23	16.50	18.46	SECURE
1943	1973EC	1.43	.256	8.7	1.06	1.80	16.50	15.45	SECURE
1980	1950LA	1.71	.365	26.8	1.08	2.33	15.00	15.42	SECURE
1221	AMOR	1.92	.436	11.9	1.08	2.76	19.16	20.40	SECURE

FIGURE CAPTIONS

Figure 1: Diameter-frequency distribution for asteroids. Points are bias-corrected counts in increments of 0.05 in log D (Zellner & Bowell 1977). Lines are possible fits and extrapolations, constrained at small D by Palomar-Leiden Survey data.

Figure 2: Proper _e_ vs proper sin _i_ values for asteroids in a small part of the belt show the very populous Eos family. It contains 78 members in a volume of proper _a_-_e_-sin _i_ space that would normally contain less than one object by chance.

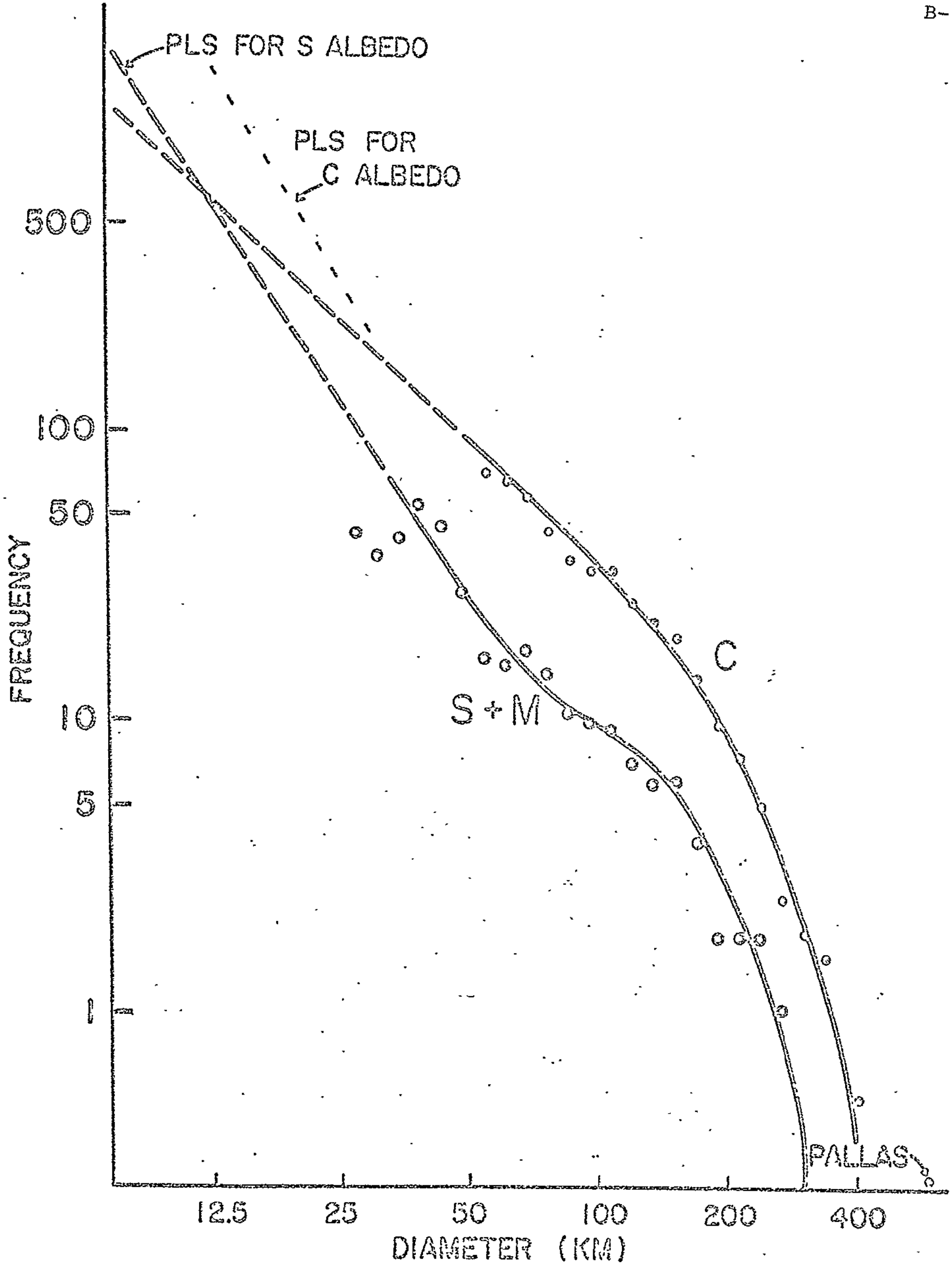
PLS FOR S ALBEDO
PLS FOR
C ALBEDO
500
100
50
10
5
1
FREQUENCY
C
S + M
PALLAS
12.5
25
50
100
200
400
DIAMETER (KM)

Figure 1

EOS FAMILY

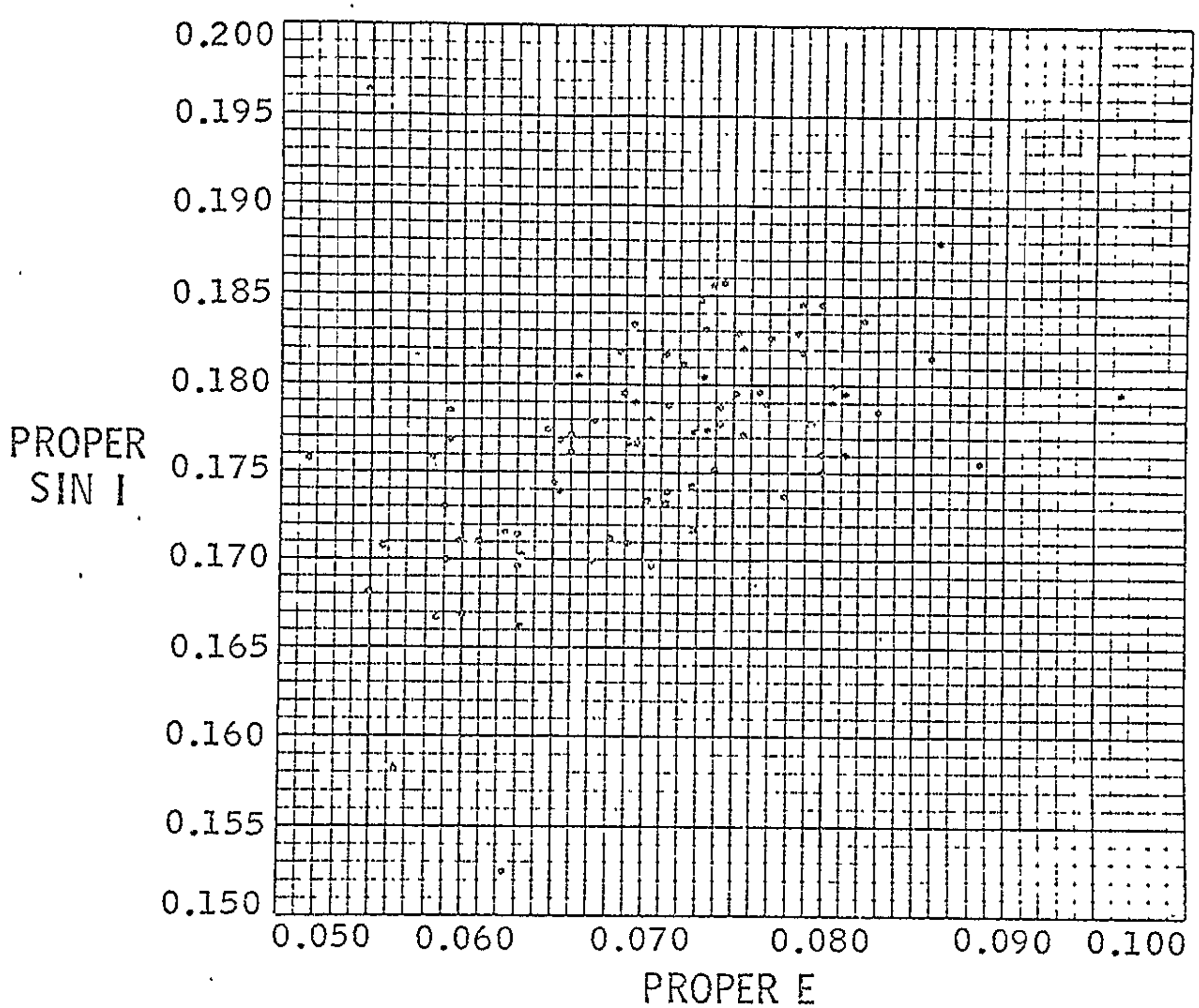

0.200
0.195
0.190
0.185
0.180
0.175
0.170
0.165
0.160
0.155
0.150
PROPER SIN I
0.050
0.060
0.070
0.080
0.090
0.100
PROPER E

APPENDIX C

<u>UBV Pinhole Scans of Saturn's Disk</u>. O. G. FRANZ, <u>Lowell Observatory</u>, and M. J. PRICE, <u>Planetary Science Institute</u>. - A photoelectric area scanner, equipped with a circular aperture of 0.64 arcsec (100 μ) diameter, was used in conjunction with the 72-inch Perkins reflector at the Lowell Observatory to obtain UBV scans of Saturn's disk on several nights in the winter and spring of 1977. The resulting intensity profiles show pronounced limb brightening in U, moderate limb brightening in B, and limb darkening in V. They also display, in all three colors, distinct east-to-west asymmetry varying with solar phase angle. In interpreting these observations, elementary radiative-transfer models are used to describe scattering in the atmosphere above the visible cloud layer. Limits are placed on the optical thickness of the gas above the clouds. The probable structure of Saturn's atmosphere is briefly discussed. This research was supported by the National Aeronautics and Space Administration under Contract NASW-2983 and by the National Science Foundation. Some of the data processing was carried out with the support of NASA Grant NGR-03-003-001.

Type of paper:
1) oral presentation [ ] 5 min.
[X] 10 min.
2) read by title only [ ]
3) invited lecture [ ]
4) percent published elsewhere____

Billing information:

We agree to pay $20 in partial support of the publication of the abstract in the B.A.A.S.

Date: 26 August 1977

Lowell Observatory
Post Office Box 1269
Flagstaff, Arizona 86002

Arthur A. Hoag
Authorized Agent

APPENDIX D

URANUS: LIMB AND POLAR BRIGHTENING AT 7300 Å

OTTO G. FRANZ AND MICHAEL J. PRICE

Reprinted for private circulation from
THE ASTROPHYSICAL JOURNAL, Vol. 214, No. 3, Part 2, 1977 June 15

THE ASTROPHYSICAL JOURNAL, 214:L145–L146, 1977 June 15

URANUS: LIMB AND POLAR BRIGHTENING AT 7300 Å

OTTO G. FRANZ
Lowell Observatory, Flagstaff, Arizona

AND

MICHAEL J. PRICE
Planetary Science Institute, Tucson, Arizona

Received 1976 November 15; revised 1977 March 15

ABSTRACT

Pinhole photoelectric area-scanning photometry of the Uranus disk demonstrates directly the existence of both limb and polar brightening in the 7300 Å CH_4 band. Polar brightening, which appears to be present also at continuum wavelengths, is interpreted as being caused by scattering in in a thin aerosol haze located over the polar region.

Subject headings: planets: atmospheres—planets: Uranus

I. INTRODUCTION

Limb brightening of Uranus was first detected by Westphal (1972), who, on 1971 March 8, obtained two simultaneous scans across the disk in the passbands 8000–8240 Å and 8720–8960 Å. The atmospheric seeing was ~0ʺ5. A circular aperture of 1ʺ was used. The long-wavelength scan, which has since been reproduced in the literature (Belton and Vesculus 1975), shows distinct limb brightening and also asymmetry, the west limb being markedly brighter than the east limb. The short-wavelength scan, which remains unpublished, shows a flat central region about 2ʺ wide together with limb darkening.

Infrared limb brightening was confirmed by Sinton (1972), who obtained several images of Uranus with a Varo tube and an 8870 Å interference filter under good seeing conditions. Both limb and polar brightening were found. Sinton explained the polar brightening as being caused by haze in the upper atmosphere, in addition to Rayleigh scattering.

Belton and Price (1973) interpreted limb brightening on the Uranus disk in terms of H_2–CH_4 pressure induced absorption in a semi-infinite, clear atmosphere. On the basis of this model, limb darkening is predicted to occur in continuum wavebands, while limb brightening is expected in *all* deep CH_4 bands.

In a recent investigation of wavelength dependence in the optical appearance of Uranus, Price and Franz (1976) used an area-scanning photometer (Franz 1970) in conjunction with the 72 inch (1.8 m) Perkins reflector at the Lowell Observatory to obtain multicolor (5500–7600 Å), narrow-band (100 Å) scans of the Uranus disk. Both slit and pinhole scanning apertures were used, each having a characteristic width of 100 μm (0ʺ65). Absolute limb brightening, i.e., limb brightening with respect to a uniform disk, was found in the 7300 Å methane band. Relative limb brightening, i.e., limb brightening with respect to the disk profile at adjacent continuum wavelengths, was detected in the 6190 Å CH_4 band. No evidence of asymmetry was found in the scan profiles. However, the point spread function (PSF) never exhibited a half-power width less than about 2ʺ. As a result, statistical methods were required to analyze the data. To demonstrate directly the existence of limb brightening in the visible region of the spectrum, observations of higher quality were clearly required. Such data are reported in this *Letter*.

II. NEW OBSERVATIONAL RESULTS

Substantial improvement of the optical performance of the 72 inch Perkins telescope was recently brought about by retouching the figure of its secondary mirror. When new scans of Uranus were subsequently obtained in winter and spring of 1976, the half-power width of the PSF was found to be on the order of 1ʺ, an improvement by a factor of 2 over typical earlier values. While equipment and observational technique were those previously used and described by Price and Franz (1976), special attention was given to pinhole scans in an effort to enhance the visibility of limb brightening.

Two sets of south-to-north (near-equatorial) scans of the Uranus disk, taken on 1976 May 18 and June 17 in the CH_4 band at 7300 Å and in adjacent continuum regions, are presented in Figure 1. All profiles are normalized at the center of the planetary disk. Both sets of scans, although of unequal quality owing largely to different seeing conditions and different effective integration times, exhibit distinct limb brightening in the light of the methane band relative to the profiles in continuum light. Note that owing to the effects of atmospheric smearing, observed relative limb brightening may indicate the presence of absolute limb brightening, as pointed out by Belton and Price (1973).

Figure 2 shows two sets of near-polar scans obtained on 1976 January 30 and June 17. The presence of limb brightening at 7300 Å, relative to scans at continuum wavelengths, is again readily apparent. But while the near-equatorial scans (Fig. 1) show symmetry about the center of the planetary disk, the near-polar scans (Fig. 2) appear distinctly asymmetric in the 7300 Å CH_4

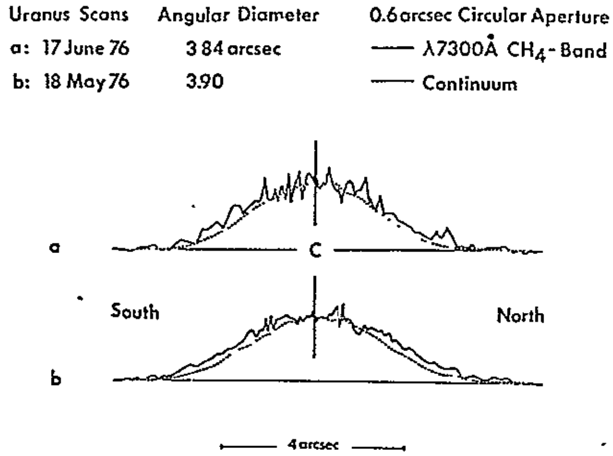

FIG. 1.—Near-equatorial (south-north) pinhole scans across the Uranus disk show limb brightening at λ7300 Å. All data are normalized at the disk center. Angular diameters of the Uranus disk are taken from the 1976 *American Ephemeris and Nautical Almanac.*

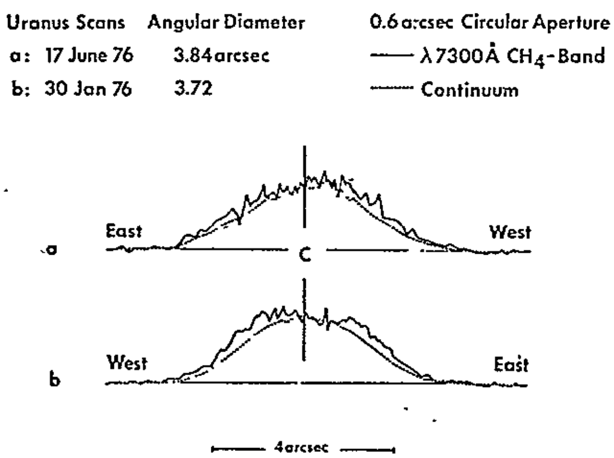

FIG. 2.—Near-polar (east-west) pinhole scans across the Uranus disk show limb brightening at 7300 Å and asymmetry in both wave bands. The sense of the asymmetry reverses with scan direction. All data are normalized at the disk center Angular diameters of the Uranus disk are taken from the 1976 *American Ephemeris and Nautical Almanac.*

band and the adjacent continuum. Note also that the near-polar scans were made in opposite directions on the two nights. The sense of the asymmetry changes accordingly, demonstrating that the effect is real and showing that in all cases Uranus appeared brighter near its western limb than near its eastern limb. It should be emphasized that this effect, now discovered in the visible spectrum, is the same as that found in the near-infrared (8870 Å) from the scans by Westphal (1972), published in part by Belton and Vesculus (1975), and from the observations by Sinton (1972).

Explanation of the observed east-west asymmetry in terms of polar brightening remains the most likely. On 1976 April 25 (opposition), the north pole of Uranus was located near the planet's western limb at position angle 278°3 and at a distance of 0.680 Uranus radii from the center of the disk.

If this polar brightening were caused by H_2–CH_4 pressure-induced absorption, its occurrence would be limited to the deep CH_4 bands. Because polar brightening is apparent in both continuum and CH_4 wavebands, it is almost certainly the result of scattering in an aerosol haze located over the polar region. This conclusion confirms that drawn by Sinton (1972). Our 1976 observations therefore suggest that such a thin polar haze on Uranus is a long-lived, perhaps even permanent, feature.

This work was carried out with the aid of the National Aeronautics and Space Administration under contracts NASW-2521, NASW-2718, and NASW-2843 and with the support of grants from the National Science Foundation. Some of the data processing was aided by NASA grant NGR-03-003-001.

REFERENCES

Belton, M. J. S., and Price, M. J. 1973, *Ap. J.*, **179**, 965.
Belton, M. J. S., and Vesculus, F. E. 1975, *Icarus*, **24**, 299.
Franz, O. G. 1970, *Lowell Obs. Bull.*, No. 154.
Price, M. J., and Franz, O. G. 1976, *Icarus*, **29**, 125.
Sinton, W. M. 1972, *Ap. J.* (*Letters*), **176**, L131.
Westphal, J. A. 1972, comment during 3d Annual Meeting of the AAS, Division for Planetary Sciences, Kailua-Kona, Hawaii, 1972 March.

OTTO G. FRANZ: Lowell Observatory, Post Office Box 1269, Flagstaff, AZ 86002
MICHAEL J. PRICE: Planetary Science Institute, Tucson, AZ 85719

APPENDIX E

REVISED MANUSCRIPT

LIMB-BRIGHTENING ON URANUS:

THE VISIBLE SPECTRUM. II

Michael J. Price
Planetary Science Institute
2030 E. Speedway Blvd., Suite 201
Tucson, Arizona 85719

and

Otto G. Franz
Lowell Observatory
P. O. Box 1269
Flagstaff, Arizona 86002

Received ______________________

Revised ______________________

No. of Copies: 3

No. of MS Pages: 35

No. of Figures: 11

No. of Tables: 2

Proposed Running Head:

LIMB-BRIGHTENING ON URANUS

Name and Address of Person to Whom Proofs Should be Sent:

Dr. Michael J. Price
Planetary Science Institute
2030 E. Speedway Blvd., Suite 201
Tucson, Arizona 85719

ABSTRACT

New narrow-band (100Å) photoelectric area-scanning photometry of the Uranus disk is reported. Observations were concentrated on the two strong CH_4 bands at λ6190Å and at λ7300Å. Adjacent continuum regions at λ6400Å and at λ7500Å were also measured for comparison. Both slit and pinhole scans were made in orthogonal directions. Disk structure in each waveband is apparent through lack of circular symmetry in the intensity distribution over the Uranus image. Polar brightening is especially prominent in the λ7500Å waveband.

Coarse quantitative determinations of the true intensity distribution over the Uranus disk were made. For the λ6190Å CH_4 band, Uranus exhibits a disk of essentially uniform intensity except for a hint of polar brightening. For the λ7300Å CH_4 band, moderate limb-brightening is apparent. Specifically, the true intensities at the center and limb of the planetary disk are approximately in the proportion 1:2. Extreme limb-brightening, with a corresponding intensity ratio greater than 1:4, is not permitted by the observational data.

I. INTRODUCTION

Belton and Vesculus (1975) pointed out that valuable information for investigating the physical structure of the Uranus atmosphere can be obtained from knowledge of the distribution of brightness over the planetary disk. Qualitative and quantitative infrared studies of the intensity profile of the Uranus disk have been reported by Westphal (1972) and by Sinton (1972), respectively. In Paper I, Price and Franz (1976) studied the wavelength variation in the optical appearance of Uranus using multi-colored (λ5500 - 7600Å), narrow-band (100Å), area-scanning photometry. Eight wavebands were selected. During the 1975 Uranus apparition, absolute limb-darkening was found in all spectral regions considered except for the two CH_4 bands at λ6190Å and λ7300Å. For the λ7300Å band, absolute limb-brightening with respect to a uniform disk was found. For the λ6190Å band, no definite conclusions could be drawn regarding the absolute nature of limb-brightening. Only limb-brightening relative to adjacent continuum regions could be demonstrated. If absolute limb-brightening did occur in the λ6190Å band, it had to be much less pronounced than in the λ7300Å band. Quantitative estimates of the degree of either limb-darkening or limb-brightening in any waveband could not be obtained from the available observational data. Spatial resolution and photometric accuracy were insufficient.

Further observations of limb-brightening on Uranus have since been carried out by other investigators. Avis et al. (1977) reported the photographic detection of albedo features in the λ6190Å CH_4 band. Image enhancement processing resulted in the discovery of local polar brightening superimposed on weak, symmetrical, absolute limb-brightening. Smith

(1977), using a CCD camera, confirmed the existence of absolute limb-brightening in the λ8900Å CH_4 band.

During the 1976 Uranus apparition, we refined our earlier observations of the planet. Spatial resolution and photometric accuracy had been much improved since 1975. Our objective was to quantitatively determine the degree of limb-brightening in each of the two CH_4 bands of interest. For the λ7300Å band, initial qualitative results were reported by Franz and Price (1977). Pinhole scans demonstrated directly the existence of both limb and polar brightening. Polar brightening appeared to be present also at adjacent continuum wavelengths. In this paper, we present a detailed analysis of our 1976 observational data. In a subsequent paper, an interpretation of our results in terms of the physical structure of the Uranus atmosphere will be given.

2. OBSERVATIONS

Using the equipment and technique described in Paper I, we carried out new photoelectric area-scanning photometry of the Uranus disk during the 1976 apparition. Measurements were restricted to four narrow-band (~100 Å) spectral regions, namely the CH_4 bands selected with Filter No. 3 (λ6200 Å) and Filter No. 7 (λ7300Å), and adjacent "continuum" regions studied through Filter No. 4 (λ6400Å) and Filter No. 8 (λ7500Å). Specifications of the filters were noted in Paper I.

Since 1975 major improvements had been made to the optical performance of the Perkins reflector. Specifically, the Cassegrain secondary was refigured to reduce spherical aberration. Typical point spread functions produced by the atmosphere-telescope combination became narrower by a factor of two compared with those previously obtained. Significant improvement in the spatial resolution of the Uranus disk was a direct result. Photometric signal-to-noise ratios were also increased by replacing the earlier EMI-9558 (S-20) tube with an ITT F4085 (S-20) photomultiplier.

Uranus was scanned with both slit and pinhole apertures. Slit scans were selected to provide the most reliable photometric data for investigating the true intensity distribution over the disk. Pinhole scans were included to enhance the visibility of limb- and polar-brightening, and to verify the interpretation of the slit-scan data. Characteristic widths of the pinhole and slit were both chosen equal to $100\mu m$ ($0\overset{''}{.}645$ arc). The slit and scan lengths were each 2 mm ($12\overset{''}{.}9$ arc). Point spread function data were obtained by slit-scanning images of individual stars located near the planet. Direct and reverse scans were made along two orientations, north-south (N-S) or east-west (E-W). For Uranus, orthogonal scans were used to examine the reality of features in the disk profiles. For stellar images, orthogonal scans were used to verify that telescope guiding errors were insignificant. Table I gives the 1976 Uranus observing log.

Visual guiding was used with no attempt made to correct for image displacement caused by the wavelength dependence of atmospheric refraction. For the maximum wavelength difference (2000Å) between guiding (λ5500Å) and scanning (7500Å), at the largest zenith distance (51 degrees) encountered in our observations, the relative image displacement never exceeded $0\overset{''}{.}5$ arc. For our slit scans, this displacement is of no consequence. Since both the slit and scan lengths (~13" arc) were much greater than the sum of both the Uranus angular diameter (~4" arc) and the maximum image displacement encountered ($0\overset{''}{.}5$ arc), no light from the planet was lost whatever the scan orientation. Furthermore, no distortion of any scan profile could occur. For our pinhole scans, however, the situation is not so clear cut. Because Uranus was always observed near the time of its local meridian transit, the N-S pinhole scans were essentially unaffected by the phenomenon of image displacement. But, the red E-W pinhole scans were located up to $0\overset{''}{.}5$ arc north of the disk center when the visual image was centered. The chord traversed was then ~3 percent shorter than the disk diameter. For the E-W scans, therefore, limb-brightening will tend to be underestimated; limb-darkening will be overestimated. We shall return to this point in our analysis of the pinhole scan data.

Composite Uranus and stellar profiles were produced to increase the effective signal-to-noise ratio in the photometry. For Uranus, on each night of observation, composite profiles in each waveband were obtained in each of the two cardinal orientations (N-S, E-W) for the slit and pinhole scans individually. The point spread function for each night was obtained by summing together all stellar slit-scans. All stellar profiles were symmetrical. Inspection of the individual stellar profiles showed no variation with waveband, scan orientation, or scan direction. Formation of the entire set of composite profiles is summarized in Table II.

Individual Uranus slit profiles were typically obtained by integrating 50 to 200 one-second scans; pinhole profiles required 200 to 500 one-second scans. Individual stellar profiles each consisted of 20 one-second scans. Colocation of the individual Uranus and stellar profiles prior to composite summation was achieved through Gaussian curve fitting by means of the least squares technique to define the centroids of the individual profiles. Where necessary, scans made in opposite directions were mirrored on their centroids prior to computer summation.

All Uranus composite profiles were normalized to an equal arbitrary integrated signal not only to facilitate interwaveband comparisons, but also to expedite comparisons with theoretical predictions. In essence, the photoelectron counts received from the planet for all points in each scan were summed to derive the total signal. Such a normalization procedure minimizes the influence of individual photometric errors within each observational scan, and eliminates the need to know the effective geometrical albedo in each waveband when comparing observation with theory. By comparison, each stellar profile was scaled to an equal arbitrary intensity at its centroid.

3. THE POINT SPREAD FUNCTION

Atmospheric turbulence, together with diffuse scattering from the telescope mirrors, produces the observed point spread function. In Paper I, we showed that a single Gaussian curve provided only a coarse fit to the distribution of intensity within the image of a point source; a Double-Gaussian curve (Fig. 1) provides a far better description of the point spread function. Line-integration, slit-broadening, and normalization of the Double-Gaussian shape are discussed in Appendix I.

Composite stellar slit-scans obtained for the nights of 1976 May 18, June 16, and June 17 are plotted individually in Fig. 1. Best-fitting theoretical scans, based on the Double-Gaussian representation of the point spread function, are shown for comparison. Optimum values of the PSF parameters for each night are tabulated in Fig. 1. Interestingly enough, the point spread functions on 1976 May 18 and June 17 were essentially identical. On 1976 June 16, to demonstrate the ability of the area-scanner to resolve the Uranus image by slit-scanning, a set of close visual binary stars was also measured. Results are illustrated in Fig. 2.

Variations in the point spread function, during each night of observation, are of special interest for the interpretation of the Uranus data. For 1976 June 16, quantitative estimates of the variation in the width of the actual point spread function may be made by fitting a single Gaussian curve to each of the 29 individual stellar slit-scans by means of the least squares technique. The derived 1/e widths provide a measure of the constancy of the point spread function. Distortion of the actual point spread function introduced by slit-scanning is not significant in the present context. Results show that the individual r.m.s. fluctuation in the 1/e width amounted to 6.0 percent. For the composite profile, the r.m.s. error in its width should therefore amount to $\sim$ 1 percent, in agreement with the observational data presented in Fig. 1. Investigation of variation in the point spread function during the nights of 1976 May 18 and 1976 June 17 produced similar results. Evidently, mean theoretical PSF parameters for each night of observation are known to an accuracy $\sim$ 1 percent.

4. URANUS SLIT SCANS

4.1. Modelling Procedures

Deriving the true intensity distribution over the Uranus disk in each waveband of interest was the objective of the slit scan analysis. Our approach was first to model both the size and shape of the planet together with the adopted "true" distribution of intensity over the disk, next to employ the known point spread function in a two-dimensional broadening procedure to derive the planetary image smeared by atmospheric seeing, then to compute the profile which would result from slit-scanning the image in one-dimension, and finally to normalize the slit-scan prediction to permit comparison with the observed profile. Full details of the mathematical formulation of the problem are contained in Appendix II.

Using Stratoscope II photographs of Uranus, Danielson et al. (1972) derived a planetary equatorial radius of 25,900 $\pm$ 300 kms together with an ellipticity of 0.01 $\pm$ 0.01. Although stellar occultations may provide improved values for both the radius and ellipticity of the planet, we adopt the values given by Danielson et al. as the best available. Our theoretical predictions assumed Uranus to be a perfect sphere of radius 25,900 kms. Circular symmetry in the distribution of intensity over the disk was also assumed. Distance from the Earth to Uranus on 1976 June 16 was taken from the American Ephemeris and Nautical Almanac to be 17.88 A.U. The corresponding angular diameter of Uranus (unbroadened) was therefore $3\overset{''}{.}99$ arc.

Simple theoretical distributions of intensity over the Uranus disk were adopted which could be described by a single parameter chosen to encompass a broad range of situations; this parameter was determined by the relative intensities at the limb and center of the disk.

Although consideration was given to the predictions by Belton and Price (1973), our choice of the radial intensity function remained largely arbitrary. Between the limb and center of the disk, the true intensity distribution was assumed to follow an elliptical curve. For both limb-brightening and limb-darkening, the slope of the function was taken to be zero at the disk center. At the limb, the slope reaches negative infinity for limb-darkening, and positive infinity for limb-brightening. Six curves, illustrated in Fig. 3, were used in our analysis. Besides the case of a uniform disk, both limb-darkened (convex) and limb-brightened (concave) intensity distributions, ranging from moderate to extreme, were adopted. For limb-darkening, the parameter (p) equal to the ratio of the intensities at the limb and center of the disk was sufficient to describe the distribution. For limb-brightening, the parameter (q) equal to the ratio of the intensities at the center and limb filled an identical role.

Distortions of the slit scans resulting from variations in atmospheric seeing need to be examined before we embark on a detailed comparison of theory with observation. Sample theoretical slit scans were computed for three extreme models of the radial intensity distribution, namely the uniform disk, extreme limb-brightening ($q = 0$), and extreme limb-darkening ($p = 0$). Each distribution was subjected to smearing by three distinct point spread functions, described by the optimum set of parameters (A, B, σ_1, σ_2) listed in Fig. 1 for 1976 June 16 together with two extreme variants obtained by changing the individual B, σ_1, and σ_2 parameters in unison by ± 5 percent. Results are illustrated in Fig. 4. Increasing the PSF width reduces the normalized intensities near the center of the slit scans; intensities in the wings are increased. For the composite Uranus slit scans, the effective PSF parameters should be uncertain by only ~ 1 percent. Evidently, variations in the seeing will have a negligible effect on the interpretation of the data. Photometric noise will be significantly greater than profile fluctuations resulting from the cumulative effects of seeing fluctuations.

Uncertainty in the slit-scan predictions introduced by inaccurate knowledge of the Uranus radius also requires examination. Sample theoretical slit scans were calculated for three distinct radii; the Danielson et al. value was adopted together with radii differing from the optimum value by ± 5 percent. Models chosen for the intensity distribution were again a uniform disk, extreme limb brightening ($q = 0$), and extreme limb-darkening ($p = 0$). The point spread function parameters for 1976 June 16 were those listed in Fig. 1. Results are illustrated in Fig. 5. Enlarging the planetary radius reduces the normalized intensities near the center of the slit scans; intensities in the wings are increased. Since the Uranus radius appears to be uncertain by only ~ 1 percent, the corresponding error introduced in the slit-scan predictions will have a negligible effect on the interpretation of the data. Photometric noise in the composite Uranus scans will be significantly greater.

4.2. Results

Observed composite Uranus slit scans, in all four wavebands of interest, are compared with theoretical predictions in Fig. 6 through 9. Discrimination between the individual intensity distributions is readily achieved near the center of the planetary image. Small uncertainties both in the planetary radius and in the point spread function then have their least influence on the interpretation. Investigation of disk structure through detection of gross asymmetries and local anomalies in the slit scans is a principal objective of our analysis. No attempts have therefore been made either to smooth out the residual photometric noise in the composite scans or to force-fit a curve through each set of observational data. For each waveband, north-south (N-S) and east-west (E-W) orthogonal scans were plotted separately. Polar brightening would manifest itself near the center of the N-S scans, and on the westerly segment of the E-W scans. Information given in the Explanatory Supplement of the American Ephemeris and Nautical Almanac shows that, on 1976 June 16, the north pole of Uranus was located at position angle 278.9 degrees at a distance of 0.69 Uranus radii from the disk center. Location of the pole on the disk did not change significantly throughout the 1976 observing season.

Data for the λ6190Å CH_4 band are presented in Fig. 6. Both N-S and E-W scans suggest that the optimum true radial intensity distribution corresponds to a uniform disk. But weak limb-darkening ($p \geq 0.5$) and weak limb-brightening ($q \geq 0.5$) are also permitted by the N-S and E-W scans respectively. Data for the adjacent "continuum" region at λ6400Å are plotted in Fig. 7. Limb-darkening is readily apparent in both the N-S and E-W scans. For the N-S scan, the true radial intensity distribution can range from a uniform disk to weak limb-darkening ($p \geq 0.5$). For the E-W scan, the distribution can range from moderate to extreme limb-darkening ($0.5 \geq p \geq 0$). Giving equal consideration to both the N-S and E-W scans, we will adopt moderate limb-darkening ($p = 0.5$) as the optimum fit to the λ6400Å data.

Data for the strong λ7300Å CH_4 band are presented in Fig. 8. In spite of the residual photometric errors in both N-S and E-W composite scans, limb-brightening is evident. Precise determination of its magnitude is difficult however. For both the N-S and E-W scans, the true radial intensity distribution can range from a uniform disk to substantial limb-brightening ($q = 0.25$). But extreme limb-brightening ($q = 0$) cannot be reconciled with the observational data. Giving equal consideration to the N-S and E-W scans, we will adopt moderate limb-brightening ($q = 0.5$) as the optimum fit to the λ7300Å data. Observations in the adjacent "continuum" region at λ7500Å are plotted in Fig. 9. For the N-S scan, the true radial intensity distribution can range from a uniform disk to moderate limb-brightening ($q = 0.5$). For the E-W scan, the distribution can range from a uniform disk to moderate limb-darkening ($p = 0.5$). Evaluating both scan directions together, one can conclude that on average the distribution of intensity in the λ7500Å band corresponds approximately to a uniform disk.

For the λ6400Å, λ7300Å, and λ7500Å wavebands, striking differences are apparent between the N-S and E-W scans. The E-W scans exhibit a distinctly greater intensity near the center of the planetary image. Since N-S and E-W scans are normalized to an identical total signal, the E-W scans must also have a slightly narrower profile than the N-S scans. Considering the scan geometry, one might conclude that Uranus is significantly oblate. But an ellipticity ~ 0.1 would be required to produce the effect. Studies by Danielson et al. (1972) appear to preclude that interpretation. If Uranus is in fact essentially spherical, one is obliged to conclude that the distribution of intensity over the disk is not circularly symmetric. Disk structure must be present in each of the above wavebands.

For the λ6190Å CH_4 band, a slight asymmetry in the E-W scan suggests the presence of weak polar brightening. One final point may be made. In all four wavebands, the N-S scans show a slight asymmetry in the wings; the northerly segment is definitely brighter than the southerly segment. One might be tempted to interpret this asymmetry in terms of the recently discovered Uranus ring system. But such an interpretation would be highly speculative. Moreover, it appears to be unwarranted.

5. URANUS PINHOLE SCANS

Our slit-scan results were confirmed by the pinhole data. Interpretation of the pinhole scans was carried out in a manner essentially identical to that employed for the slit scans. No changes were made in the Uranus disk model. Only diametric scanning of the Uranus image was considered. Uncertainties both in the atmospheric seeing and in the planetary radius were insignificant when considered in the context of the photometric noise remaining in the composite pinhole scans. Modifications to the theoretical formulation introduced by changing the scanning aperture from a slit to a pinhole are discussed in Appendix II.

Theoretical pinhole scans were calculated for the six radial intensity distributions illustrated in Fig. 3. Atmospheric seeing was described by the optimum set of PSF parameters (A, B, σ_1, σ_2) listed in Fig. 1 for both the 1976 May 18 and 1976 June 17 observations. For the two nights in question, a mean Earth-Uranus distance of 17.74 A.U. was obtained from the American Ephemeris and Nautical Almanac. The corresponding mean angular diameter (unbroadened) of Uranus was $4\overset{''}{.}03$ arc. Adopting a mean diameter introduces an error of less than 1 percent in the value for each night.

Observed composite Uranus pinhole scans, for the λ7300Å and λ7500Å wavebands, are compared with theoretical predictions in Figs. 10 and 11, respectively. For each waveband, north-south (N-S) and east-west (E-S) scans are plotted separately to investigate the presence of disk structure. Compared with the slit-scan observations, significantly greater photometric noise remains in the pinhole data. But, fortuitously, the theoretical pinhole scans exhibit a far greater sensitivity to the shape of the true intensity distribution. Note, however, that telescope guiding errors (rms deviation ~0".2 arc) are potentially more serious for pinhole scans than for slit scans. Errors in guiding can cause the observed pinhole scans to exhibit rather <u>less</u> limb-brightening, and rather <u>more</u> limb-darkening than is actually present in the Uranus image. Earlier, we pointed out that, for the E-W pinhole scans only, an identical effect is introduced by image displacement (< 0".5 arc) resulting from atmospheric dispersion. For the pinhole observations, the observable pole of Uranus lies 2".7 arc west, 0".2 arc north of the center of the planetary disk. Northerly displacement of the E-W pinhole scans, with respect to the pole, will therefore amount to less than 0".3 arc. Since our pinhole diameter was 0".645, the pole will always be included in the E-W scans, but will always be excluded from the N-S scans. Differences in the visibility of polar brightening should therefore be apparent between the E-W and N-S pinhole scans.

For the λ7300Å CH_4 band, Fig. 10 shows that polar brightening is present in the E-W scan and, as expected, not in the N-S scan. Using the N-S scan to derive limits to the shape of the true intensity distribution, we conclude that limb-brightening is definitely present in this waveband. Extreme possibilities range from a uniform disk to moderate limb-brightening ($q = 0.25$). Extreme limb-brightening ($q = 0$) is excluded. The best match between observation and theory is achieved for moderate limb-brightening ($q = 0.5$). Evaluating the pinhole and slit scan data together, we estimate that the maximum permitted degree of limb-brightening corresponds to $q = 0.25$.

For the λ7500Å data, Fig. 11 shows that polar brightening is present in the E-W scan, but not in the N-S scan. Evidently, polar brightening must be highly localized on the Uranus disk. Using the N-S scan to derive limits to the shape of the true intensity distribution, we estimate that limb-darkening may be present in this waveband. Possibilities range from weak limb-brightening ($q = 0.5$) to extreme limb-darkening. The best match between observation and theory appears to lie between a uniform disk and moderate limb-darkening ($p = 0.5$). For the E-W scan, polar brightening is so significant that it grossly affects the overall shape of the profile. Possibilities for the true intensity distribution appear to range from a uniform disk to extreme limb-darkening ($p = 0$). Even the latter distribution is not sufficiently extreme to completely encompass the polar brightening. Considering the pinhole- and slit-scan results together, we conclude that the basic distribution of intensity in this waveband corresponds to an essentially uniform disk upon which is superimposed significant polar brightening.

4. CONCLUSIONS AND DISCUSSION

Coarse quantitative information on the true radial intensity distribution over the Uranus disk has been derived in four selected wavebands. Lack of circular symmetry in the intensity distributions indicates the presence of disk structure, especially polar brightening, in each waveband. For the λ6190Å CH_4 band, the distribution corresponds to a uniform disk upon which a hint of polar brightening is superimposed. For the λ6400Å region, moderate limb-darkening ($p = 0.5$) was found. For the λ7300Å CH_4 band, moderate limb-brightening ($q = 0.5$) was discovered. Extreme limb-brightening ($q < 0.25$) was not permitted by the observational data. For the λ7500Å waveband, the distribution corresponds to a uniform disk upon which significant localized polar brightening is superimposed. While the λ7300Å CH_4 band observations exhibit absolute limb-brightening with respect to a uniform disk, the λ6190Å CH_4 band data show only relative limb-brightening with respect to nearby continuum regions.

Our results may be compared with those obtained by Sinton (1972) for the λ8900Å CH_4 band. Both limb and polar brightening were found. Sinton fitted his observations with a radial intensity distribution consisting of a uniform disk combined with limb-brightening proportional to $1/\mu$, where μ equals the cosine of the angle made by the incident/emergent ray with respect to the local outward normal to the atmosphere. Both components of the intensity were taken to contribute equally at the center of the Uranus disk. In the notation of Appendix II, the limb brightening component takes the functional form $(1 - r^2)^{-1/2}$, $0 \leq r \leq 1$.

Our coarse analytical technique used in this paper to explore the information content of the photometric scans of Uranus has several basic limitations. First, the assumption of smooth elliptical distributions of radial intensity over the disk is entirely arbitrary. Second, the use of circular symmetry prevents investigation of azimuthal structure on the disk. In fact, direct deconvolution of the Uranus scans is required to thoroughly investigate the two-dimensional photometric structure of its disk. In principle, Fourier analytical techniques, operating on the Uranus slit scans made in orthogonal directions, can be used. But practical application of Fourier analysis to the Uranus images remains to be demonstrated.

APPENDIX I: THE POINT SPREAD FUNCTION

Our empirical studies show that the two-dimensional (x, y) image of an astronomical point source formed by the Flagstaff atmosphere-Perkins telescope combination can be accurately described by a circularly symmetric normalized intensity profile given by

$$F(r) = \frac{1}{\pi(A\sigma_1^2 + B\sigma_2^2)} \left\{ A \exp\left(-\frac{r^2}{\sigma_1^2}\right) + B \exp\left(-\frac{r^2}{\sigma_2^2}\right) \right\} \tag{1.1}$$

where

$$r = (x^2 + y^2)^{1/2} \tag{1.2}$$

and A, B, σ_1 and σ_2 are constants for the image under consideration.

Next, consider a slit of indefinite length, and infinitesimal width, scanning the two-dimensional image in one-dimension (x). Line-integration of the point spread function produces a profile given by

$$L(x) = \int_{-\infty}^{+\infty} F(x,y)\, dy \tag{1.3}$$

which reduces to

$$L(x) = \frac{1}{\sqrt{\pi}(A\sigma_1^2 + B\sigma_2^2)} \left\{ A\sigma_1 \exp\left(-\frac{x^2}{\sigma_1^2}\right) + B\sigma_2 \exp\left(-\frac{x^2}{\sigma_2^2}\right) \right\} . \tag{1.4}$$

For a slit of finite width, Δ, the line-integrated profile is broadened to produce

$$S(x) = \frac{1}{\Delta} \int_a^b L(\zeta)\, d\zeta \tag{1.5}$$

where the integration limits are

$$a = x - \frac{\Delta}{2} \quad , \qquad b = x + \frac{\Delta}{2} \tag{1.6}$$

The slit-scan profile of the point spread function reduces to

$$S(x) = \frac{1}{2\Delta\left(A\sigma_1^{\,2} + B\sigma_2^{\,2}\right)} \left\{ A\sigma_1^{\,2}\left[\operatorname{erf}\left(\frac{b}{\sigma_1}\right) - \operatorname{erf}\left(\frac{a}{\sigma_1}\right)\right] + B\sigma_2^{\,2}\left[\operatorname{erf}\left(\frac{b}{\sigma_2}\right) - \operatorname{erf}\left(\frac{a}{\sigma_2}\right)\right]\right\} . \tag{1.7}$$

Optimum values for the parameters A, B, σ_1, σ_2 are obtained by direct comparison of theoretical predictions with the observational data

APPENDIX II: THE URANUS IMAGE

1. True Disk Profiles

The Uranus disk is taken to be circular and of unit radius. Its true intensity profiles, D(r), were chosen to encompass the possibilities of extremes in both limb-darkening and limb-brightening. Limb-darkening was described by

$$D(r) = p + (1 - p)\sqrt{1 - r^2} \quad , \qquad 0 \leq r \leq 1 \tag{2.1}$$

where

$$p = D(1)/D(o) \quad . \tag{2.2}$$

Limb-brightening was described by

$$D(r) = 1 - (1 - q)\sqrt{1 - r^2} \quad , \qquad 0 \leq r \leq 1 \tag{2.3}$$

where

$$q = D(o)/D(1) \quad . \tag{2.4}$$

The uniform disk is described by

$$D(r) = 1 \quad , \qquad 0 \leq r \leq 1 \tag{2.5}$$

2. Seeing Broadening

Every element of the Uranus disk will be affected by seeing broadening. Smearing by the point spread function will produce a circularly symmetric intensity profile of the planetary image given by

$$I(u) = \int_0^{2\pi} \int_0^{1} D(r)\ F(\rho)\, r\, d r\, d\theta \tag{2.6}$$

where the radial distance, u, from the center of the image is given by

$$u = (x^2 + y^2)^{1/2} \tag{2.7}$$

and

$$\rho^2 = r^2 + u^2 - 2ru\cos\theta \quad . \tag{2.8}$$

Equation (2.6) reduces to

$$I(u) = \frac{2}{(A\sigma_1^{\,2} + B\sigma_2^{\,2})} (T_1 + T_2) \tag{2.9}$$

where

$$\left.\begin{aligned} T_1 &= A\exp\left(-\frac{u^2}{\sigma_1^{\,2}}\right)\int_0^1 D(r)\, r\, I_0\left(\frac{2ru}{\sigma_1^{\,2}}\right) \exp\left(-\frac{r^2}{\sigma_1^{\,2}}\right) dr \\ T_2 &= B\exp\left(-\frac{u^2}{\sigma_2^{\,2}}\right)\int_0^1 D(r)\, r\, I_0\left(\frac{2ru}{\sigma_2^{\,2}}\right) \exp\left(-\frac{r^2}{\sigma_2^{\,2}}\right) dr \end{aligned}\right\} \tag{2.10}$$

and I_0 denotes the modified Bessel function.

3. Line-Integration and Slit-Broadening

Consider a slit of infinite length, and infinitesimal width, scanning the Uranus image in one-dimension (x). Line-integration produces

$$L(x) = \int_{-\infty}^{+\infty} I(x,y)\, dy \quad . \tag{2.11}$$

For a slit of finite width, Δ, the line-integrated profile is broadened to produce a scan profile given by

$$S(x) = \frac{1}{\Delta}\int_a^b L(\zeta)\, d\zeta \tag{2.12}$$

where the integral limits are given by

$$a = x - \frac{\Delta}{2} \quad , \qquad b = x + \frac{\Delta}{2} \tag{2.1}$$

4. Pinhole Integration

Our pinhole calculations consider only diametric scans across the Uranus image. For a pinhole of radius r_1, numerical integration over the pinhole aperture is required to obtain the pinhole scan profile, given by

$$P(x) = \int_0^{2\pi} \int_0^{r_1} I(\eta, \psi)\, \eta\, d\eta\, d\psi \tag{2.1}$$

where

$$I(\eta, \psi) \equiv I(u) \tag{2.15}$$

with

$$u^2 = x^2 + \eta^2 + 2x\eta \cos \psi \tag{2.1}$$

ACKNOWLEDGMENTS

This research was supported by the National Aeronautics and Space Administration under contract NASW-2983, and with the support of grants from the National Science Foundation. Some of the data processing was carried out with the support of NASA grant NGR-03-003-001. The U.S. Naval Observatory, Flagstaff Station, generously lent us an ITT F4085 photomultiplier for the project. This is Planetary Science Institute Contribution No. 71.

REFERENCES

Avis, C.A., Smith, H.J., Bergstralh, J.T., Sandmann, W.H. (1977). "Photometric Determination of the Rotation Period of Uranus." Paper presented at the Eighth Annual Meeting of the American Astronomical Society/Division for Planetary Sciences, Honolulu, Hawaii, 1977 January 19-22.

Belton, M.J.S. and Price, M.J. (1973). "Limb-Brightening on Uranus: A Prediction." Astrophys. J. 179, 965-970.

Belton, M.J.S. and Vesculus, F.E. (1975). "Why Image Uranus?" Icarus 24, 299-310.

Danielson, R.E., Tomasko, M.G. and Savage, B.D. (1972). "High resolution imagery of Uranus obtained by Stratoscope II." Astrophys. J. 178, 887-900.

Franz, O.G. and Price, M.J. (1977). "Uranus: Limb and Polar Brightening at λ7300Å." Astrophys. J. 214, L145-L146.

Price, M.J. and Franz, O.G. (1976). "Limb-Brightening on Uranus: The Visible Spectrum." Icarus 29, 125-136.

Sinton, W.M. (1972). "Limb and Polar Brightening of Uranus at 8870Å." Astrophys. J. 176, L131-L133.

Smith, B.A. (1977). "Uranus Photography in the 890 -nm Absorption Band of Methane." Paper presented at the Eighth Annual Meeting of the American Astronomical Society/Division for Planetary Sciences, Honolulu, Hawaii, 1977 January 19-22.

Westphal, J.A. (1972). Comment at the Third Annual Meeting of the American Astronomical Society/Division for Planetary Sciences, Kona, Hawaii, 1972 March 21-24.

TABLE I

URANUS OBSERVING LOG*

DATE (U.T.)	SCAN[1]		FILTER NO.	SKY[2]		REMARKS [3], [4]
	TYPE	DIRECTION		TRANSPARENCY	SEEING	
1976 May 18	P	S→N	7, 8	4	2-3	PSF (ι Vir)
1976 June 16	S	N↔S, E↔W	3, 4, 7, 8	5	3-4	PSF (ι Vir and Double Stars)
1976 June 17	P	E→W	7, 8	5	2-3	PSF (ι Vir)

*Notes:

1. Scan type is either pinhole (P) or slit (S)
2. Sky transparency and seeing conditions are given on scale 0-5 (i.e. worst-best)
3. All PSF data were taken using slit scanning. Scan directions and filters used were identical with those employed to obtain the Uranus profiles.
4. Angular scales of both the Uranus and stellar profiles were identical for all scans on all nights. Scale calibration was achieved using double stars of known separation.

TABLE II

FORMATION OF COMPOSITE PROFILES

Date (U.T.)	Object	Scan Type	Scan Direction	Filter	Integrated Scans	Total one-sec scans/ Integration	Total one-sec scans/ Composite
1976 May 18	Uranus	P	N-S	7	2	500-801	1301
"	Uranus	P	N-S	8	2	200	400
"	PSF	S	All	All	4	20	80
1976 June 16	Uranus	S	N-S	3	5	50	250
"	Uranus	S	N-S	4	4	50	200
"	Uranus	S	N-S	7	3	100-200	400
"	Uranus	S	N-S	8	4	50	200
"	Uranus	S	E-W	3	4	50	200
"	Uranus	S	E-W	4	4	50	200
"	Uranus	S	E-W	7	6	100-200	700
"	Uranus	S	E-W	8	8	50	400
"	PSF	S	All	All	29	20	580
1976 June 17	Uranus	P	E-W	7	3	500	1500
"	Uranus	P	E-W	8	2	100-200	300
"	PSF	S	All	All	5	20	100

FIGURE CAPTIONS

Fig. 1. The composite stellar slit scans for each night of observation. Theoretical point spread function predictions are compared with observation. Optimum curve fitting only is illustrated. The corresponding PSF parameters are tabulated.

Fig. 2. Illustration of atmospheric seeing quality on 1976 June 16. Specimen double star scans obtained in the direction of maximum separation are shown. Scans were obtained by integrating over 20 individual one-second sweeps.

Fig. 3. Theoretical intensity distributions over the Uranus disk selected for the analysis. Intensity, I(r), is considered to be a smooth function of radial distance, r, from the center of the disk. Azimuthal symmetry is assumed.

Fig. 4. Analytical uncertainties introduced by atmospheric seeing fluctuations. Theoretical Uranus slit scans are shown computed for 1976 June 16. The Uranus disk was taken as circularly symmetric with an apparent angular diameter of 3."99 arc. Seeing broadening was computed for a uniformly bright disk, and for the two cases of extreme limb-darkening and extreme limb-brightening shown in Fig. 3. The optimum PSF parameters tabulated in Fig. 1 were used together with two alternate sets of parameters obtained by varying B, σ_1 and σ_2 together by ± 5 percent.

Fig. 5. Analytical uncertainties introduced by changes in the Uranus radius. Theoretical Uranus slit scans are shown computed for 1976 June 16. Three models for the radial distribution of intensity over the disk were used. Computations were made for a uniformly bright circular disk, and for the two cases of extreme limb-darkening and extreme limb-brightening shown in Fig. 3. Seeing broadening was described by the optimum set of PSF parameters tabulated in Fig. 1. The optimum Uranus radius was taken as 25,900 kms; Two alternative Uranus radii, obtained by varying the optimum value by ±5 percent, were also used.

Fig. 6. Composite Uranus slit scans obtained on 1976 June 16 for the λ6200Å waveband. Theoretical slit scans are compared with observation. The Uranus disk was taken as circularly symmetric with an apparent angular diameter of 3".99 arc. Seeing broadening was described by the optimum set of PSF parameters tabulated in Fig. 1. All six models for the radial distribution of intensity over the Uranus disk shown in Fig. 3 were used. All theoretical and observational scans were normalized to a fixed arbitrary flux from the planet. In the abscissa, the zero point corresponds to the centroid of each observed and theoretical scan profile. Centroids of the observed scans will coincide with the physical center of the disk only if the intensity distribution is circularly symmetric. For information purposes, the observable pole of Uranus is located 2".7 arc west, 0".2 arc north of the physical center of the disk.

Fig. 7. Composite Uranus slit scans obtained on 1976 June 16 for the λ6400Å waveband. Theoretical slit scans are compared with observation. The Uranus disk was taken as circularly symmetric with an apparent angular diameter of 3.″99 arc. Seeing broadening was described by the optimum set of PSF parameters tabulated in Fig. 1. All six models for the radial distribution of intensity over the Uranus disk shown in Fig. 3 were used. All theoretical and observational scans were normalized to a fixed arbitrary flux from the planet. In the abscissa, the zero point corresponds to the centroid of each observed and theoretical scan profile. Centroids of the observed scans will coincide with the physical center of the disk only if the intensity distribution is circularly symmetric. For information purposes, the observable pole of Uranus is located 2.″7 arc west, 0.″2 arc north of the physical center of the disk.

Fig. 8. Composite Uranus slit scans obtained on 1976 June 16 for the λ7300Å waveband. Theoretical slit scans are compared with observation. The Uranus disk was taken as circularly symmetric with an apparent angular diameter of 3.″99 arc. Seeing broadening was described by the optimum set of PSF parameters tabulated in Fig. 1. All six models for the radial distribution of intensity over the Uranus disk shown in Fig. 3 were used. All theoretical and observational scans were normalized to a fixed arbitrary flux from the planet. In the abscissa, the zero point corresponds to the centroid of each observed and theoretical scan profile. Centroids of the observed scans will coincide with the physical center of the disk only if the intensity distribution is circularly symmetric. For information purposes, the observable pole of Uranus is located 2.″7 arc west, 0.″2 arc north of the physical center of the disk.

Fig. 9. Composite Uranus slit scans obtained on 1976 June 16 for the λ7500Å waveband. Theoretical slit scans are compared with observation. The Uranus disk was taken as circularly symmetric with an apparent angular diameter of 3."99 arc. Seeing broadening was described by the optimum set of PSF parameters tabulated in Fig. 1. All six models for the radial distribution of intensity over the Uranus disk shown in Fig. 3 were used. All theoretical and observational scans were normalized to a fixed arbitrary flux from the planet. In the abscissa, the zero point corresponds to the centroid of each observed and theoretical scan profile. Centroids of the observed scans will coincide with the physical center of the disk only if the intensity distribution is circularly symmetric. For information purposes, the observable pole of Uranus is located 2."7 arc west, 0."2 arc north of the physical center of the disk.

Fig. 10. Composite Uranus pinhole scans obtained on 1976 May 18 and on 1976 June 17 for the λ7300Å waveband. Theoretical pinhole scans through the image center are compared with observation. The Uranus disk was taken as circularly symmetric with a mean apparent angular diameter of 4."03 arc. Seeing broadening was described by the optimum set of PSF parameters tabulated in Fig. 1. All six models for the radial distribution of intensity over the Uranus disk shown in Fig. 3 were used. All theoretical and observational scans were normalized to a fixed arbitrary flux from the planet. In the abscissa, the zero point corresponds to the centroid of each observed and theoretical scan profile. Centroids of the observed scans will coincide with the physical center of the disk only if the intensity distribution

is circularly symmetric. Moreover, the scans must be precisely across a diameter of the planetary disk. For information purposes, the observable pole of Uranus is located $2.''7$ arc west, $0.''2$ arc north of the physical center of the disk.

Fig. 11. Composite Uranus pinhole scans obtained on 1976 May 18 and on 1976 June 17 for the λ7500Å waveband. Theoretical pinhole scans through the image center are compared with observation. The Uranus disk was taken as circularly symmetric with a mean apparent angular diameter of $4.''03$ arc. Seeing broadening was described by the optimum set of PSF parameters tabulated in Fig. 1. All six models for the radial distribution of intensity over the Uranus disk shown in Fig. 3 were used. All theoretical and observational scans were normalized to a fixed arbitrary flux from the planet.
In the abscissa, the zero point corresponds to the centroid of each observed and theoretical scan profile. Centroids of the observed scans will coincide with the physical center of the disk only if the intensity distribution is circularly symmetric. Moreover, the scans must be precisely across a diameter of the planetary disk. For information purposes, the observable pole of Uranus is located $2.''7$ arc west, $0.''2$ arc north of the physical center of the disk.

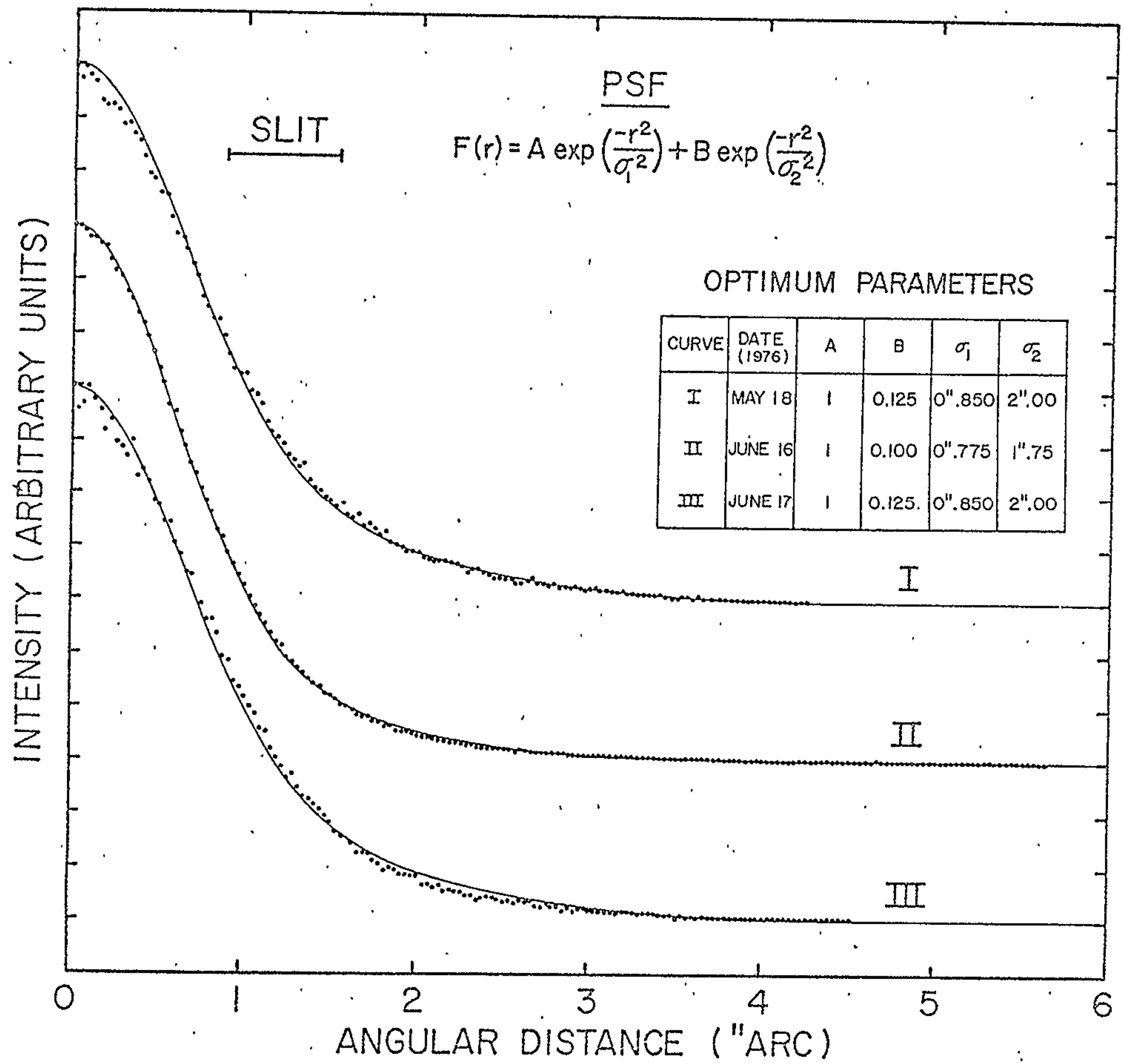

CURVE	DATE (1976)	A	B	σ_1	σ_2
I	MAY 18	1	0.125	0".850	2".00
II	JUNE 16	1	0.100	0".775	1".75
III	JUNE 17	1	0.125.	0".850	2".00

Fig

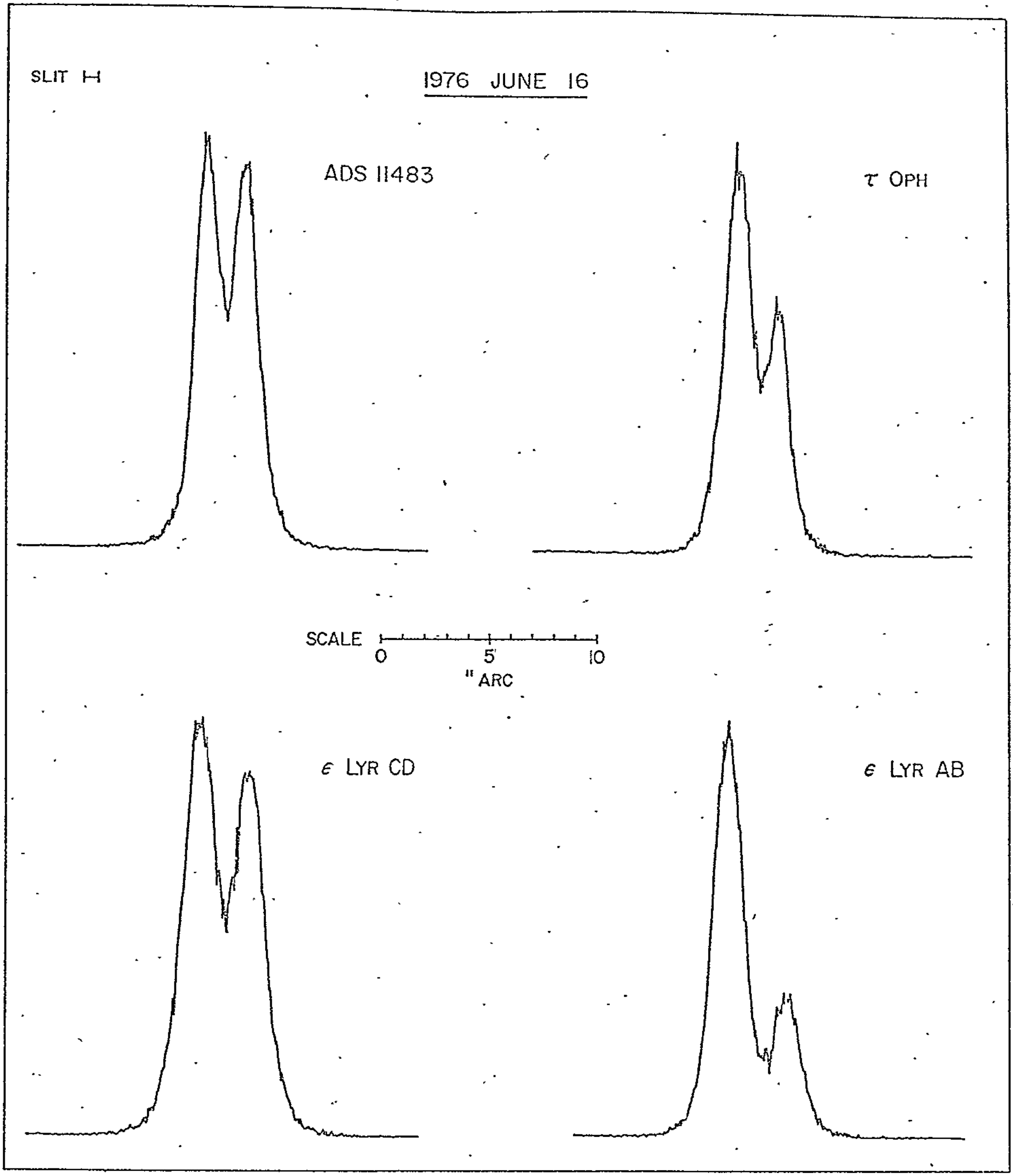
SLIT ⊢⊣
1976 JUNE 16
ADS 11483
τ OPH
SCALE
0
5
10
" ARC
ε LYR CD
ε LYR AB

Fig. 2

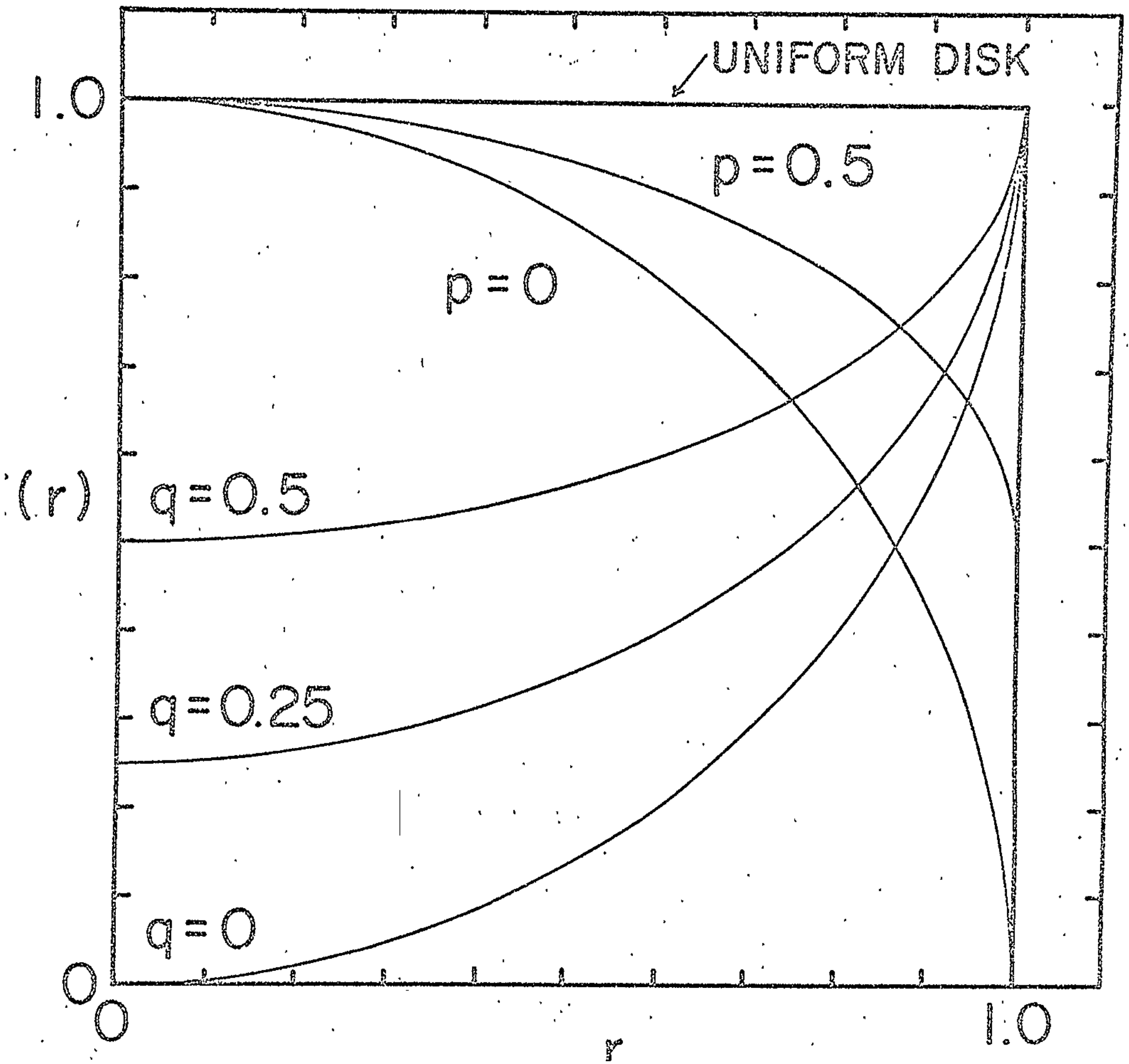

Fig. [redacted]

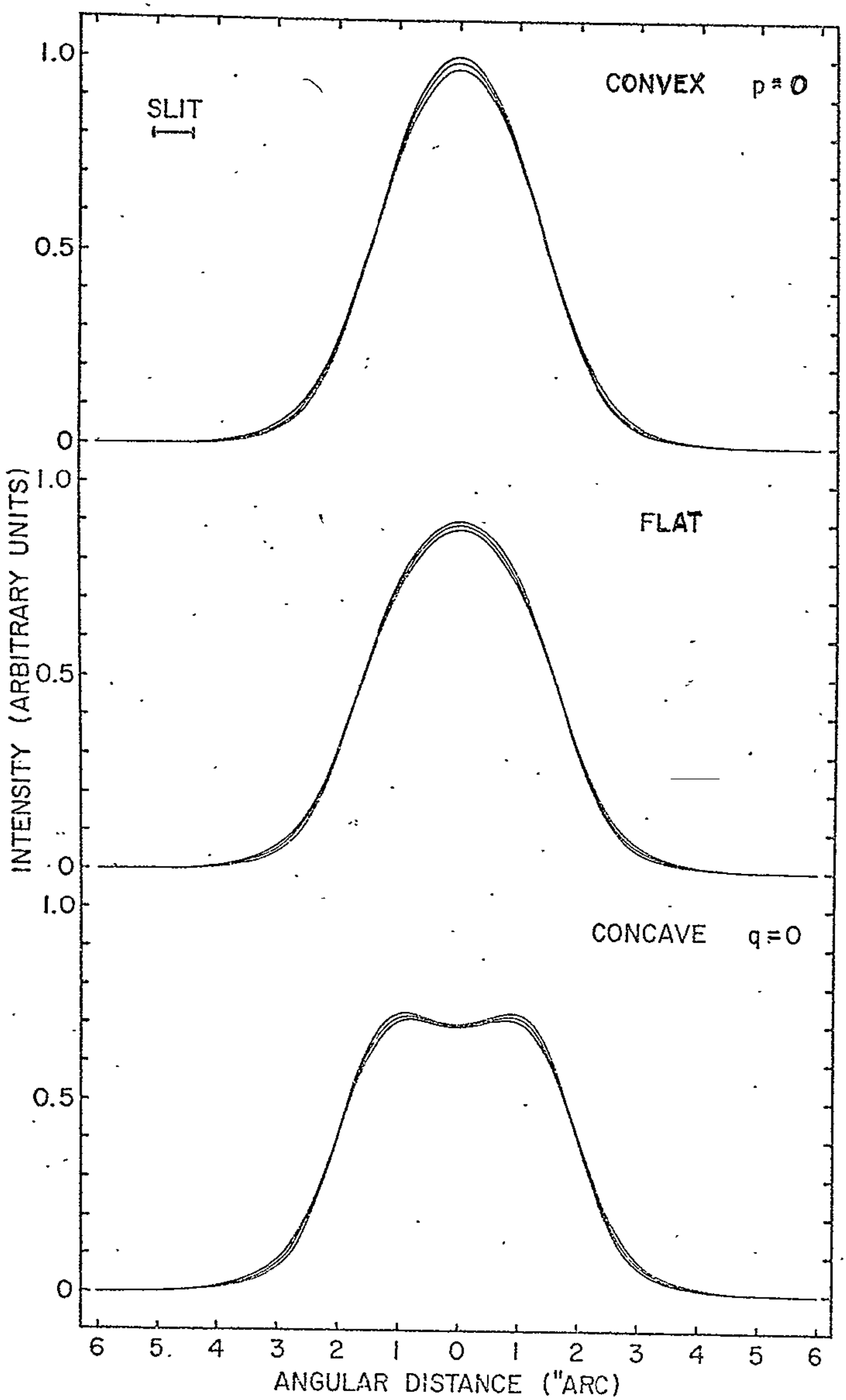
1.0
0.5
0
CONVEX p = O
SLIT
1.0
0.5
0
FLAT
1.0
0.5
0
CONCAVE q = O
INTENSITY (ARBITRARY UNITS)
6 5. 4 3 2 1 0 1 2 3 4 5 6
ANGULAR DISTANCE ("ARC)

FIG.

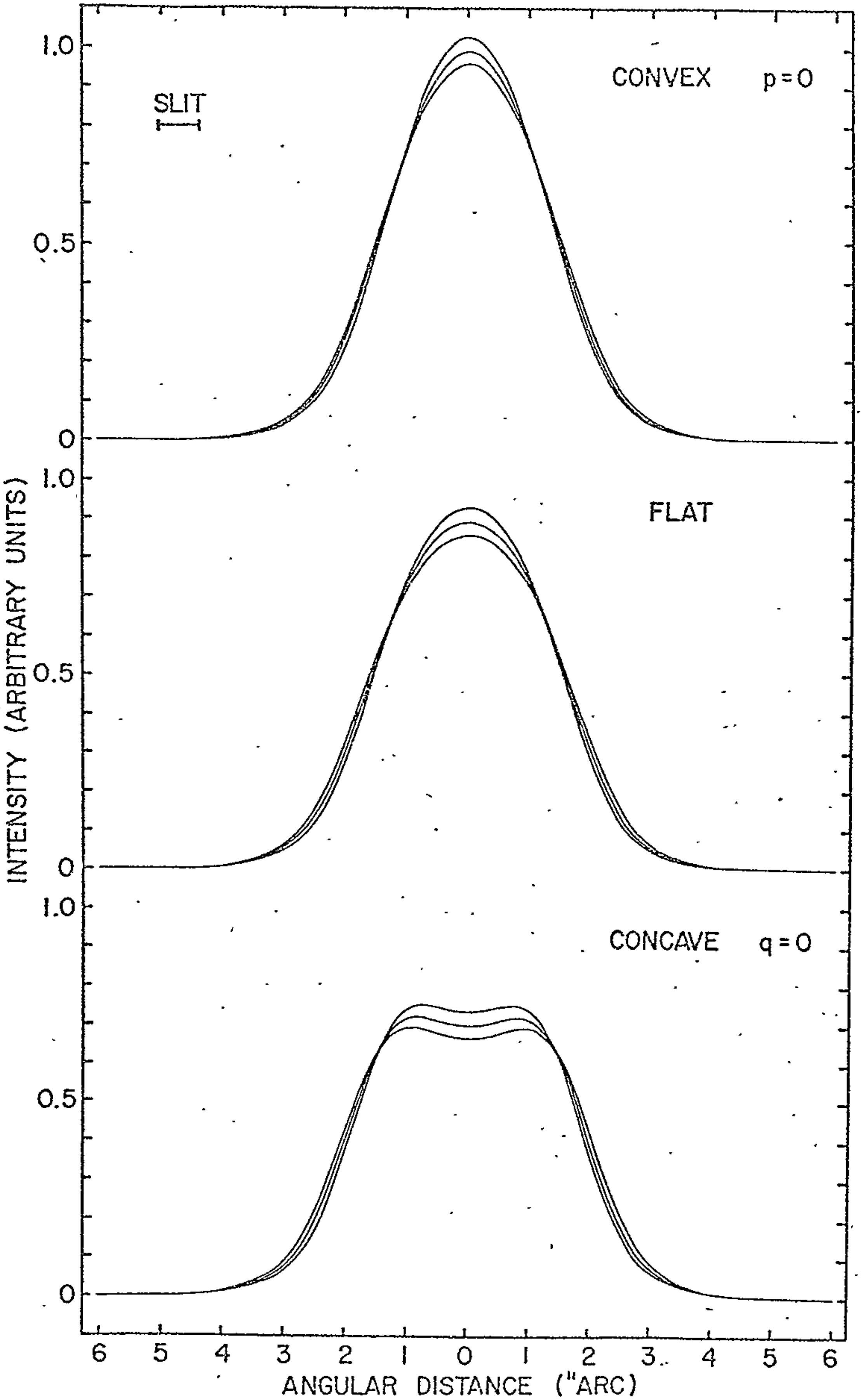
CONVEX p = 0
SLIT
FLAT
CONCAVE q = 0
INTENSITY (ARBITRARY UNITS)
ANGULAR DISTANCE ("ARC)
1.0
0.5
0
6 5 4 3 2 1 0 1 2 3 4 5 6

Fig

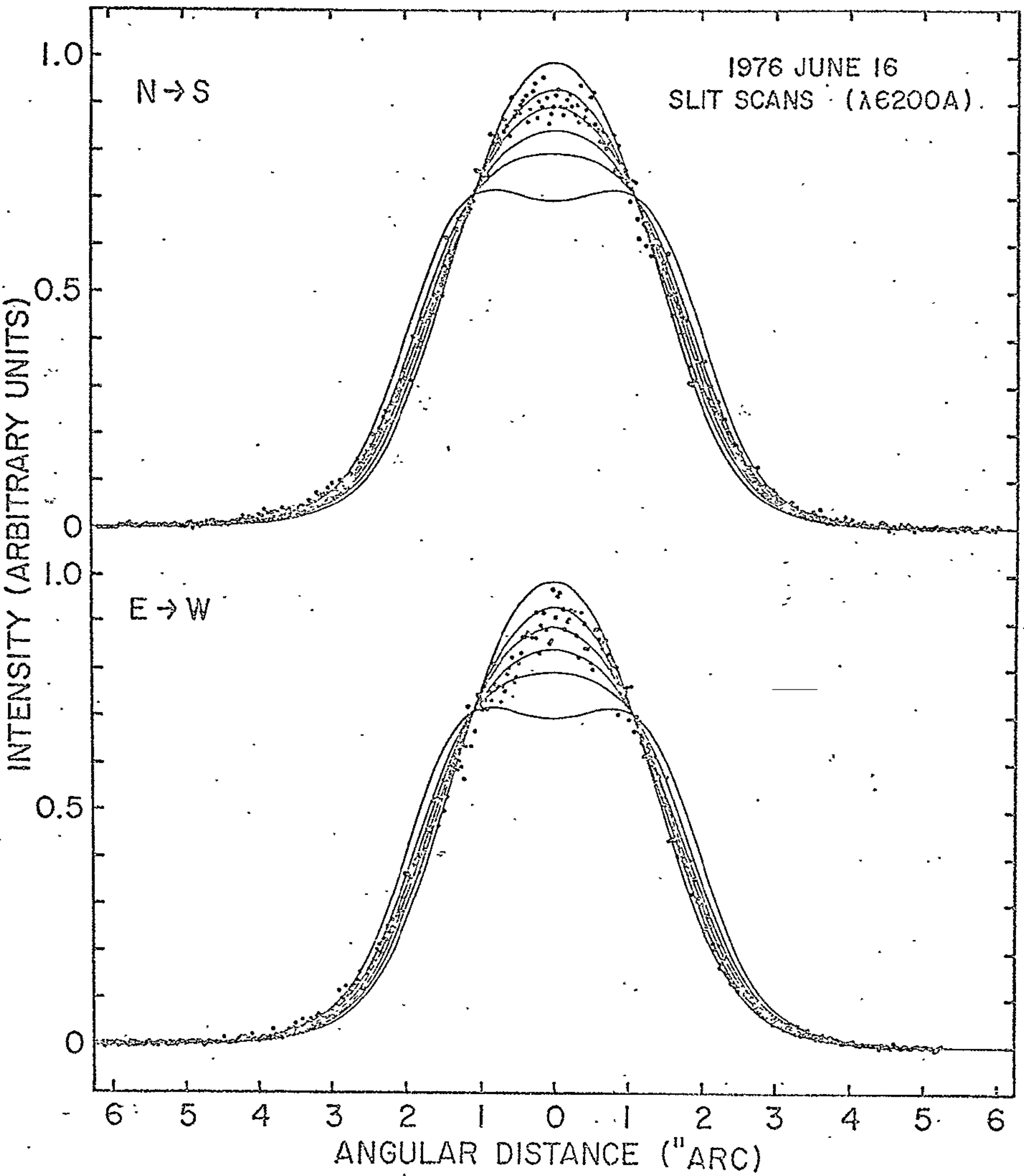

1976 JUNE 16
SLIT SCANS (λ6200A)
N → S
E → W
INTENSITY (ARBITRARY UNITS)
1.0
0.5
0
ANGULAR DISTANCE ("ARC)
6 5 4 3 2 1 0 1 2 3 4 5 6

Fig.

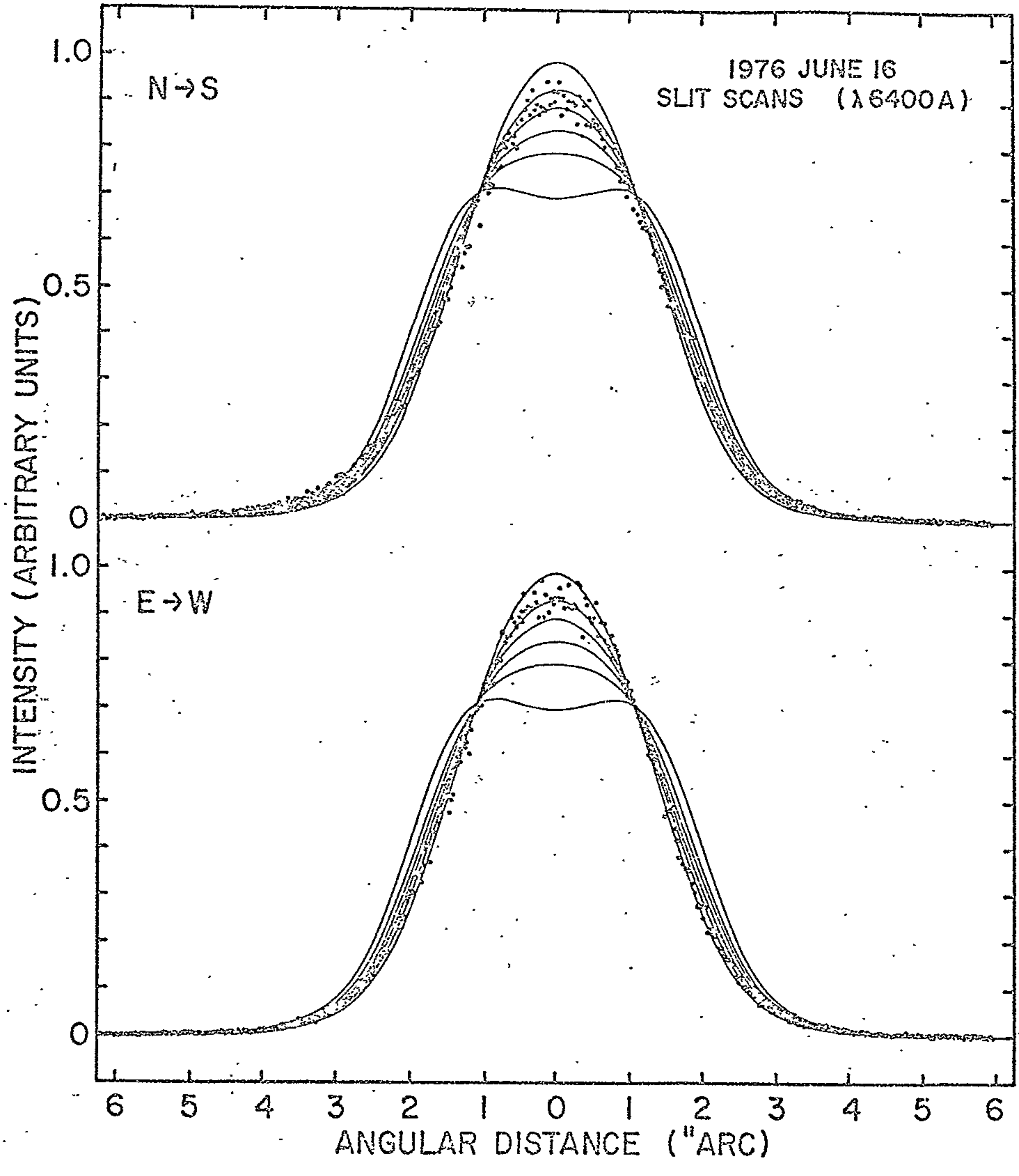
1976 JUNE 16
SLIT SCANS (λ6400A)
N→S
E→W
INTENSITY (ARBITRARY UNITS)
1.0
0.5
0
1.0
0.5
0
6 5 4 3 2 1 0 1 2 3 4 5 6
ANGULAR DISTANCE ("ARC)

Fig. 7

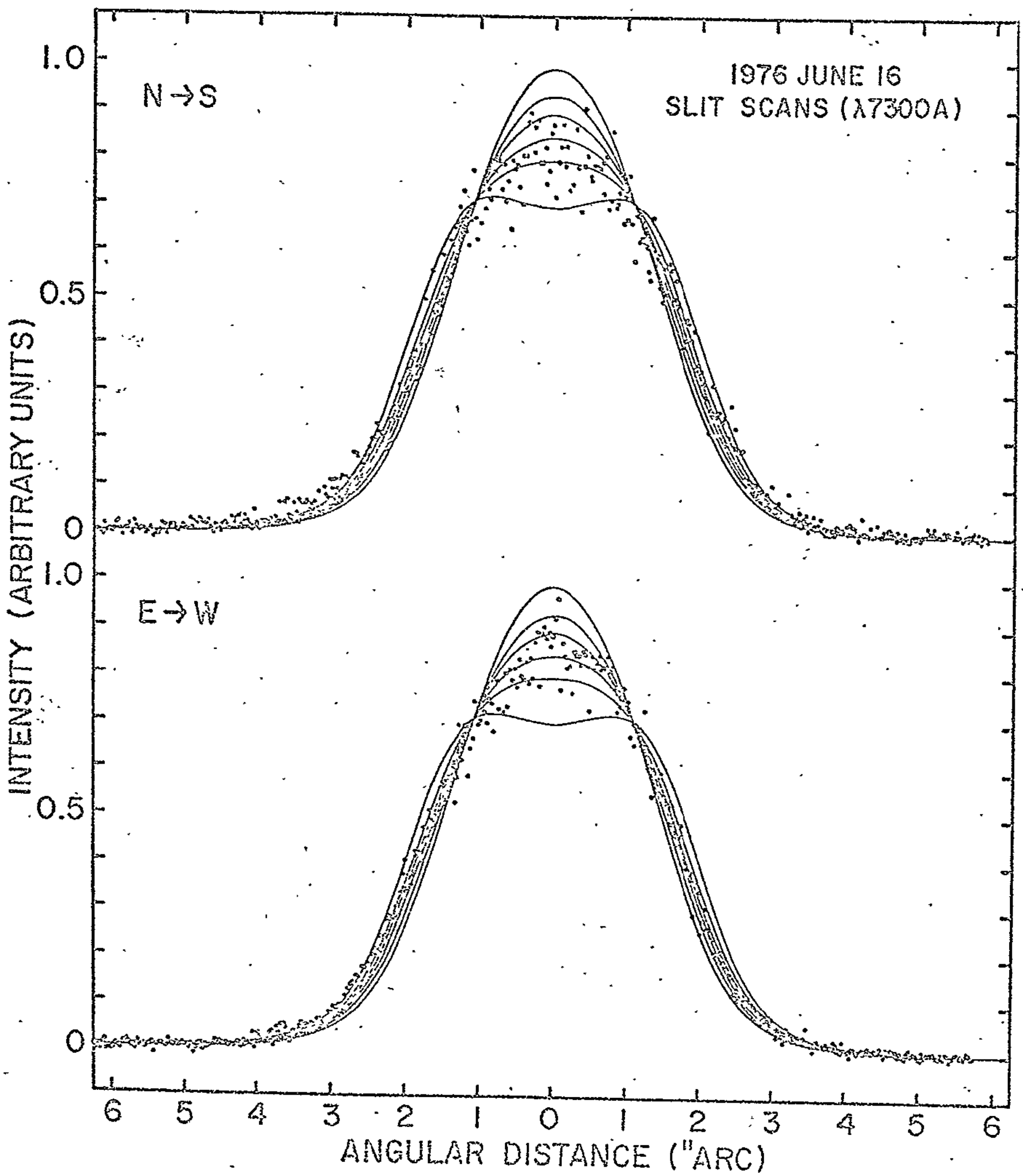
1.0
0.5
0
1.0
0.5
0
N→S
E→W
1976 JUNE 16
SLIT SCANS (λ7300A)
INTENSITY (ARBITRARY UNITS)
6 5 4 3 2 1 0 1 2 3 4 5 6
ANGULAR DISTANCE ("ARC)

Fig.8

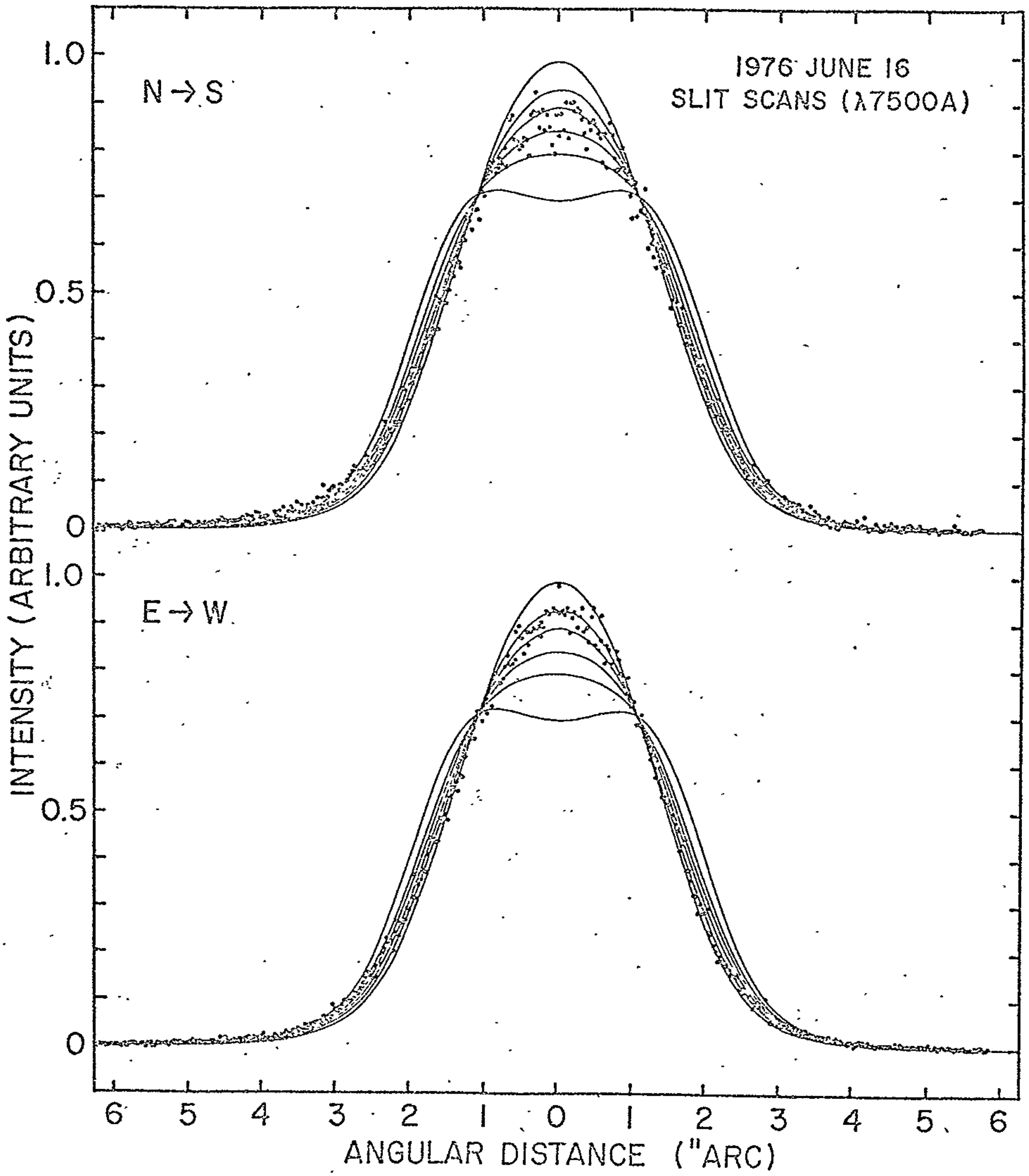

1976 JUNE 16
SLIT SCANS (λ7500A)
N → S
E → W
INTENSITY (ARBITRARY UNITS)
1.0
0.5
0
1.0
0.5
0
6 5 4 3 2 1 0 1 2 3 4 5 6
ANGULAR DISTANCE ("ARC)

Fig

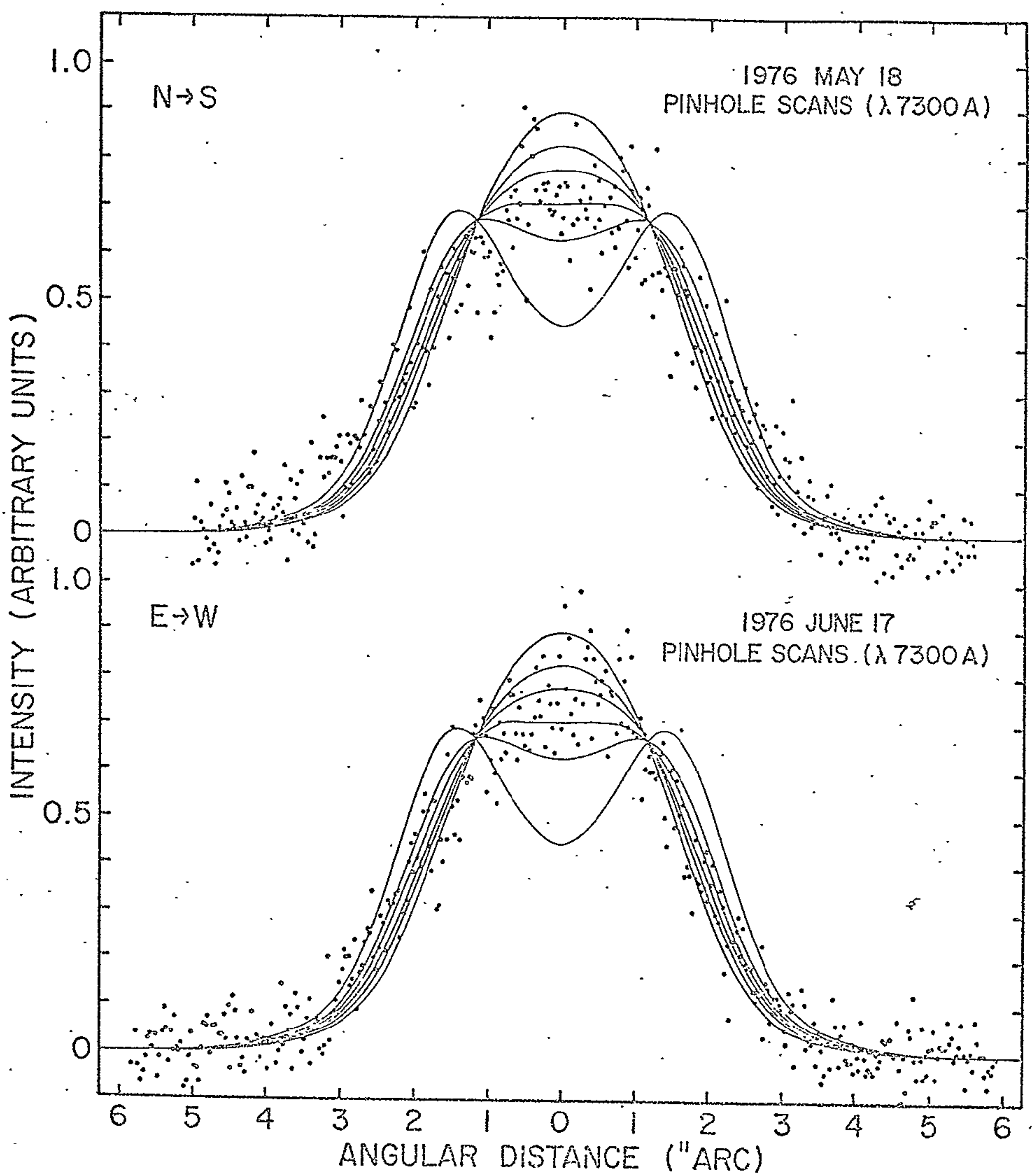
1.0
N→S
1976 MAY 18
PINHOLE SCANS (λ7300 A)
0.5
0
1.0
E→W
1976 JUNE 17
PINHOLE SCANS (λ7300 A)
0.5
0
INTENSITY (ARBITRARY UNITS)
6 5 4 3 2 1 0 1 2 3 4 5 6
ANGULAR DISTANCE ("ARC)

Fig. 1

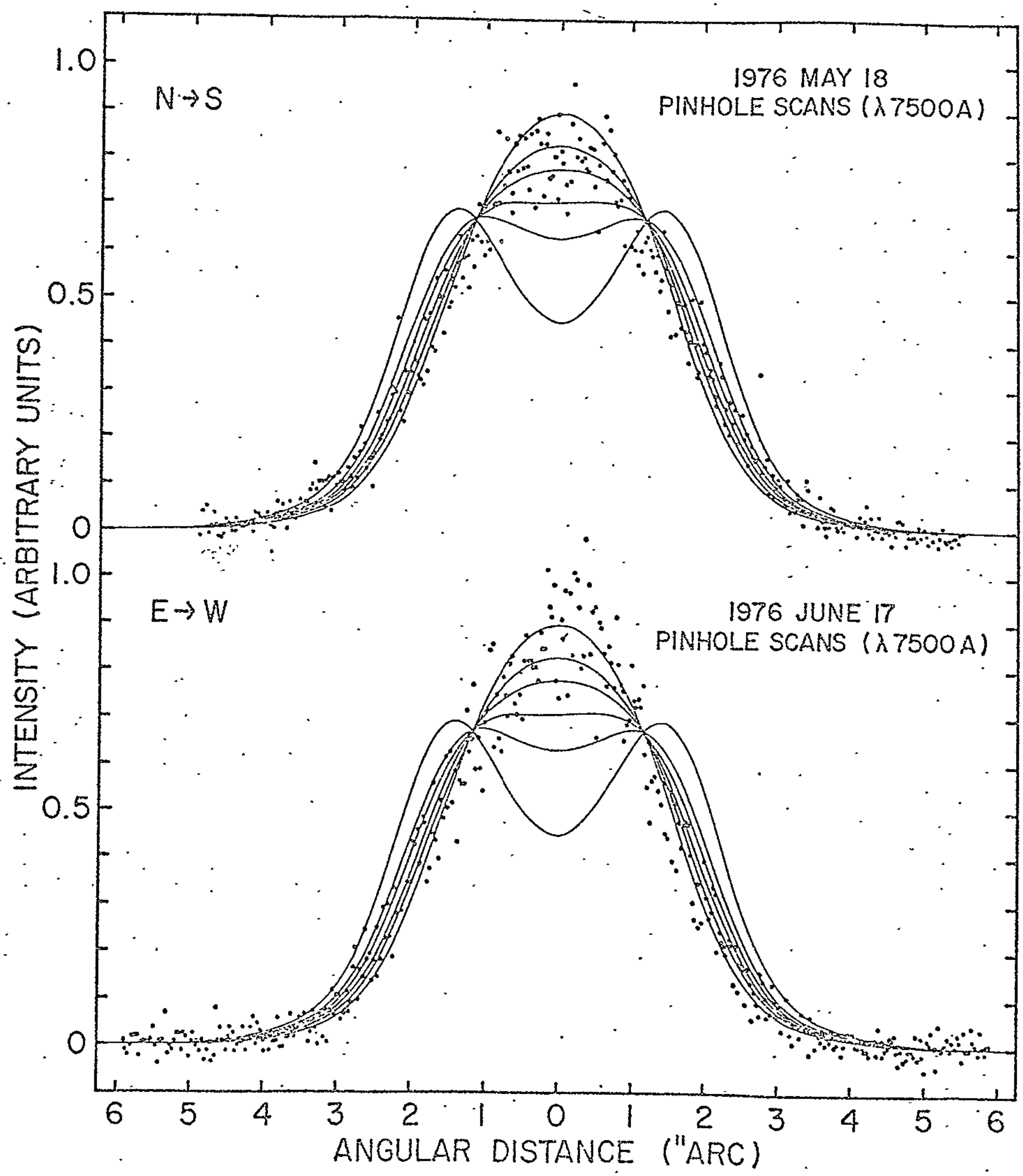

1.0
N→S
1976 MAY 18
PINHOLE SCANS (λ7500A)
0.5
0
1.0
E→W
1976 JUNE 17
PINHOLE SCANS (λ7500A)
0.5
0
INTENSITY (ARBITRARY UNITS)
6 5 4 3 2 1 0 1 2 3 4 5 6
ANGULAR DISTANCE ("ARC)

Fig.

APPENDIX F

Limb-Brightening on Uranus in the λ7300Å CH_4 Band. M. J. PRICE, Planetary Science Institute, and O. G. FRANZ, Lowell Observatory - New narrow-band (100Å) photoelectric area-scanning photometry of the Uranus disk in the strong λ7300Å CH_4 band is reported. Coarse quantitative studies of the true radial intensity profile of the disk show moderate limb-brightening to be present. Specifically, the true intensities at the center and limb of the planetary disk are approximately in the proportion 1:2. Extreme limb-brightening, with a corresponding intensity ratio greater than 1:4 is not permitted by the observational data. Our results are interpreted on the basis of a simple radiative transfer model containing an elementary vertical inhomogeneity. The Uranus atmosphere is approximated by a finite upper layer of conservatively scattering particles below which lies a semi-infinite homogeneous H_2-CH_4 gas. Isotropic scattering is assumed. The measured degree of limb-brightening is consistent with an upper layer of optical thickness $\sim$0.1 together with a CH_4/H_2 mixing ratio $\sim 2 \times 10^{-3}$ in the lower atmosphere.

KEY WORDS: (list up to ten)
URANUS, PLANETARY ATMOSPHERES, AREA-SCANNING PHOTOMETRY

Type of paper (check one)

1) oral presentation ☒ 5 min.
   ☐ 10 min.
2) read by title only ☐
3) invited lecture ☐
4) percent published elsewhere 0

Billing information:
We agree to pay $20 in partial support of the publication of the abstract in the B.A.A.S.

Date: 8/25/77

Planetary Science Institute
Institution to be billed

2030 East Speedway, Suite 201

Tucson, Arizona 85719

Joanne Metcalfe
Signature of Authorized Agent